GL-TR-90-0194   SSS-TR-90-11757
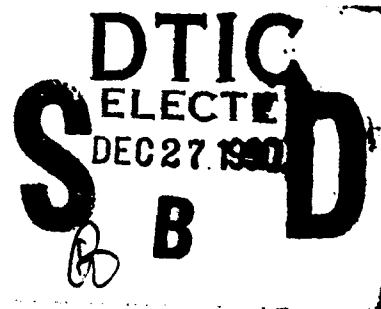
AD-A230 251

Regional Discrimination Research and Methodology
Implementation: Analyses of CDSN and Soviet IRIS Data

T. J. Bennett
J. F. Scheimer
A. K. Campanella
J. R. Murphy

S-CUBED
A Division of Maxwell Laboratories, Inc.
P. O. Box 1620
La Jolla, CA 92038-1620

DTIC
ELECTE
DEC 27 1990
S B D

July 1990

Scientific Report No. 4

GEOPHYSICS LABORATORY
AIR FORCE SYSTEMS COMMAND
UNITED STATES AIR FORCE
HANSCOM AIR FORCE BASE, MASSACHUSETTS 01731-5000

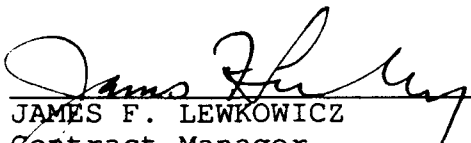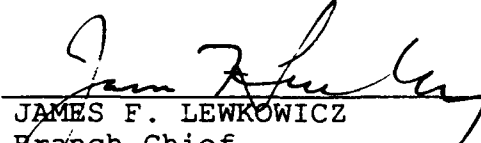The views and conclusions contained in this document are those of
the authors and should not be interpreted as representing the
official policies, either expressed or implied, of the Defense
Advanced Research Projects Agency or the U.S. Government.

This technical report has been reviewed and is approved for
publication.

JAMES F. LEWKOWICZ
Contract Manager
Solid Earth Geophysics Branch
Earth Sciences Division

JAMES F. LEWKOWICZ
Branch Chief
Solid Earth Geophysics Branch
Earth Sciences Division

FOR THE COMMANDER

DONALD H. ECKHARDT, Director
Earth Sciences Division

REPORT DOCUMENTATION PAGE

Public reporting burden for this collection of information is estimated to average 1 hour per response, including the time for reviewing instructions, searching existing data sources, gathering and maintaining the data needed, and completing and reviewing the collection of information. Send comments regarding this burden estimate or any other aspect of this collection of information, including suggestions for reducing this burden, to Washington Headquarters Services, Directorate for Information Operations and Reports, 1215 Jefferson Davis Highway, Suite 1204, Arlington, VA 22202-4302, and to the Office of Management and Budget, Paperwork Reduction Project (0704-0188), Washington, DC 20503.

1. AGENCY USE ONLY *(Leave blank)*	2. REPORT DATE July 1990	3. REPORT TYPE AND DATES COVERED Scientific No. 4

4. TITLE AND SUBTITLE
Regional Discrimination Research and Methodology Implementation: Analyses of CDSN and Soviet IRIS Data

5. FUNDING NUMBERS
F19628-89-C-0043
PE62714E
PR9A10 TA 0A WUBG

6. AUTHOR(S)
Bennett, T. J., Scheimer, J. F., Campanella, A. K., Murphy, J. R.

7. PERFORMING ORGANIZATION NAME(S) AND ADDRESS(ES)
S-CUBED
Division of Maxwell Laboratories, Inc.
P. O. Box 1620
La Jolla, California 92038-1620

8. PERFORMING ORGANIZATION REPORT NUMBER
SSS-TR-90-11757

9. SPONSORING/MONITORING AGENCY NAME(S) AND ADDRESS(ES)
Geophysics Laboratory
Hanscom Air Force Base
Massachusetts 01731-5000

Contract Manager: James Lewkowicz/LWH

10. SPONSORING/MONITORING AGENCY REPORT NUMBER
GL-TR-90-0194

11. SUPPLEMENTARY NOTES

12a. DISTRIBUTION/AVAILABILITY STATEMENT
Approved for public release; distribution unlimited.

12b. DISTRIBUTION CODE

13. ABSTRACT *(Maximum 200 words)*

The objective of this research is to evaluate the capability of regional stations in discrimination of underground nuclear explosions from earthquakes and non-nuclear explosions. Efforts during the first year of this program have focused on studies of regional data from the Chinese Digital Seismic Network (CDSN) and Incorporated Research Institutions for Seismology (IRIS) stations in the Soviet Union.

In a previous report we described observations from the CDSN station at WMQ which indicated differences in relative spectral content of L_g versus regional P for explosions and earthquakes. In the current research we used different spectral analyses to study the signals from a larger event sample including 27 East Kazakh explosions and 32 regional earthquakes. L_g/P ratios for regional earthquakes were found to be enriched at high frequencies compared to similar explosions. In comparing explosions from Shagan River and Degelen Mountain areas

(over)

14. SUBJECT TERMS
Seismic
Discrimination
Regional Phases
Soviet Explosions
Attenuation
CDSN
IRIS

15. NUMBER OF PAGES
106

16. PRICE CODE

17. SECURITY CLASSIFICATION OF REPORT	18. SECURITY CLASSIFICATION OF THIS PAGE	19. SECURITY CLASSIFICATION OF ABSTRACT	20. LIMITATION OF ABSTRACT
UNCLASSIFIED	UNCLASSIFIED	UNCLASSIFIED	UNLIMITED

NSN 7540-01-280-5500

Standard Form 298 (Rev. 2-89)
Prescribed by ANSI Std. 239-18
298-102

13. ABSTRACT (Continued)

it was found that regional P signals are relatively stronger from SR than from DM explosions with similar L_g signals.

Analysis of East Kazakh explosion signals recorded at Soviet IRIS stations indicates that regional signals are observable down to very low magnitudes. L_g magnitude residuals from these stations have been used to derive effective Q values for these paths.

Accession For	
NTIS GRA&I	☑
DTIC TAB	☐
Unannounced	☐
Justification	

By	
Distribution/	
Availability Codes	

Dist	Avail and/or Special
A-1	

Table of Contents

List of Illustrations

List of Tables

I. Introduction

1.1 Background

Over the years the DARPA research program to develop regional discrimination procedures has produced numerous advances in our understanding of the regional phase signals generated by seismic sources. However, the progress toward determination of reliable discriminants has been slow and there have been no true breakthroughs. The principal hindrances in this regard appear to be lack of complete theoretical understanding of factors affecting regional phase generation and propagation and inadequate regional phase data from Soviet events in areas of interest to test the portability of promising discrimination procedures.

Two factors suggest that it may now be possible to make significant improvements to our understanding of regional discriminants as they apply to Soviet events. Principal among these is the recent availability of high-quality digital seismic data from stations within the Soviet Union and in adjacent border regions. These data are expected to be particularly important for monitoring smaller events which would be undetected at most teleseismic stations. The second factor is the improvement in theoretical studies. Findings from such studies are expected to be useful in identifying new, more-powerful regional discrimination measures which can be tested on relevant event databases both in a controlled environment like the NTS region and in the region surrounding the Soviet testing areas where the procedures ultimately need to be applied.

1.2 Research Summary

Research described in this report summarizes the results of the first year's effort of a three year program. This program is designed to systematically evaluate the capability of regional stations to discriminate underground nuclear explosions from earthquakes and non-nuclear explosions for various environments of interest. During the first year of this program, efforts have focused on

1

empirical studies utilizing regional data from the Chinese Digital Seismic Network (CDSN) in the People's Republic of China (PRC) and the Incorporated Research Institutions for Seismology (IRIS) stations in the Soviet Union. These stations provide good, strong P_n, P_g, and L_g signals from underground nuclear explosions at the East Kazakh test sites and earthquakes in the region.

In previous studies we had found that triggered seismic stations of the CDSN frequently missed the L_g signals from Soviet underground nuclear tests. Only the nearest station, WMQ at Urumchi (R ≃ 960 km), appeared to have recorded L_g signals consistently from the Soviet events. However, additional investigation has revealed that CDSN station HIA (R ≃ 2910 km) also records L_g signals from many of the larger East Kazakh explosions. In addition, review of the data recorded at the Soviet IRIS stations at ranges between 1380 km and 2880 km reveals that they also record strong regional signals, in some cases to magnitudes as low as 4.0 m_b or so. We have found that the regional signals from such small events can normally be enhanced relative to noise by band-pass filtering with a center frequency near 1 Hz.

As a follow-up to preliminary analyses of the regional signals at WMQ which suggested differences in the relative spectral content of L_g versus regional P for explosions and earthquakes, in the current research we conducted a different spectral analysis with a larger sample of earthquake and explosion records. The analyzed database included 27 East Kazakh explosions and 32 regional earthquakes. The latter were selected to provide a variety of propagation paths with epicentral distances which encompassed those of the East Kazakh explosions. These studies again showed that L_g/P ratios for regional earthquakes were relatively enriched at high frequencies compared to similar explosions. Comparison of events with similar magnitudes indicated that regional P signals appeared to have similar spectral shapes while the L_g signals were enriched at high frequencies. L_g/P ratios which were intermingled at 1 Hz were completely separated at the one sigma level at frequencies of 2 Hz and greater for the SR explosions and regional earthquakes.

Of the 27 East Kazakh explosions in the WMQ database, 18 were at Shagan River (SR) and 9 were at Degelen Mountain (DM). These provided an opportunity to study differences in the relative signal excitation between the two source areas. We found from our analyses that the regional phase signals appeared to show different effects than those observed by Nuttli (1987) in comparing L_g amplitudes with teleseismic P. In particular, our studies suggest that the regional P signals are relatively stronger from SR explosions than from DM explosions with similar L_g signals. This appears to be the opposite of Nuttli's finding in comparing teleseismic P from the two sites. We also analyzed the spectral behavior of the P and L_g signals recorded at WMQ from DM versus SR explosions. These results revealed a tendency for the DM explosions to have L_g/P spectral ratios which were slightly more earthquake-like (i.e. larger L_g/P at high frequencies), but not enough for the source site differences to jeopardize the discrimination capability of the measurement.

An issue which needs further study is the degree to which propagation path differences might affect the L_g/P spectral ratios. Since co-located earthquake and explosion sources do not exist, we are forced to compare events which have somewhat different propagation paths to the available regional monitoring stations. In principle, such comparisons would be most valid if the signal measurements were compensated for attenuation differences. To obtain some insight into these effects, we have made some preliminary computations of the Q values for L_g signals propagating from the East Kazakh test sites to the regional CDSN and Soviet IRIS stations. These Q values were derived from an analysis of the L_g magnitude residuals and gave values ranging from a low value of 428 for station GAR to a high value of 761 for station OBN.

1.3 Report Organization

The report is divided into six sections including this introduction. Section II summarizes the regional network used in these studies and summarizes the general characteristics of the regional signals recorded at the CDSN stations and the Soviet IRIS stations from East Kazakh explosions and regional earthquakes. Section III provides information on the spectral analyses performed on the WMQ database and gives the results of the L_g/P spectral ratio measurements. In Section IV we present the results comparing the relative L_g and

3

regional P excitation for SR and DM explosions. Section V contains the preliminary analysis performed on the L_g magnitude residuals to derive effective Q values for the paths to the regional stations from the East Kazakh test sites. Finally, Section VI provides a summary and identifies future research plans.

II. Database for CDSN and Soviet IRIS Stations

2.1 The Regional Network

As noted in the Introduction, research efforts during the past year under this contract have focused on analyses of the regional signals recorded at stations in the CDSN and Soviet IRIS networks. Figure 1 shows the locations of these stations with respect to the principal Soviet underground nuclear test sites at Shagan River (SR) and Degelen Mountain (DM). The CDSN stations range in distance (cf. Table 1) from about 960 km for station WMQ to 4380 km for the station designated QIO on the map. The distance to the test sites for the Soviet IRIS stations is between about 1380 km for station GAR and 2880 km for station OBN. As can be seen from the map in Figure 1, the broadest gap in azimuthal coverage ($\approx 125°$) is to the north of the test site. A smaller gap ($\approx 80°$) occurs to the south. However, it should be noted that seismic data are not currently available from the Soviet IRIS station at IRK or from three of the CDSN stations designated as ENS, QIO, and SSH on the map; so actual regional coverage is not as good as it may appear from the station map.

The stations of both the CDSN and Soviet IRIS networks include high-quality, broad-band three-component systems with digital recording at sampling rates of 20 samples per second and, for CDSN, also 40 samples per second. The stations in both networks also include low-frequency elements with lower sampling rates, but these latter have not been analyzed in the current investigation. An important difference between the CDSN and Soviet IRIS recording systems is that the CDSN is a triggered system while the IRIS stations record continuously. As a result, the CDSN stations record only those events which produce ground motion at the individual stations above some signal-to-noise threshold. This triggering system has been a persistent problem for recording longer-range regional events since this network first became operational. In particular, the triggering algorithm is not optimized for detection of L_g signals from events at ranges comparable to SR/DM. Regional signals from SR/DM explosions below about 4.8 m_b are missed at even the nearest CDSN station (viz WMQ); and at the distant CDSN stations the trigger algorithm usually

5
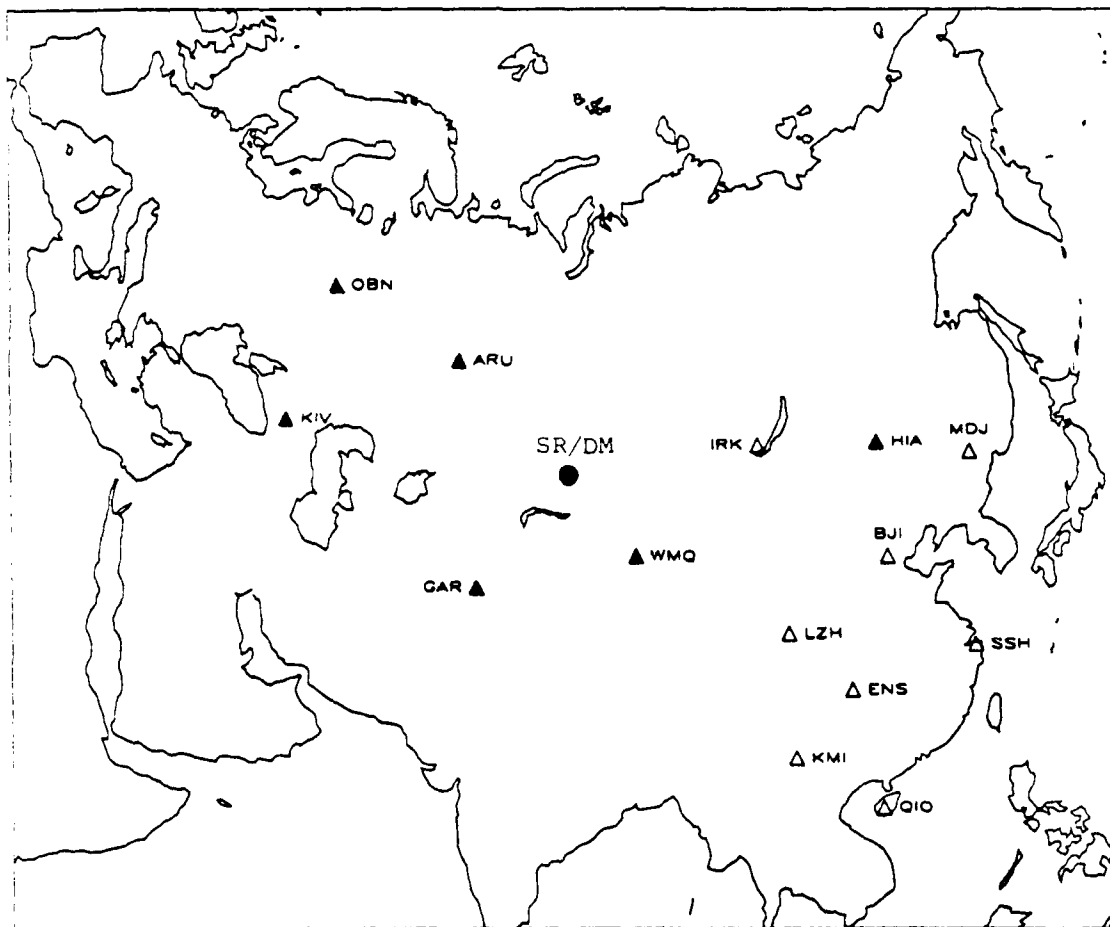
Figure 1. Locations of CDSN and Soviet IRIS stations with re-
spect to principal East Kazakh test sites at SR/DM.
Solid triangles indicate stations from which useful
L_g signals are obtained.

Table 1. Distance From Soviet Test Sites For CDSN and Soviet IRIS Stations

Station Designation	Distance (km)	Azimuth (°)
WMQ (CDSN)	960	133
GAR (IRIS)	1380	212
ARU (IRIS)	1530	306
IRK*(IRIS)	1780	72
LZH (CDSN)	2530	118
KIV (IRIS)	2800	270
OBN (IRIS)	2880	298
HIA (CDSN)	2910	76
BJI (CDSN)	3100	97
ENS*(CDSN)	3350	120
KMI (CDSN)	3440	135
MDJ (CDSN)	3800	79
SSH*(CDSN)	4100	105
QIO*(CDSN)	4380	131

*No useful explosion data is available from these stations at this time.

shuts-off, for even the largest SR/DM explosions, prior to the L_g signal and, in most cases, doesn't reactivate. Therefore, the analysis of the CDSN data presented here focuses on two stations, WMQ and HIA, which have frequently recorded L_g signals from SR/DM explosions. The other CDSN stations normally record only the regional P phases from SR/DM explosions and occasionally L_g phases from earthquakes nearer individual stations. Analyses of the latter data will be included in subsequent years of this research effort.

With regard to the Soviet IRIS stations, although the systems are designed to record continuously, in reality this goal has not always been met during the initial year or so of network operation. Station down-time has been a recurring problem particularly at some of the stations. As a result, several SR/DM explosions and regional earthquakes have been missed at various IRIS stations. Furthermore, during this start-up phase of network operation, instrumentation and gain levels have occasionally changed and, in some cases, have been incorrectly reported. This has provided some obstacles to the determination of absolute ground-motion levels associated with the regional signals recorded at the Soviet IRIS stations, but most of these have now been resolved.

2.2 The CDSN Database

The high-quality CDSN network has been in routine, nearly continuous operation since late 1986. Over this period the network stations have recorded numerous underground nuclear explosions from the SR/DM test site. For analyzing the characteristics of regional signals from these events, we have found the broadband channels, with a digitizing rate of 20 samples per second, to be most useful. This band appears adequate to recover the spectral characteristics over most frequencies for which the signal-to-noise level is above 1.0 for the SR/DM explosions. The broadband database is also somewhat more complete than the short-period band (digitized at 40 samples per second), which experienced more of the triggering problems described above.

Figure 2 shows the broadband, vertical-component records at station WMQ (R = 960 km) from 27 underground nuclear explosions. Information on the locations and magnitudes of these explosions obtained from NEIS are shown in Table 2. Of these 27 events 18 were located at SR and 9 at DM.

8
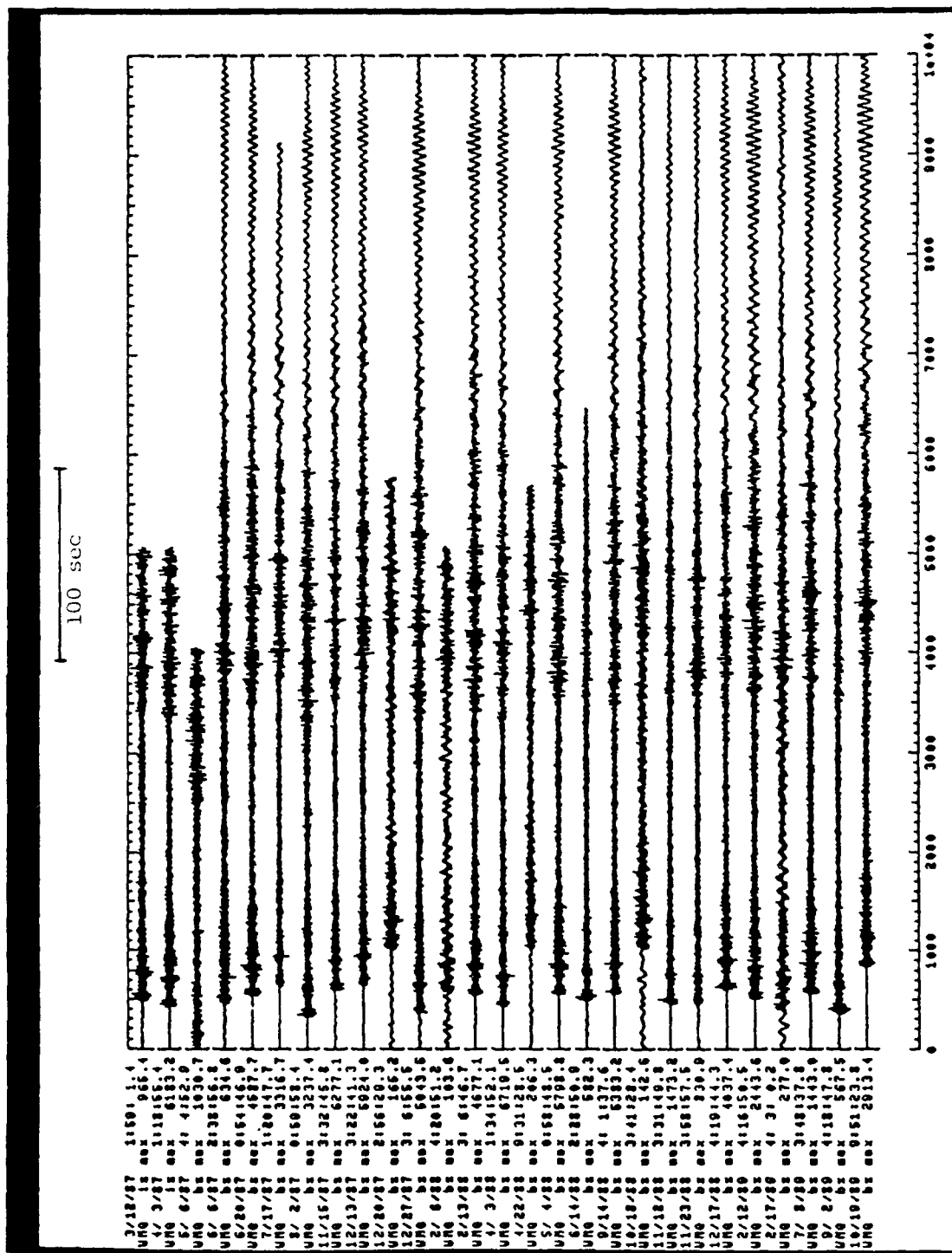
Figure 2.   Vertical-component records at station WMQ from 27 SR/DM explosions.

9

Table 2. Information on SR & DM Explosions Recorded at CDSN Stations

Date	Origin Time	Lat(°N)	Lon(°E)	Site	m_b	$m_b(L_g)$ - NOR	WMQ	HIA
03/12/87	01:57:17.2	49.94	78.82	SR	5.5	5.22	x	-
04/03/87	01:17:08.0	49.93	78.83	SR	6.2	6.05	x	x
05/06/87	04:02:05.6	49.83	78.13	DM	5.6	-	x	-
06/06/87	02:37:07.0	49.86	78.11	DM	5.3	-	x	-
06/20/87	00:53:04.8	49.91	78.74	SR	6.1	5.97	x	x
07/17/87	01:17:07.0	49.80	78.11	DM	5.8	-	x	-
08/02/87	00:58:06.8	49.88	78.93	SR	5.9	5.87	x	x
11/15/87	03:31:06.7	49.87	78.79	SR	6.0	5.97	x	x
12/13/87	03:21:04.8	49.99	78.84	SR	6.1	6.09	x	x
12/20/87	02:55:06.7	49.83	78.00	DM	4.8	-	x	-
12/27/87	03:05:04.7	49.86	78.76	SR	6.1	6.05	x	x
02/06/88	04:19:06.3	49.80	78.06	DM	5.0	-	x	-
02/13/88	03:05:05.9	49.95	78.91	SR	6.1	6.04	x	-
04/03/88	01:33:05.8	49.92	78.95	SR	6.1	6.06	x	x
04/22/88	09:30:06.9	49.82	78.12	DM	4.9	-	x	-
05/04/88	00:57:06.8	49.93	78.77	SR	6.1	6.04	x	-
06/14/88	02:27:06.4	50.05	79.01	SR	5.0	-	x	-
09/14/88	04:00:00.0	49.83	78.81	SR	6.1	5.97	x	x
10/18/88	03:40:06.6	49.87	78.08	DM	4.9	-	x	-
11/12/88	03:30:03.7	50.08	78.99	SR	5.3	5.26	x	-
11/23/88	03:57:06.7	49.82	78.07	DM	5.3	-	x	-
12/17/88	04:18:06.9	49.89	78.93	SR	5.9	5.80	x	x
01/22/89	03:57:06.6	49.92	78.83	SR	6.1	5.96	-	x
02/12/89	04:15:06.8	49.93	78.74	SR	5.9	5.79	x	x
02/17/89	04:01:06.9	49.87	78.08	DM	5.0	-	x	-
07/08/89	03:47:01.9	50.66	78.51	SR	5.6	-	x	x
09/02/89	04:17:01.6	50.85	78.94	SR	5.4	-	x	-
10/19/89	09:49:59.7	50.47	78.72	SR	6.0	5.79	x	x

For purposes of associating these events with a particular test site, we have used the observation that the event locations fall into two clusters with the DM cluster located about 50 km west of the SR cluster. The events cover a magnitude range from 4.8 to 6.2 m_b with many of the smaller magnitude explosions having locations at DM. East Kazakh explosions with magnitudes below about 4.8 m_b apparently do not trigger the detector at WMQ. It can be noted in Figure 2 that even the magnitude 4.8 m_b explosions appear to have large signal-to-noise levels; and it should, therefore, be possible to detect regional P and L_g signals at WMQ from much smaller East Kazakh explosions. Although some modifications to the automatic detection algorithm at WMQ have been made over the years and have improved acquisition of East Kazakh explosion data, it seems clear that continuous recording or changes to the detector could enable recovery of much smaller events at WMQ. One or two larger events were also not recorded at WMQ because the station was down at the time of the events.

As can be seen in Figure 2, the regional P and L_g signals at WMQ from the East Kazakh explosions are strong. The records also show a strong R_g phase whose dispersion characteristics seem to be remarkably consistent from event to event but whose excitation relative to the other regional phases appears to be somewhat variable. This latter observation needs further investigation. We have described the general characteristics of the regional signals recorded at WMQ in a previous report (cf. Bennett *et al.*, 1989) and won't describe them further here. In the previous report we also described spectral analyses performed on the regional P and L_g signals at WMQ from several East Kazakh explosions. Spectral analyses of the L_g signals revealed that they were peaked in a relatively narrow frequency band between 0.3 and 1.0 Hz. The regional P waves showed somewhat broader peaks with maxima in the band from about 0.5 to 3 Hz. We will address the spectral characteristics of the regional signals at WMQ more fully in the next section of this report.

Our earthquake database at WMQ currently includes 32 events. These are listed in Table 3 and their locations are plotted in Figure 3. The earthquakes ranged in magnitude from 4.3 to 5.9 m_b. Because the area in the immediate vicinity of the East Kazakh test sites is generally aseismic, the comparative earthquake sample was selected to give events with epicentral distances which bounded the explosion distance range. In addition, some events

11

Table 3. Information on Earthquakes Recorded at WMQ

Date	Origin Time	Lat(°N)	Lon(°E)	m_b	R(km)
11/18/86	13:27:01.0	40.06	77.56	4.7	938
12/14/86	03:19:17.0	47.31	83.31	5.0	517
12/20/86	23:08:16.5	36.75	93.66	5.3	935
01/05/87	22:52:46.5	41.96	81.32	5.9	560
01/24/87	08:09:21.0	41.53	79.32	5.9	732
01/24/87	13:40:40.0	41.44	79.25	5.2	741
03/05/87	02:33:39.0	35.41	87.39	4.5	935
04/09/87	07:25:35.7	35.50	87.07	4.8	926
04/09/87	20:01:18.0	35.59	80.47	4.9	1103
04/30/87	05:17:37.0	39.76	74.57	5.7	1179
06/08/87	13:30:36.0	39.79	74.69	5.1	1169
08/05/87	10:24:21.0	41.36	82.11	4.8	534
09/03/87	09:08:12.0	38.83	75.32	4.8	1174
09/16/87	17:57:26.4	52.09	95.70	4.8	1096
09/18/87	21:58:41.0	47.02	89.66	5.3	387
10/06/87	13:06:20.3	43.44	88.55	4.8	81
12/03/87	23:51:43.0	39.54	77.55	4.7	969
12/06/87	16:20:45.2	37.44	94.61	4.7	919
12/17/87	12:17:25.0	41.94	83.20	5.1	423
12/22/87	00:16:39.0	41.36	89.64	5.9	317
01/02/88	22:02:36.0	40.06	77.34	4.9	954
01/09/88	03:55:05.3	39.09	71.50	5.4	1449
02/08/88	17:49:19.8	43.73	83.76	4.3	317
03/25/88	02:07:56.0	44.71	79.60	4.5	654
04/01/88	01:27:16.2	47.53	89.65	4.6	439
05/02/88	02:13:26.0	40.26	82.20	4.9	603
05/25/88	00:05:23.0	40.57	77.62	4.9	907
05/25/88	18:21:58.0	42.01	85.69	5.2	259
06/17/88	13:30:45.0	42.94	77.50	5.3	832
06/30/88	15:25:15.5	50.23	91.14	5.0	759
07/23/88	07:38:09.0	48.72	90.51	5.5	586
11/15/88	16:56:45.9	42.08	89.40	5.0	238
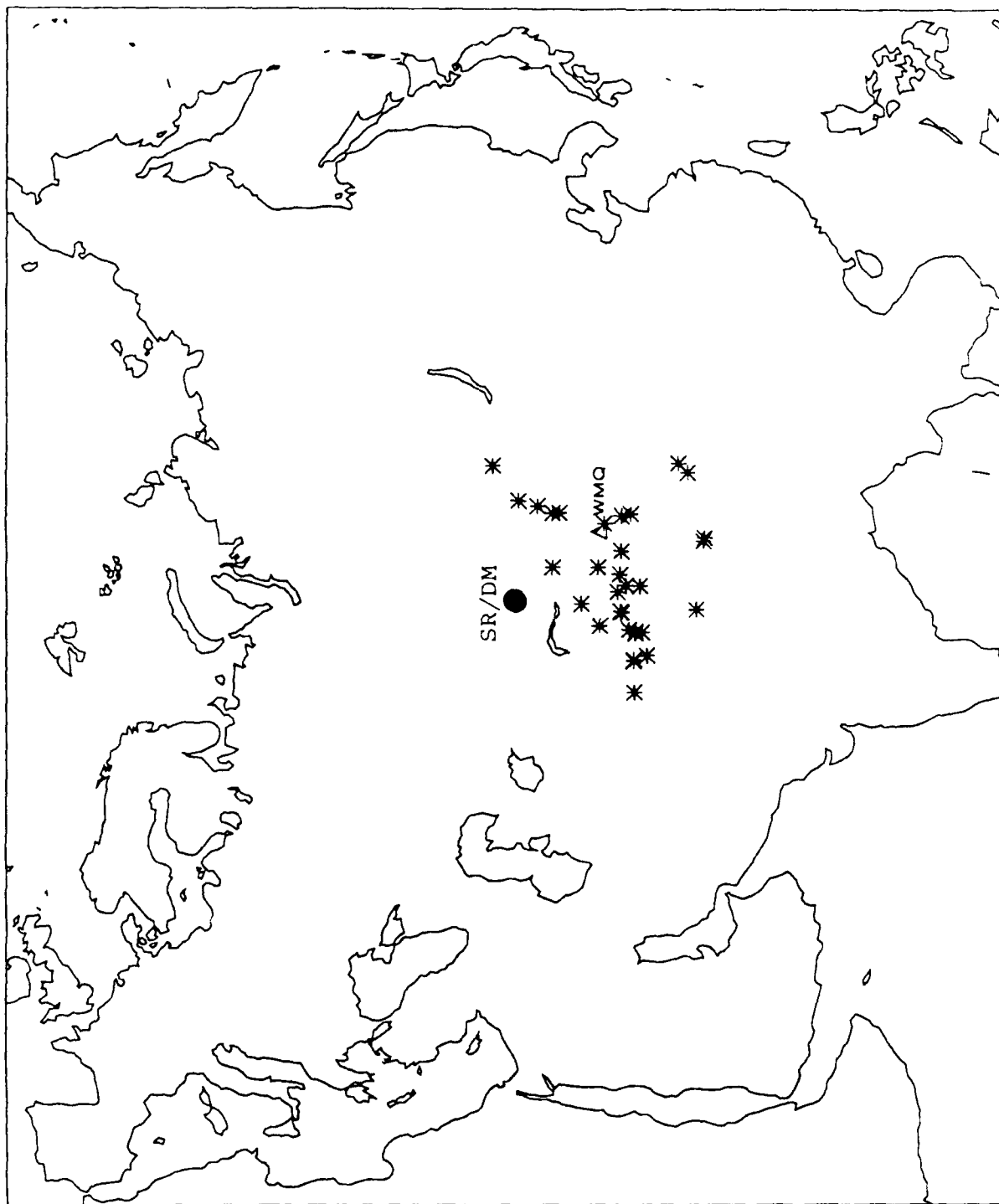
Figure 3. Locations of 32 earthquakes recorded at WMQ with respect to Soviet nuclear explosion tests at SR/DM.

at smaller and larger ranges from WMQ were selected to enable a more complete analysis of attenuation and other path-dependent effects for the region. As a result the earthquakes cover an epicentral distance range from about 80 km to 1450 km. The earthquakes recorded at WMQ typically show strong L_g signals which, in most cases, are larger than the frequently emergent P phases. Some of these characieristics, based on a smaller data sample, were described in our previous report (cf. Bennett et al., 1989) and examples of the observed signals were presented. In Section III of this report, we describe the results of spectral analysis performed on the regional earthquake signals recorded at WMQ and identify diagnostic differences in the signal behavior between the earthquake and explosion samples.

Figure 4 shows the broadband, vertical-component records at station HIA (R = 2910 km) from 12 SR underground nuclear explosions. Information on the locations and magnitudes of these explosions is presented in Table 2 above. The events recorded at HIA cover a very limited range of magnitudes between 5.6 and 6.2 m_b. Smaller magnitude explosions at the East Kazakh test sites apparently do not trigger the detector. From the broadband recordings in Figure 4, it appears that the magnitude 5.6 event has a signal-to-noise level of about 3:1. Some enhancement of the recording capability at HIA for East Kazakh explosions again might be achieved by continuous recording or modifying the triggering algorithm, but the signal-to-noise level suggests that it may not be possible to push the threshold at HIA below about magnitude 5.0 m_b. It should also be noted in Figure 4 that the records of earlier explosions obtained from HIA consist of interrupted P and L_g segments. The intervening trace dead time corresponds to a time interval during which the automatic detector shuts off before retriggering on the L_g arrival. This problem appears to have been corrected for the more recent explosions producing the continuous records shown for the bottom five events.

The SR explosion records obtained at HIA in Figure 4 show relatively strong L_g signals following a relatively weak P phase. The relative phase characteristics are observed to be very consistent from event to event. The L_g window includes a higher-frequency segment followed by a dispersed packet of low-frequency energy apparent on most records. Typical P and L_g spectra for SR explosions at HIA are shown in Figure 5. As with the WMQ signals, the L_g

14
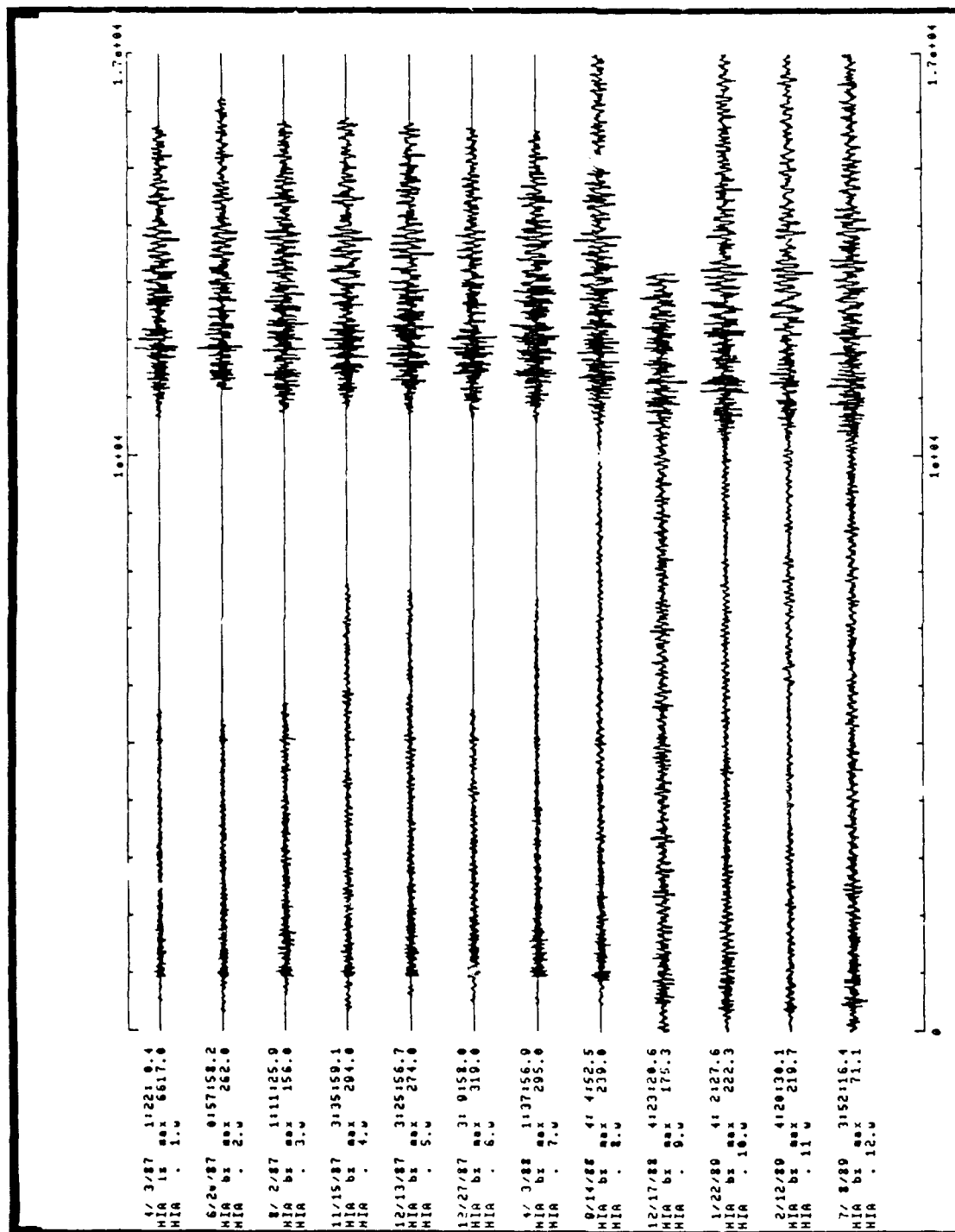
Figure 4. Vertical-component records at HIA from 12 SR explosions.

15
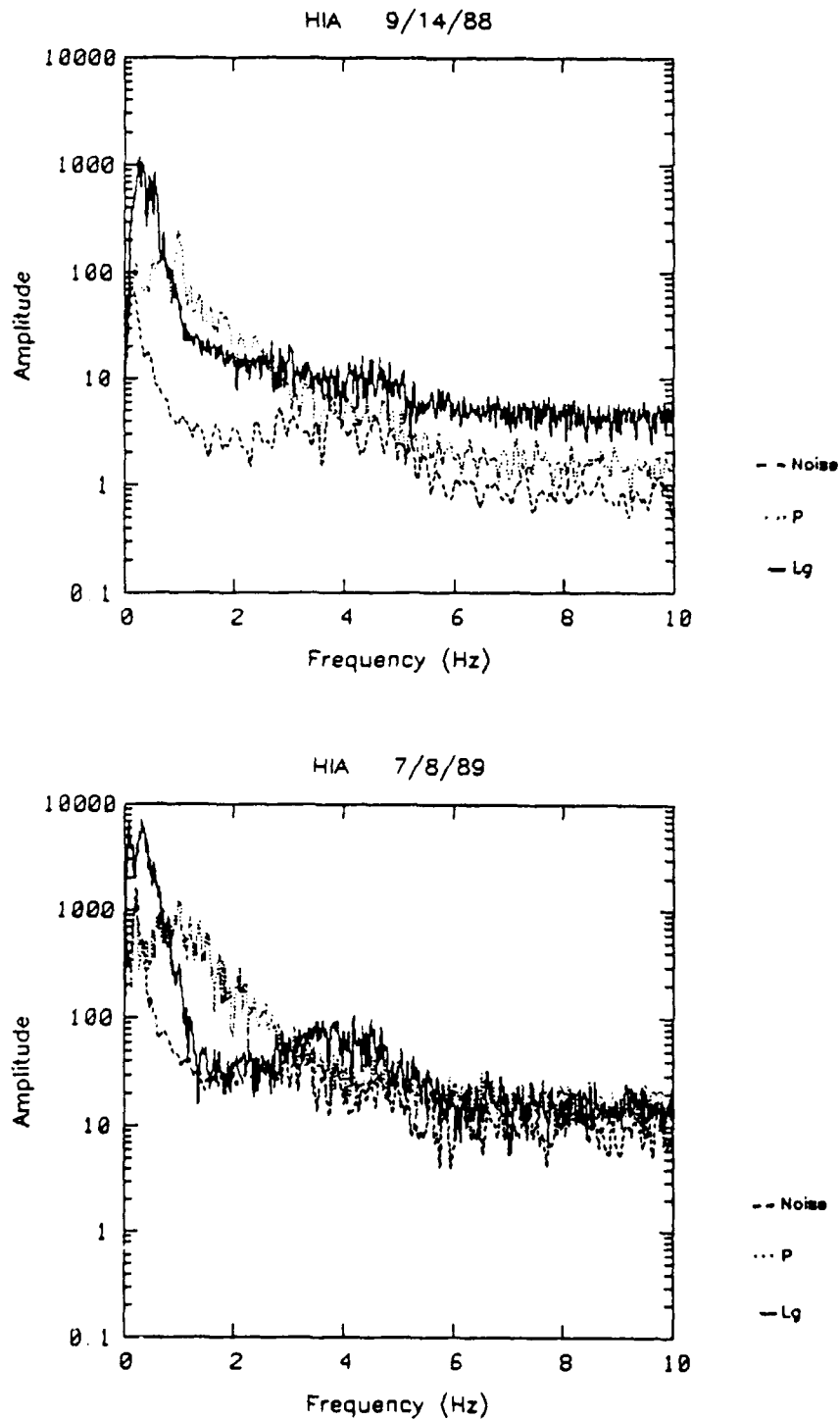
Figure 5. Regional P, L_g and noise spectra measured at station HIA for Soviet nuclear tests at SR on 09/14/88 (JVE, top) and 07/08/89 (bottom).

16

spectra at HIA are sharply peaked at a frequency less than 1 Hz (viz between about 0.3 and 0.8 Hz). There is some evidence of a secondary peak in the L_g spectra at a somewhat higher frequency (around 4 Hz); but the signal-to-noise level in this band is low and the peak could be related to noise. The L_g spectra are generally at or near the noise level for frequencies of 2 Hz and higher. The regional P-wave spectra from the East Kazakh explosions recorded at HIA are peaked at a higher frequency (around 1 Hz) than the L_g. Furthermore, the P-wave spectra are somewhat broader than the L_g with relatively more energy at frequencies above 1 Hz. One peculiarity of the L_g signal spectrum for the September 14, 1988 explosion at SR is its failure to return to the noise level at high frequencies. We are attempting to ascertain whether this is somehow related to the signal processing, but most obvious causes have been eliminated.

2.3 The Soviet IRIS Database

The network of Soviet IRIS stations began operation in September, 1988. As noted above, the operation of individual stations in the network has been somewhat sporadic during the initial start-up phase. This has resulted in a failure to record several explosions at the East Kazakh test sites because stations were not operating at these times. Nevertheless, excellent regional seismic records have been obtained from several Soviet IRIS stations starting with the Soviet JVE shot on September 14, 1988. Figure 6 shows the available vertical-component records obtained from nine explosions through July, 1989. Two additional explosions since that time are in the process of being installed into the CSS database. Table 4 shows the location and magnitude information on the nine explosions. Seven of the events were located at SR and two at DM. The magnitudes range from 3.8 to 6.1 m_b. The smallest event magnitude (viz 3.8 m_b) was estimated by Hansen et al. (1990) based on NOR-SAR m_b measurements with a bias correction applied to adjust to a large, global-network m_b. All nine of the explosions were recorded at ARU, and only one other Soviet IRIS station (viz GAR) recorded more than half of the events. This is not a detection problem; the missing stations were simply not operating.

As can be seen in Figure 6, the Soviet IRIS stations generally record strong, rather complex regional P phases and equally strong L_g on these

17
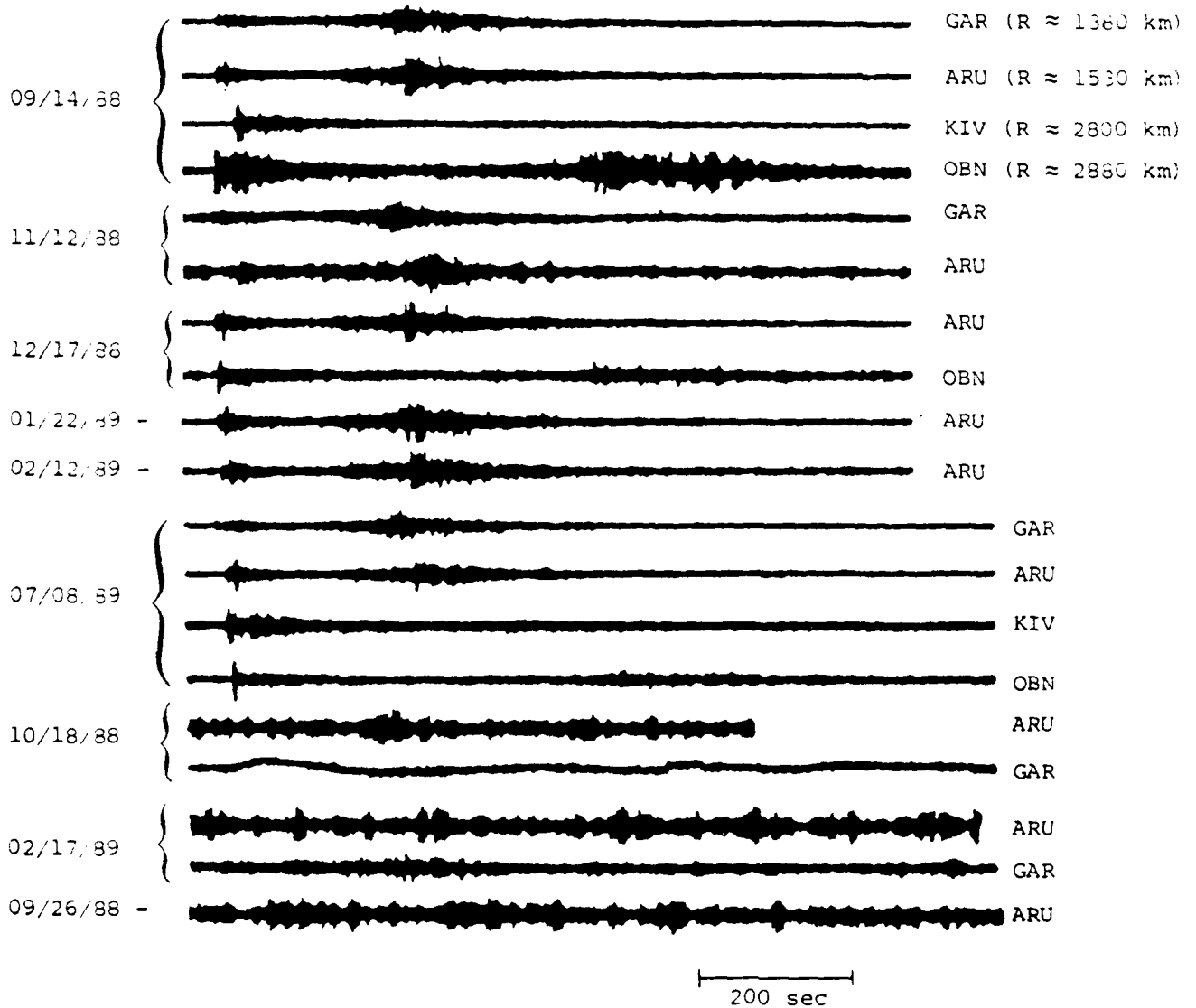
Figure 6. Available vertical-component records at Soviet IRIS
stations from nine SR/DM explosions.

Table 4. Information on SR & DM Explosions
Recorded at Soviet IRIS Stations

Date	Origin Time	Lat(°N)	Lon(°E)	Site	m_b	$m_b(L_g)$ - NOR	GAR	ARU	KIV	OBN
09/14/88	04:00:00.0	49.83	78.81	SR	6.1	5.97	x	x	x	x
09/26/88*	07:45:00.0	49.90	78.00	SR	3.8	-	-	x	-	
10/18/88	03:40:06.6	49.87	78.08	DM	4.9	-	x	x	-	-
11/12/88	03:30:03.7	50.08	78.99	SR	5.3	5.26	x	x	-	-
12/17/88	04:18:06.9	49.89	78.93	SR	5.9	5.80	-	x	-	x
01/22/89	03:57:06.6	49.92	78.83	SR	6.1	5.96	-	x	-	-
02/12/89	04:15:06.8	49.93	78.74	SR	5.9	5.79	-	x	-	-
02/17/89	04:01:06.9	49.87	78.08	DM	5.0	-	x	x	-	-
07/08/89	03:47:01.9	50.66	78.51	SR	5.6	-	x	x	x	x

*Source information on this event is from Hansen *et al.* (1990); the location and origin time are approximate.

19

broadband systems. The only exception with regard to L_g is station KIV for which the propagation path from the East Kazakh test sites crosses the northern Caspian Sea, which has previously been recognized as blocking L_g propagation (cf. Piwinskii and Springer, 1978; Bennett et al., 1981). The L_g signal at KIV in the records of Figure 6 appears to be at the P-coda level and indistinct. In contrast, L_g signal levels at the two nearest IRIS stations (ARU and GAR) from East Kazakh explosions are particularly strong for even small magnitude events. Although this observation may not be immediately obvious from the broadband records in Figure 6, we will show later that even the five records from the smaller magnitude events at the bottom of the figure have signal-to-noise levels well above 1.0 over some frequency bands.

Spectral analyses were performed on waveform segments corresponding to P, L_g, and pre-P noise for each of the records in Figure 6. Examples of the spectra for two explosions at each station are shown in Figures 7 and 8. The analyses revealed that the energy in the L_g spectra is concentrated in a narrow frequency band which peaks at a frequency less than 1.0 Hz. The P-wave spectra at the various Soviet IRIS stations are generally much broader and remain above the noise level to higher frequencies. The noise spectra themselves show a null at a frequency near 1 Hz. This seems to be fairly consistent between all stations and events. The noise spectra reach a peak at a somewhat higher frequency before declining again above 5 Hz, as the antialiasing filter in the IRIS recording system takes effect. The spectral behavior of the P and L_g signals at the Soviet IRIS stations is in general consistent with what would be expected from an attenuation model; spectral decay with frequency above the peak values is more rapid at the more distant stations because of higher attenuation. As a result of this attenuation, the L_g signals in particular are dominated by low frequencies at the more-distant stations. It can be seen from the spectral plots in Figure 8 that the L_g signals at OBN and KIV have low signal-to-noise levels above about 2 Hz for even large explosions at the East Kazakh test sites. It is apparent from this observation that to resolve high-frequency characteristics of regional L_g signals from most Soviet underground nuclear explosions will require regional stations at ranges much closer than those of OBN and KIV (i.e. $R \ll 2900$ km). The regional P-wave spectra in Figure 8 indicate a somewhat broader band of useful frequencies. For the P-wave windows signal-to-noise levels are greater than 1.0 to
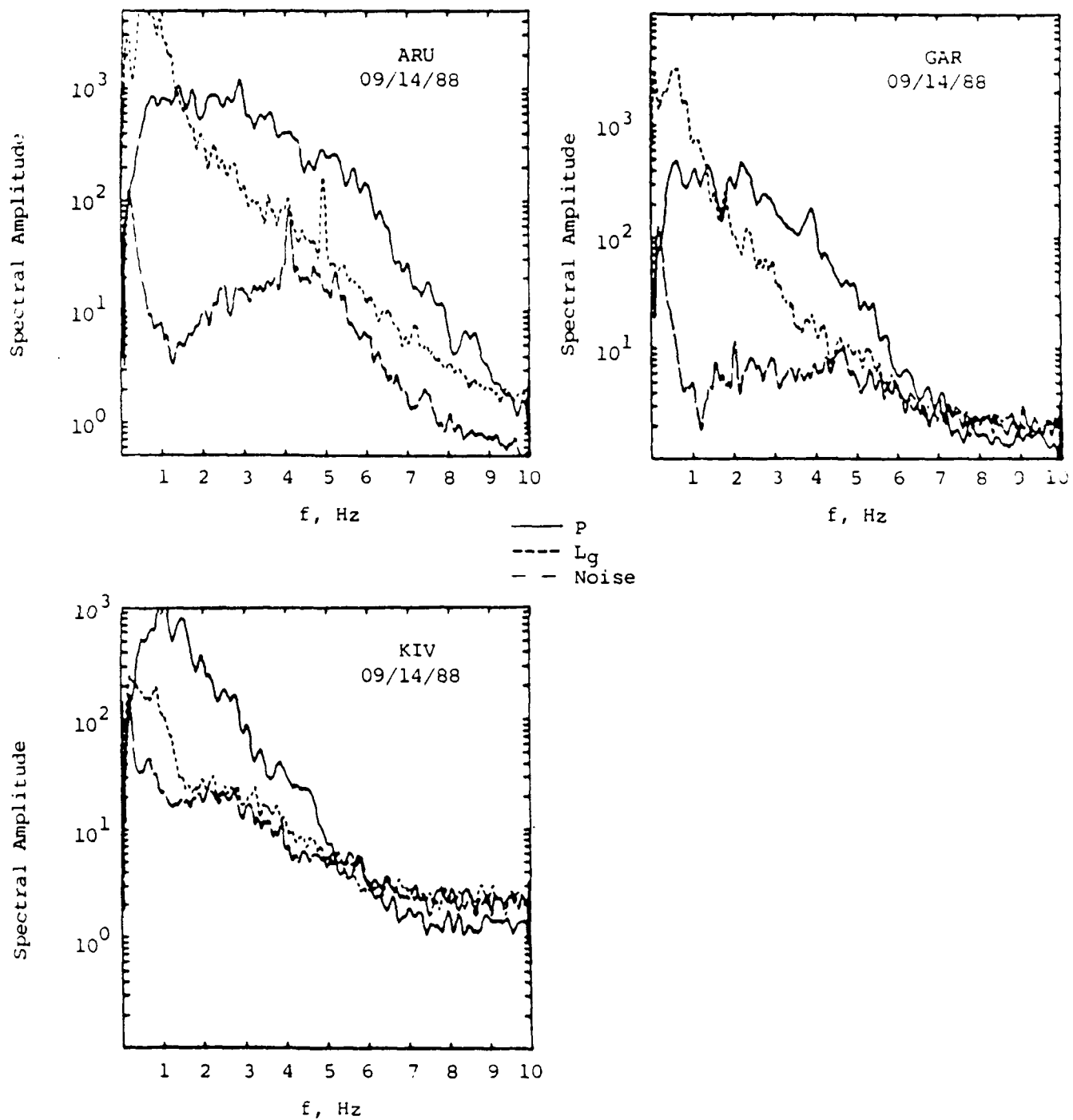
Figure 7. Regional P, L_g and noise spectra measured at Soviet IRIS stations from the SR explosion of 09/14/88 (JVE).

21
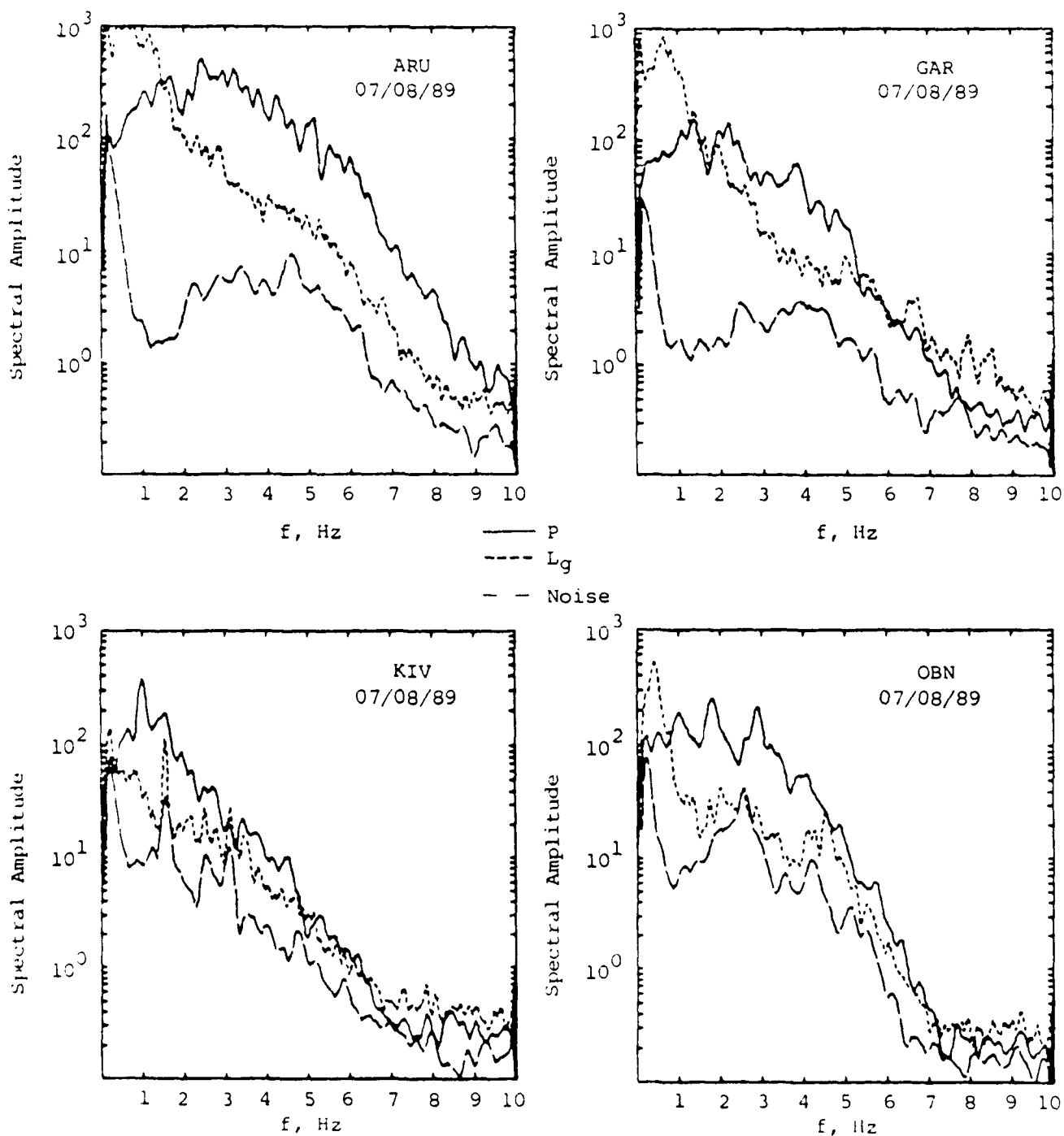
Figure 8. Regional P, L_g and noise spectra measured at Soviet IRIS stations from the SR explosion of 07/08/89.

frequencies of 5 Hz or more at the more distant stations and to 10 Hz at the two nearer stations.

One clear result of the spectral analyses of the regional signals from East Kazakh explosions measured at Soviet IRIS stations is that the signal-to-noise level is maximum at a frequency of about 1 Hz for both L_g and regional P. Although this frequency range may vary slightly from station to station and may be somewhat less for L_g (cf. Figure 8), the observation suggests that useful regional signals can be extracted from the background noise by bandpass filtering at a frequency of about 1 Hz. This is illustrated in Figure 9 where we have applied a narrow band-pass filter with corners at 0.8 and 1.6 Hz to the ground motion time histories recorded at station ARU for several underground nuclear tests at the East Kazakh test sites. The events shown ranged in magnitude from 6.1 m_b to 3.8 m_b. The raw, unfiltered traces are shown on the left and the filtered traces are on the right. It can be seen that, for the magnitude 6.1 and 5.9 explosions, the signal-to-noise level is good prior to application of the filter. For these events the filter reduces some of the longer- period energy arriving late in the L_g or at the beginning of the R_g windows. For the magnitude 5.3 m_b explosion, the signal is visible in the raw, broad-band record in spite of rather strong lower-frequency noise. The signal appearance is greatly enhanced by the filtering operation. The signal-to-noise improvement is even more dramatic for the three smaller-magnitude events. The raw traces for the magnitude 5.0 and 4.9 m_b explosions show little evidence of signal except for a few higher-frequency segments. When filtered these high-frequency segments are greatly enhanced and revealed to be clear regional P, S, and L_g signals. The smallest magnitude explosion for which Soviet IRIS data are available was estimated to have a magnitude of 3.8 m_b by Hansen et al. (1990). Though the magnitude of this event is somewhat questionable, since it was based on a single amplitude measurement, it seems unlikely from the relative amplitude of the L_g that this explosion had a magnitude much greater than 4 m_b. For this magnitude 3.8 event, the raw trace, on the left in Figure 9, shows very little evidence of signal. The filtered trace on the right, however, shows L_g signals with amplitudes more than three times the noise level. The regional P signal for this explosion, however, is not much bigger than the ambient noise even after filtering. We performed similar analyses on the records at GAR for the lower-magnitude explosions in Figure 7 and found that they also showed clear

23
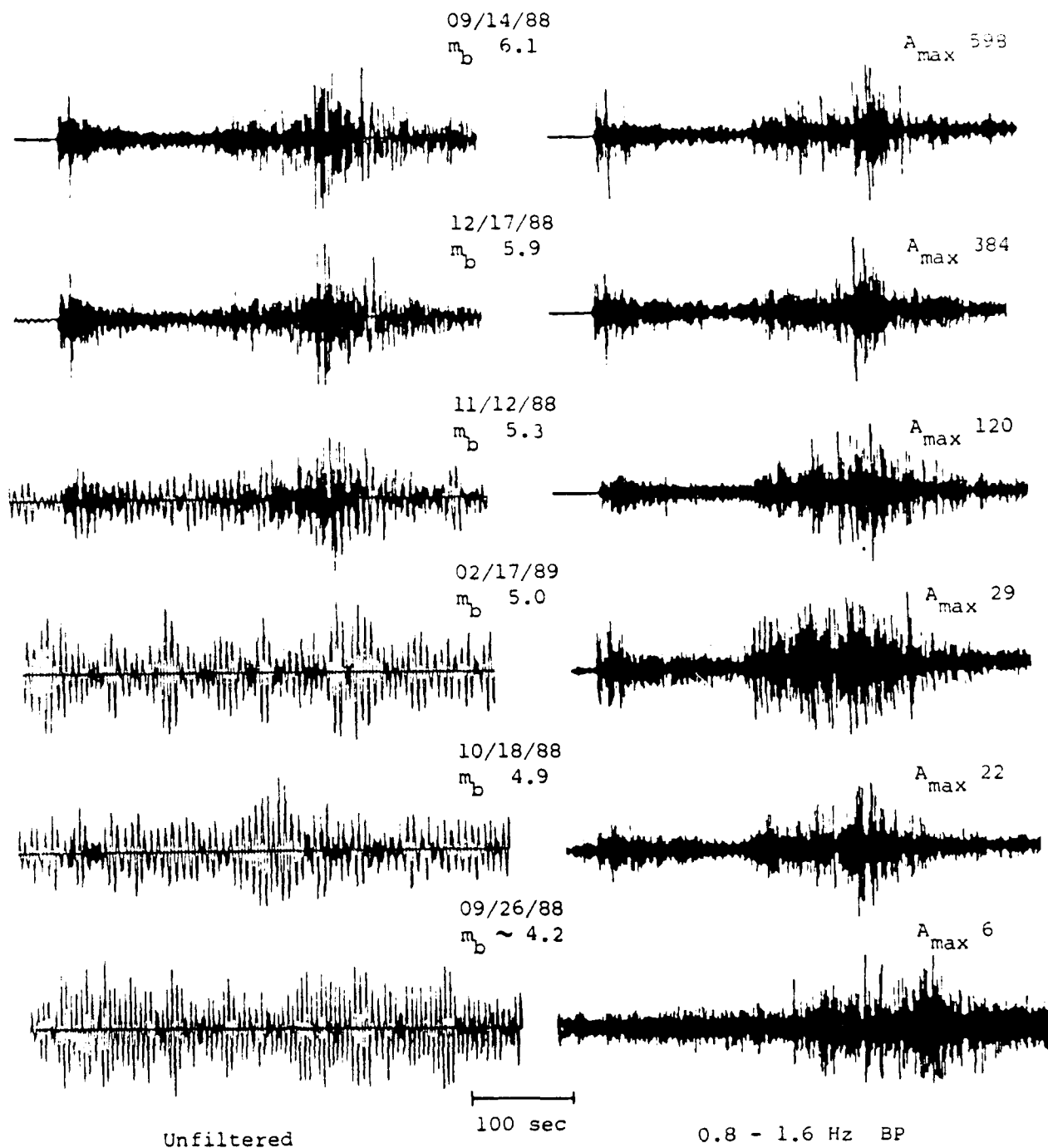
Figure 9. Application of bandpass filter to ARU records of SR/DM explosions to enhance signal relative to background noise.

24

regional signals when bandpass filtered at about 1 Hz.

During the first year of this contract, we have recovered only a small amount of earthquake data recorded at the Soviet IRIS stations. Soviet IRIS stations GAR and KIV are located in active seismic zones along the southern Soviet border region and have recorded numerous local events. However, in our discrimination efforts we have attempted to focus on earthquakes which are similar in magnitude or have comparable paths to the available explosions in the database. These restrictions severely limit the available data and may need to be relaxed to increase the database of regional signals from natural events recorded at the Soviet IRIS stations.

Two prominent sources of regional signals from larger earthquakes, with magnitudes comparable to Soviet underground nuclear explosions, during the relatively recent operating history of the IRIS stations have been the 12/07/88 earthquake in Armenia and its aftershocks and also several larger earthquakes in the Pamir-Hindu Kush region. We have recovered Soviet IRIS station data for some of these events. Initial indications are that the earthquakes produce strong L_g signals which frequently have larger amplitudes than the regional P phases on the 20 samples per second channels at the IRIS stations. In several cases the dominant frequencies of the L_g signals from these earthquakes appear to occur at lower frequencies than comparable explosions. This is particularly true for some of the larger-magnitude earthquakes. It should be noted, however, that the propagation paths for these events are also different than for the explosions. In future analyses we plan to take into account such propagation differences and make appropriate adjustments for attenuation effects which could alter the spectral content of the regional P and L_g signals. In these analyses we hope to incorporate a much larger sample of regional earthquakes recorded at all the available Soviet IRIS stations which will permit more complete investigation of path effects.

III. Analyses of Spectral Differences Between Explosions and Earthquakes Recorded at WMQ

3.1 Objectives of Discrimination Analyses

The primary goal of this research program is to develop reliable regional discrimination procedures which can be applied to identify seismic events in the Soviet Union. The focus of our studies to date under this contract has been empirical observations and analyses of the characteristics of regional phase signals from Soviet underground nuclear explosions and comparable earthquakes recorded at high-quality digital seismic stations in the regional distance range. Such data are likely to be extremely important to the identification of small events under a low-threshold testing limit. Over the years several time-domain and spectral measures of seismic signals have been proposed as potential regional discriminants (cf. Blandford, 1981; Pomeroy et al., 1982). However, these regional discrimination techniques have not been completely reliable; and, furthermore, capability to extend the techniques to aseismic regions of the Soviet Union (including the principal Soviet test sites in East Kazakh) has not been demonstrated. The latter situation is partly due to limitations on our theoretical understanding of regional phase generation (particularly for explosion sources) and a lack of high-quality seismic data at regional distances from events in the Soviet Union. It is only recently that such data have become available with the advent of the CDSN stations in China and the even more recent installation of the Soviet IRIS stations. In a previous report (cf. Bennett et al., 1989) we presented preliminary results describing general characteristics of the regional signals measured at a selected CDSN station, WMQ, from explosions at the East Kazakh test sites and nearby earthquakes. We also presented a band-pass filter analysis of those data which indicated diagnostic differences in the relative amplitudes of the L_g and regional P phases at certain frequencies from explosions and earthquakes recorded at WMQ. In the current study we have attempted to follow-up these observations with more thorough spectral analyses which were performed on a larger data sample.

3.2 Preliminary Observations of Spectral Behavior

CDSN station WMQ is the nearest station to the principal Soviet test sites at East Kazakh for which high-quality digital data are routinely available. As pointed out in the preceding section of this report, WMQ records strong regional P and L_g signals from Soviet underground nuclear tests at East Kazakh (R = 960 km) and also from earthquakes at epicentral distances which encompass the range to the East Kazakh test sites. The instrument response for the WMQ records used in our analyses were broadband, and we applied different narrow band-pass filters to derive S_{max}/P_{max} and L_g/P_{max} ratios as a function of frequency. Figure 10, taken from our previous report, shows S_{max}/P_{max} ratios measured from the raw broadband vertical-component records for a sample consisting of 12 East Kazakh explosions and 20 nearby earthquakes. The earthquakes were basically a subset of those shown above in Figure 3 and Table 3 with magnitudes between 4.5 and 5.9 m_b and ranges between 423 and 1176 km. The earthquakes were located mainly along the southern Soviet border, so that their paths to WMQ were somewhat different from those of the explosions. This raises some concern about the effects of dissimilar paths on the signal measurements. Nevertheless, the results indicated a fairly large separation by about a factor of four, on average, between explosions and earthquakes with the explosion ratio being much smaller. A few anomalous events at lower magnitudes had S_{max}/P_{max} ratios which were intermingled between earthquakes and explosions.

The bandpass filter analyses were performed to explore this observation more fully and possibly to increase the separation between the two source types. Figure 11 shows the results of the preliminary analyses which were applied to 10 East Kazakh explosions and 13 earthquakes. The L_g/P_{max} ratios determined from the filtered data for explosions and earthquakes are observed to be intermingled at filter center frequencies of 1 Hz and lower but separated in all cases above 3 Hz. The average L_g/P_{max} ratio was found to be only about 30 percent larger for earthquakes than for explosions in the low-frequency passband. However, the explosion ratio fell off much faster toward higher frequencies and, as a result, was about a factor of ten smaller than the average earthquake ratio at high frequencies. We concluded that care needed to be exercised in dealing with regional discriminants which rely on signal differences
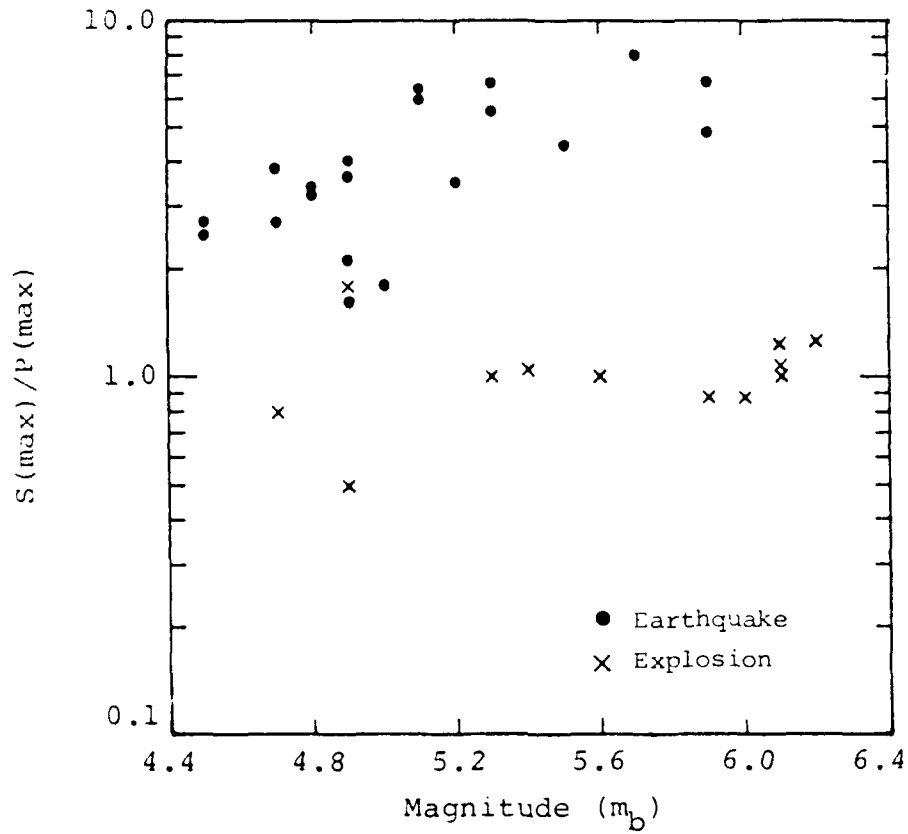
27

Figure 10. S_{max}/P_{max} ratios for regional earthquakes and SR/DM explosions measured from broadband, vertical-component records at WMQ.

28
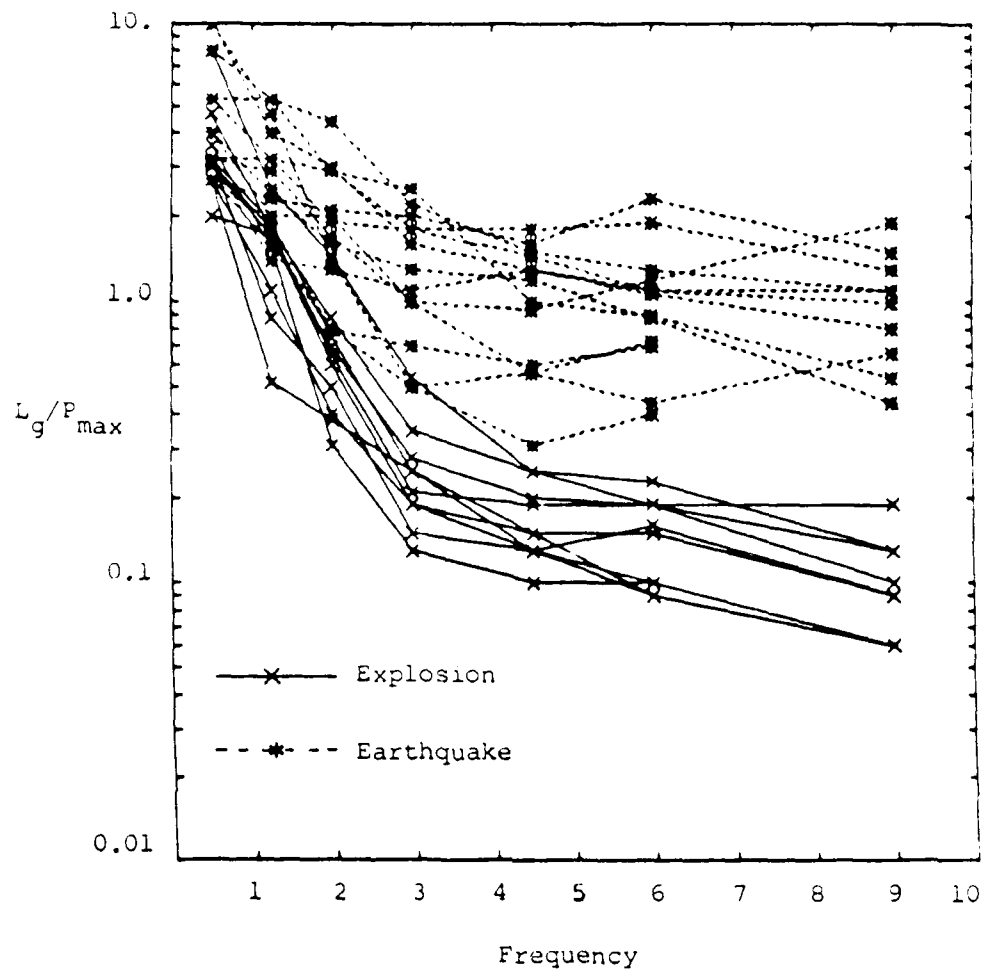
Figure 11. S_{max}/P_{max} ratios determined from bandpass filter analyses of WMQ records for 10 SR/DM explosions and 13 regional earthquakes.

29

in limited frequency bands. Some recording systems may have responses which are too narrow to resolve the differences. For example, a system with a relatively narrow response peaked near 1 Hz, such as WWSSN, might not see the differences in the L_g/P_{max} ratios which were found. This might be an explanation why L_g/P_{max} ratio observations have not always provided reliable discrimination of explosions and earthquakes.

3.3 Further Spectral Analysis of WMQ Data

In the current study we performed an alternate spectral analysis on the regional P and L_g signals from a larger sample of East Kazakh explosions and earthquakes recorded at WMQ. Instead of narrow band-pass filtering, discrete Fourier transforms were computed for the regional P and L_g signals; and spectral ratios were derived from those. For these analyses we used the vertical-component signals which were described in Section II. As can be seen in Figure 2 above, the regional P signals from East Kazakh explosions recorded at WMQ are quite complex with apparent multiple phases of approximately equivalent amplitudes on the broadband recordings. The earthquake P phases, although normally smaller and more variable, were also seen to be complex in most distance intervals apparently indicating multiple P paths in the crust and upper mantle.

From the WMQ data identified in Tables 2 and 3 above a sample of 19 East Kazakh explosions and 27 regional earthquakes were analyzed. The earthquakes were chosen to provide a distance range which encompassed the distances from WMQ to the East Kazakh test sites, but several different azimuths are represented in the data sample. It was anticipated that, by allowing these kinds of variations in propagation path, bias associated with particular paths could be avoided or at least diminished. We also performed some preliminary tests on the P-wave window length in an attempt to establish a stable measurement scheme. Pre-P noise spectra were also calculated for each record to verify the frequency range over which the individual phase spectra and the corresponding ratios could be considered valid.

The initial P-wave arrivals were timed using a phase picker based on the Stewart-Allen algorithm (cf. Allen, 1982). The automatic picks were then

30

verified by the analyst. The data were of sufficiently high quality that the automatic picker failed to find the correct P-wave arrival time for only one earthquake. Time marks were placed on the records corresponding to the P-arrival times and to the group velocity interval between 3.5 and 2.9 km/sec, which includes most of the L_g energy for these events. The pre-P noise time segment was defined as being from 1 second before the initial P arrival to 30 seconds before that time. In cases where the P arrival occurred less than 30 seconds after the record start, the noise window was taken from the beginning of the record.

In order to avoid spurious high-frequencies, each window was tapered using a Hanning window applied over 5 percent of each end of the time segment. The discrete Fourier transforms were then calculated for each window producing amplitude and phase spectra. The spectra were not always consistent in length or frequency spacing because of the varying sizes of the time windows, so they were all resampled to 120 evenly spaced frequencies using the interpolation method of Wiggins (1976). The spectra were then convolved with a boxcar function 10 points wide to provide some smoothing. All spectral ratios were calculated using these resampled, smoothed spectra.

3.4 Comparison of P-Wave Windows

As pointed out above, the regional P-wave signals recorded on the broadband records at WMQ from East Kazakh explosions and regional earthquakes are frequently complex. The vertical-component records in Figure 2 above for East Kazakh explosions show two or three distinct regional P phases rising above the general P coda level. To test the sensitivity of the spectral measurements to the P-wave window, we analyzed the P-wave signals for two different windows, both starting 1 second prior to the detected P arrival. The short P-wave window extended to 10 seconds after the P arrival and the long window to 25 seconds after the P arrival. The short window included mainly the energy in the first distinct P phase seen in the explosion records of Figure 2 above. The long P window appears to include most of the P-wave energy seen on these records.

31

Figures 12 and 13 show the analyses performed on the P-wave signals for two East Kazakh explosions: one at SR (viz 03/12/87) and one at DM (viz 05/06/87). The expanded playouts of the P phases at the tops of each figure illustrate the complexity of the regional signals. Several arrivals are apparent in the first 25 seconds of the signals. One interesting feature in comparing Figures 12 and 13 is that the initial P for the DM event appears to have a somewhat lower predominant frequency, even though the events have similar body-wave magnitudes (viz 5.5 for the 03/12/87 explosion and 5.6 for the 05/06/87 explosion). We will address differences in the regional signals between SR and DM events more completely in a subsequent section of this report.

The plots in the lower left corners of Figures 12 and 13 show the spectra computed for these events. Spectra are shown for both the short and long regional P windows, the L_g windows and the noise. In addition, the lower solid line shows the ratio of the spectra for the short P-wave window to the long window. First, it can be noted that the signal spectra generally lie well above noise over the entire band of frequencies plotted here. It should be pointed out that the instrument response has not been removed from the spectra presented in this section. Focusing on the P-wave spectra, the short- and long-window spectra are seen to match quite closely at high frequencies; but the short-window spectra fall below the long-window spectra at frequencies less than about 3 Hz. Thus, the general tendency is for the long-window spectra to have higher values than the spectra for the shorter P-wave windows. For the 05/06/87 DM event the difference between the short- and long-window P-wave spectra is seen as a steady decline in the short-window to long-window ratio. For the 03/12/87 SR event, the short-window P spectrum is most severely depleted relative to the long-window P spectrum at specific frequencies (viz between 1.0 and 2.0 Hz).

The lower right-hand plots in the figures show the effects on the L_g/P spectral ratios. As would be expected from individual spectral observations, the L_g/P ratios for the short P-wave windows fall below those obtained for the longer P-wave windows over most of the frequency band from 1.0 to 8.0 Hz. This tendency appears to be the same for events at both the SR and DM test sites.
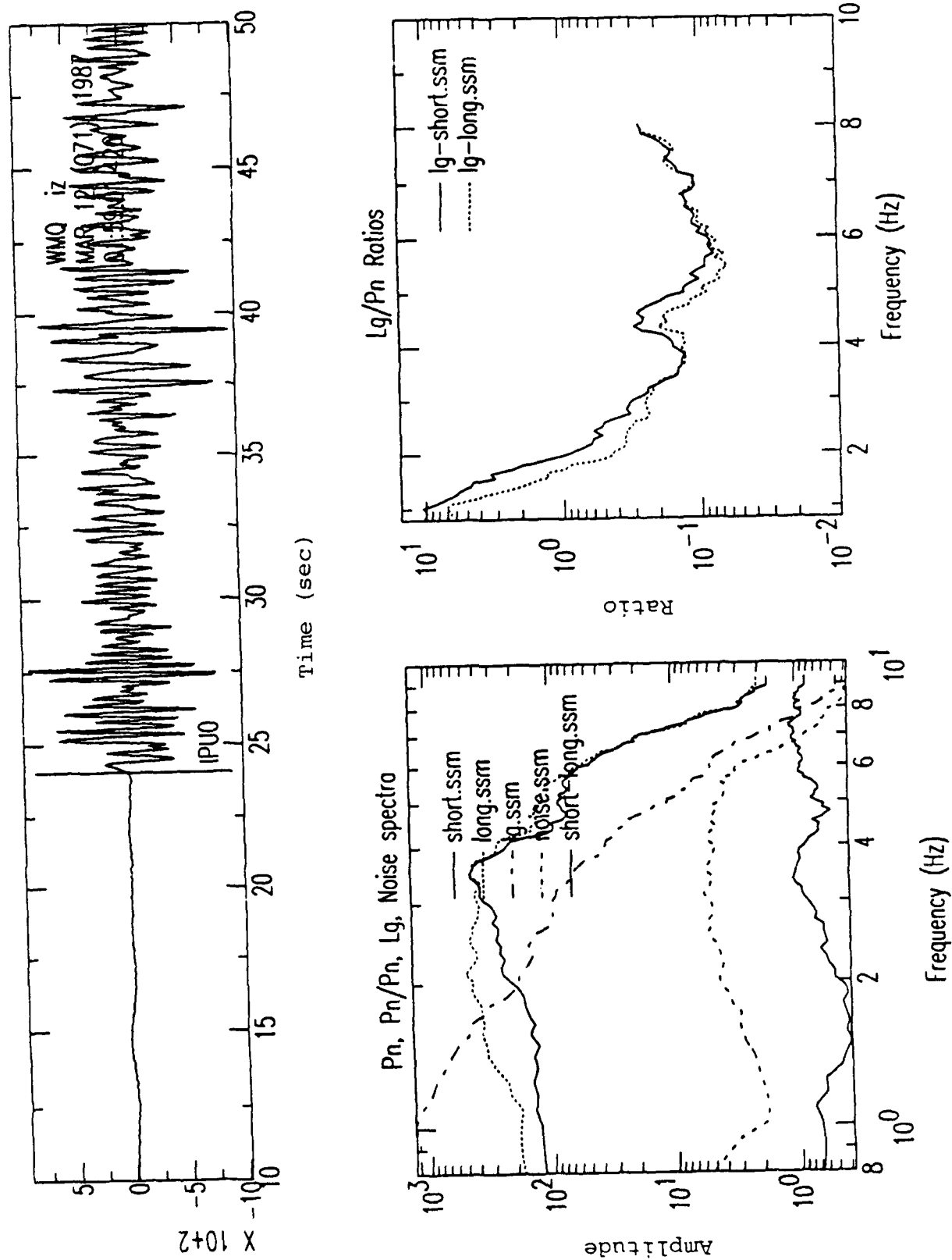
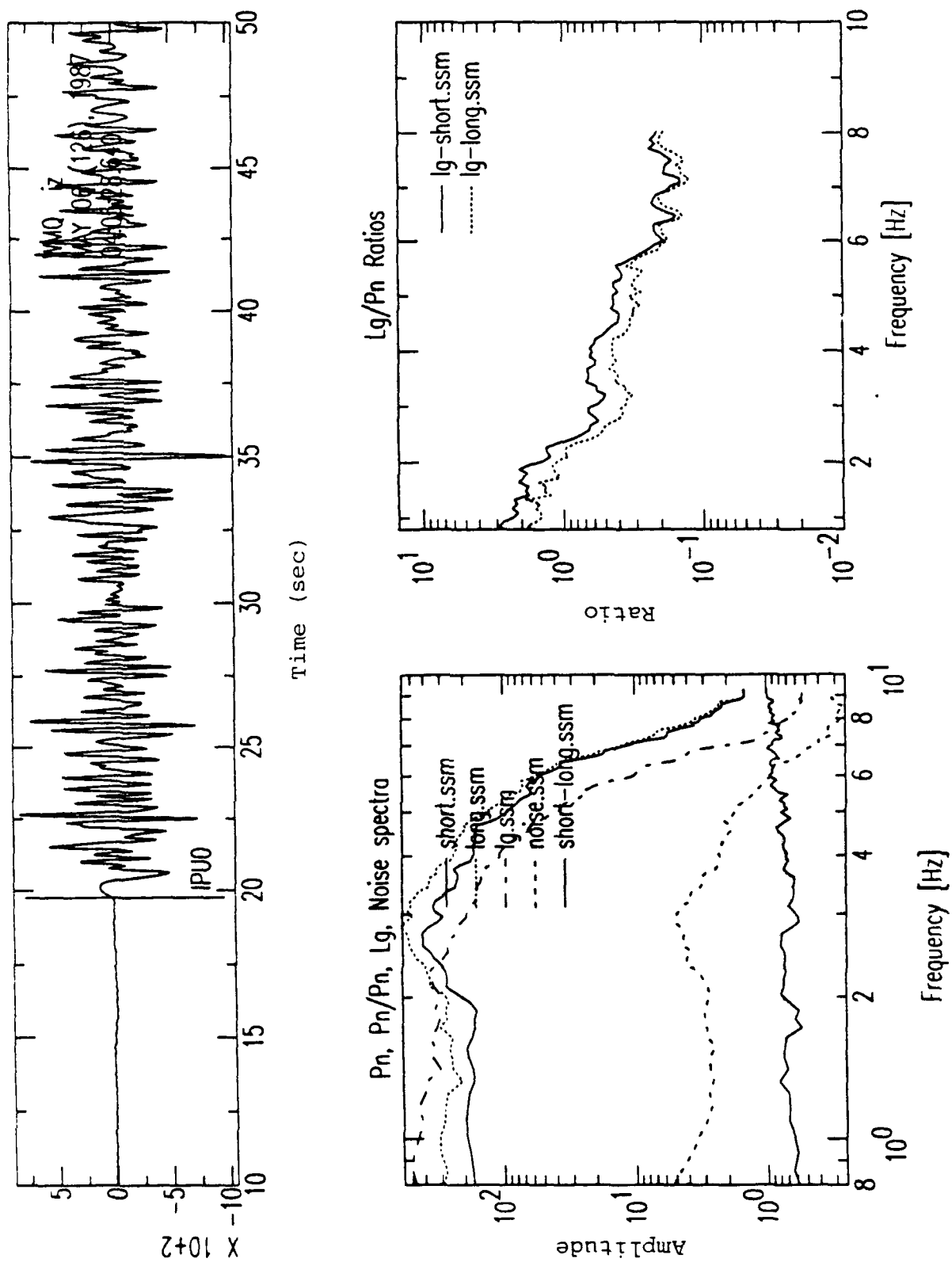Figure 12. Spectral analysis of the WMQ record from the 03/12/87 SR explosion.

Figure 13. Spectral analysis of the WMQ record from the 05/06/87 DM explosion.

In the subsequent analyses we have used only the longer (viz 25 seconds) P-wave windows. The main effect on the L_g/P ratios presented below of using the long versus the short window is expected to be an overall decrease in the ratio. Although we would not expect this effect to change too drastically from event to event, there is some evidence from the studies just described that some differences with frequency could occur between events at different sites. This problem will require further study.

3.5 L_g/P Spectral Ratios

L_g/P spectral ratios were computed for the 19 East Kazakh explosions and 27 regional earthquakes in the WMQ sample. Figures 14 through 18 show the results of the processing performed on three SR explosions and two regional earthquakes. Comparing the spectra for the explosions, the shapes appear remarkably consistent over the magnitude range from 5.0 m_b to 6.1 m_b covered by these events. In all cases the regional P spectra show a relatively flat portion extending from 0.8 Hz to more than 3 Hz. Above 3 Hz the spectra show a steady, rapid decline. The L_g spectra for the same explosions show a less rapid but steady decline over the entire frequency range plotted, with amplitudes falling below the regional P spectral level between 1.0 Hz and about 2.0 Hz. The regional P and L_g spectra for the two earthquakes also have roughly similar shapes (cf. Figures 17 and 18) even though the two events are at somewhat different ranges. The regional P spectra again show a nearly flat portion from 0.8 Hz to about 3.0 Hz followed by a rapid decline toward higher frequencies. The L_g spectra show a steady decline starting at low frequencies and extending to 4 Hz or so before decreasing much more rapidly at higher frequencies. In contrast to the explosions, the L_g spectra for the earthquakes do not reach the P-wave spectral level until a frequency of 5 Hz or more.

Perhaps more interestingly, comparing the earthquake and explosion of equivalent magnitude (viz the 12/14/86 and the 06/14/88 events), the regional P-wave spectra for the two events match very closely even though the ranges are again quite different. In contrast, the L_g spectrum for the earthquake has much more high-frequency energy. It needs to be emphasized, however, that it is unclear to what extent attenuation differences because of the different ranges and paths may affect this observation. Next, comparing the spectra for

35

Figure 14. Spectral analysis of the WMQ record from the 09/14/88 (JVE) SR explosion.

36

Figure 15. Spectral analysis of the WMQ record from the 03/12/87 SR explosion.
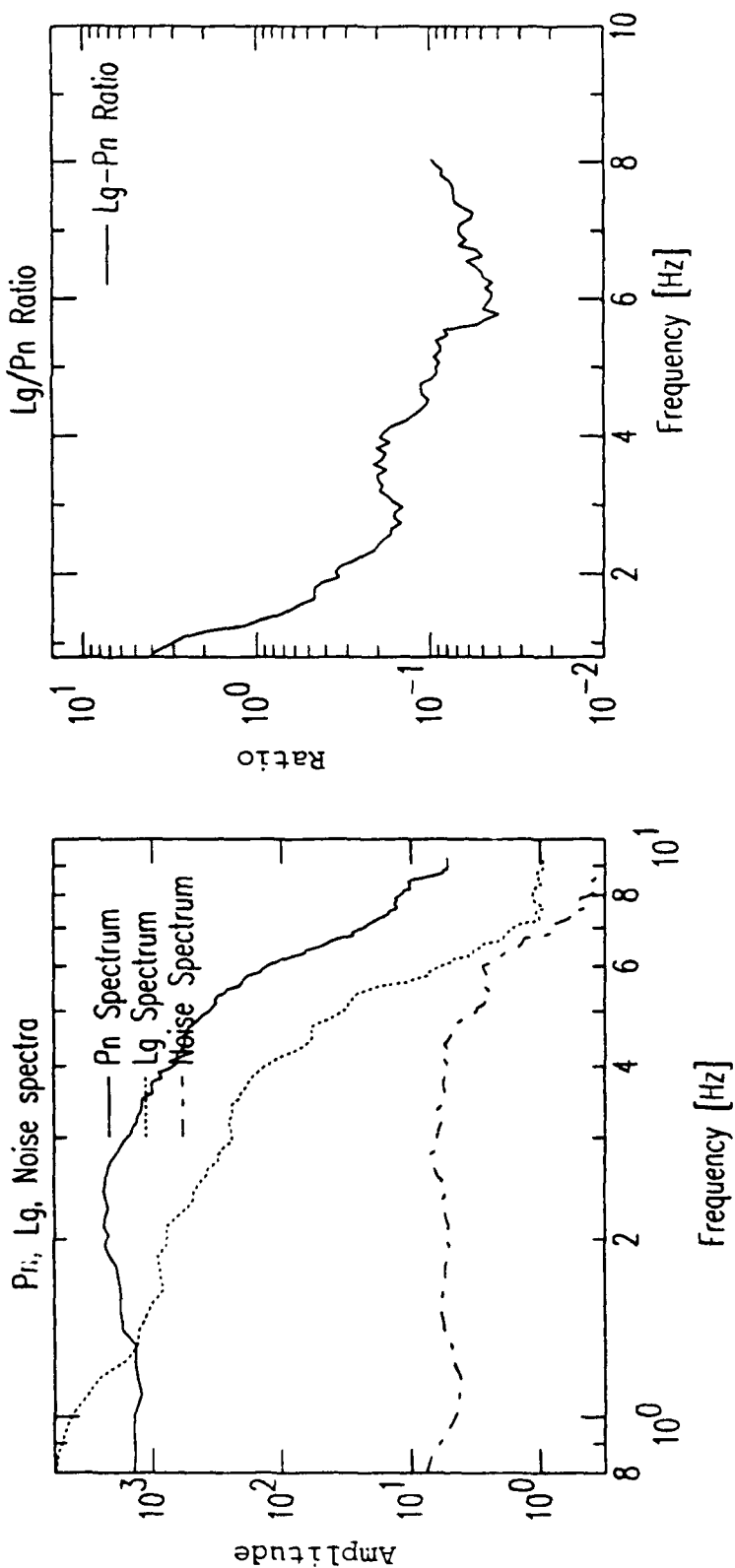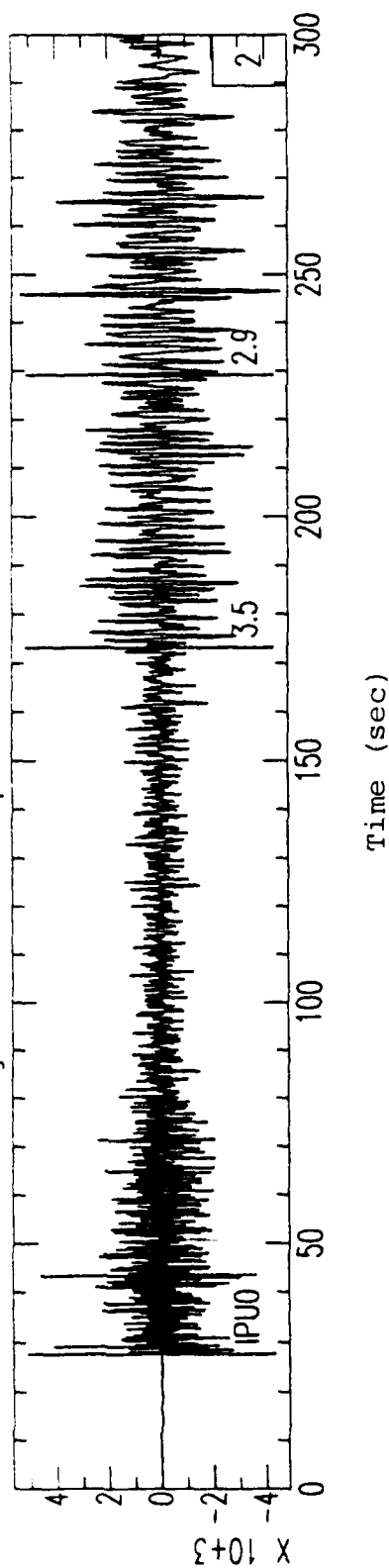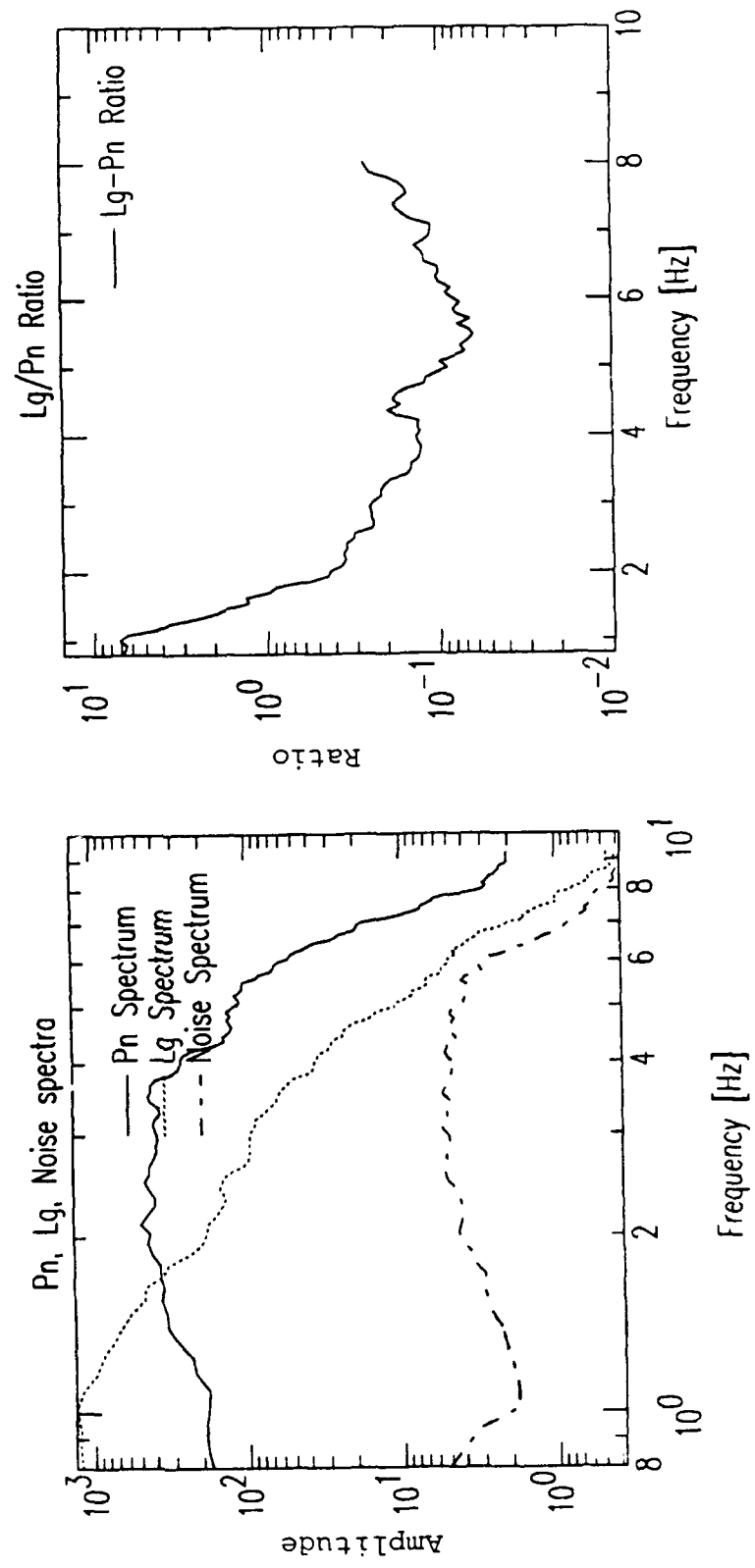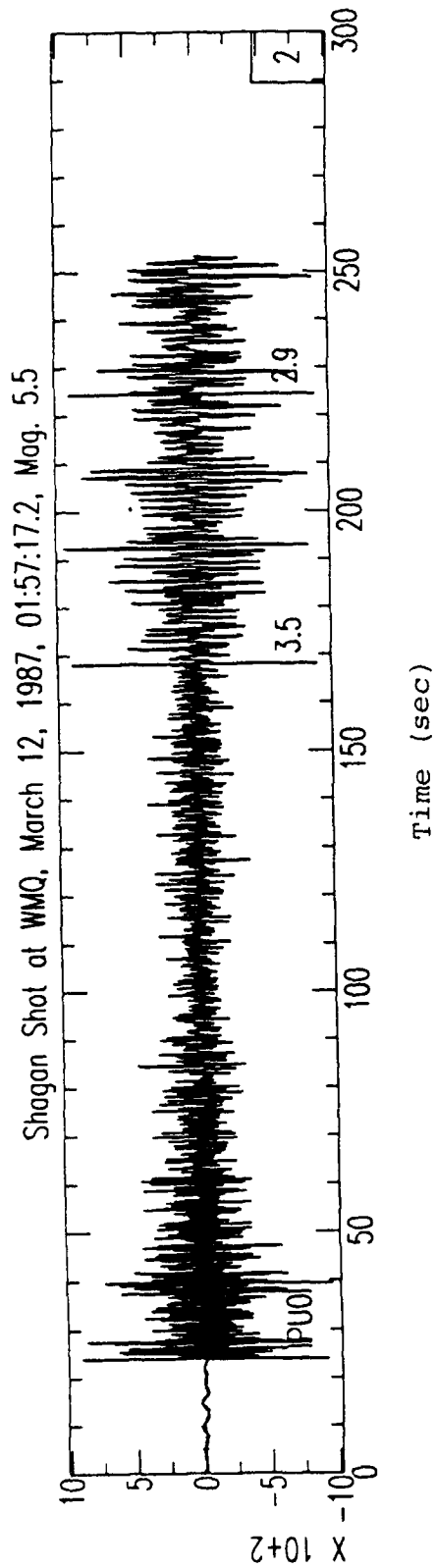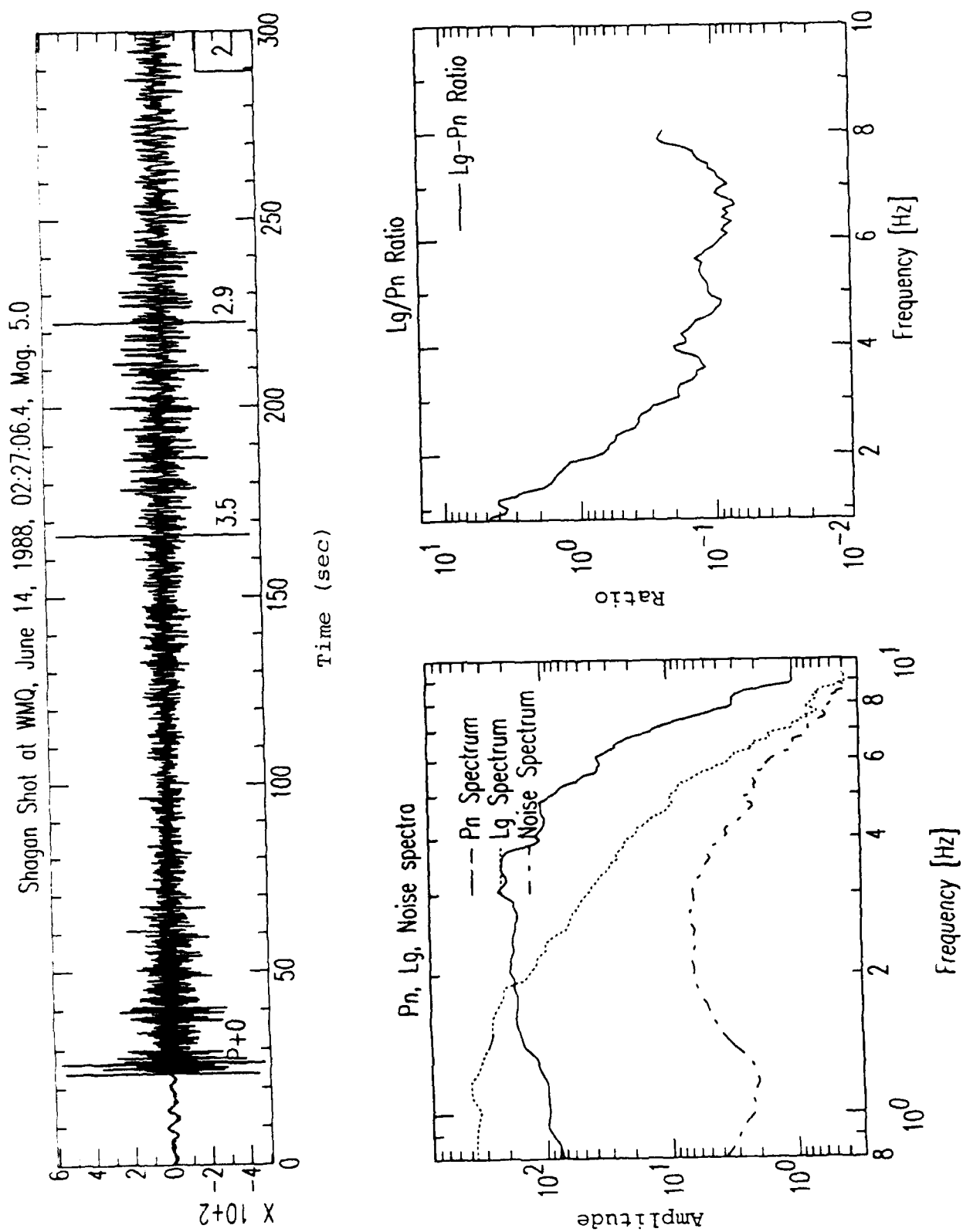
Figure 16. Spectral analysis of the WMQ record from the 06/14/88 SR explosion.
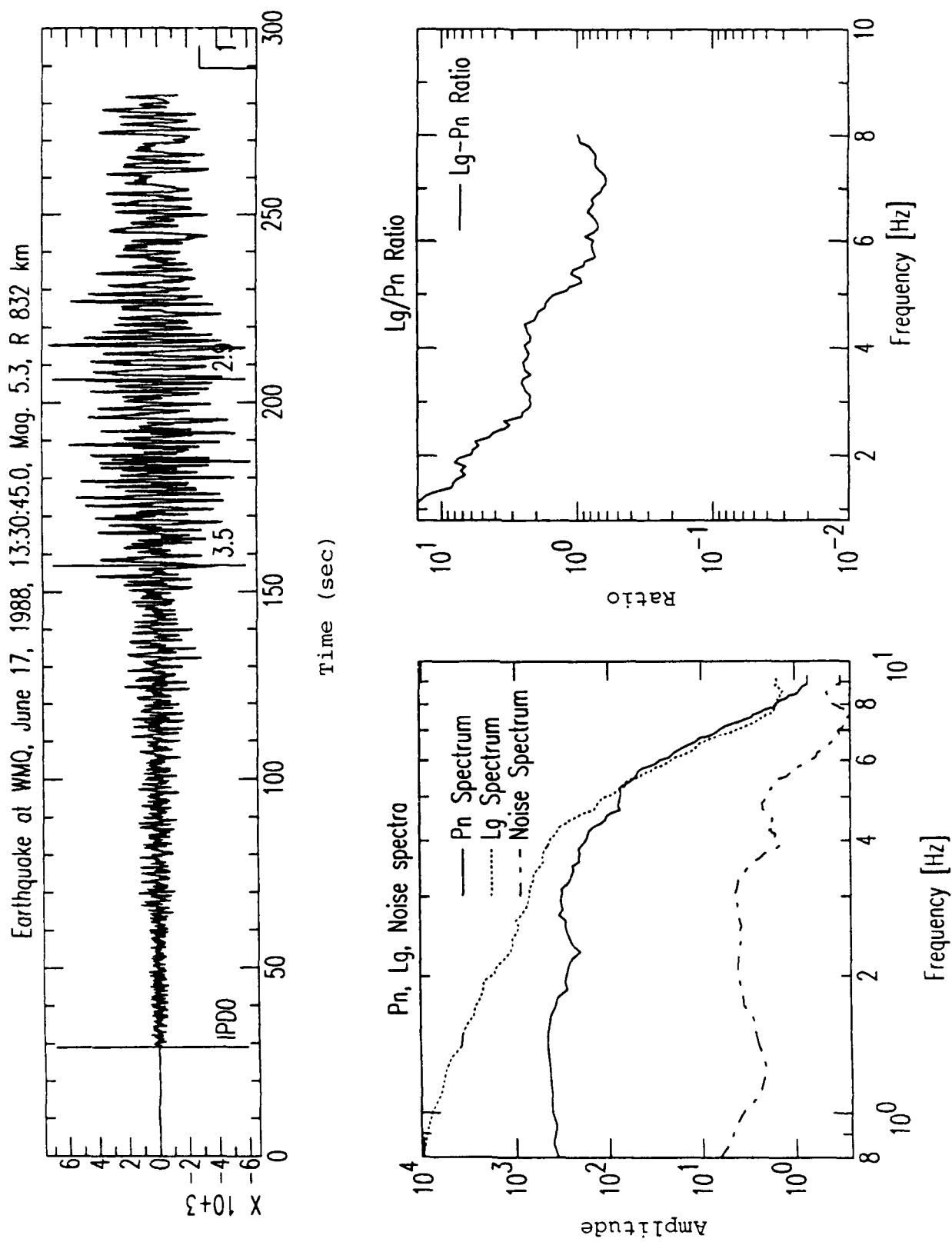
Figure 17. Spectral analysis of the WMQ record from the 06/17/88 regional earthquake.
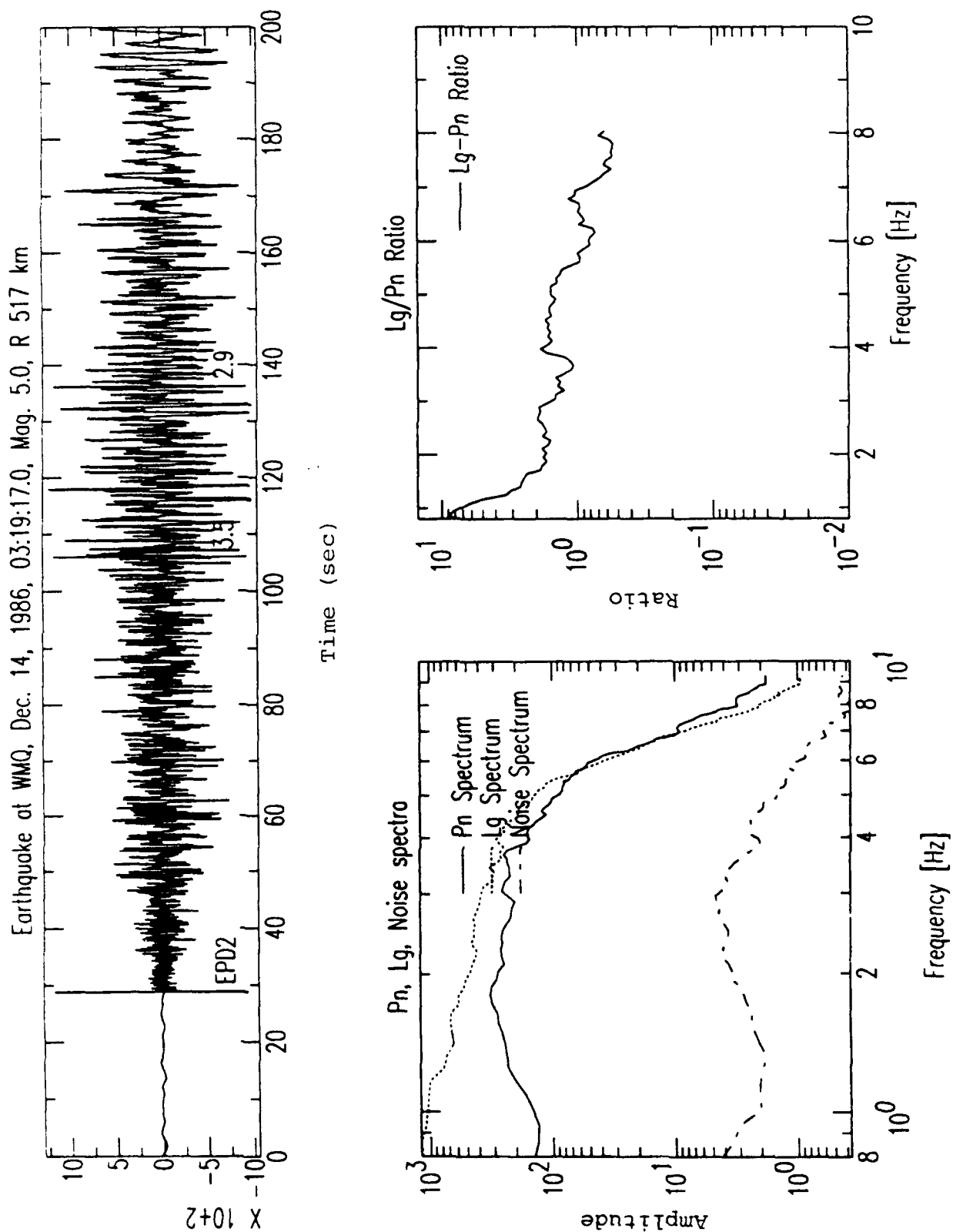
Figure 18. Spectral analysis of the WMQ record from the 12/14/86 regional earthquake.

the 5.3 m_b earthquake (06/17/88) and the 5.5 m_b explosion (03/12/87), the regional P-wave spectra are again seen to match quite closely between the two events. However, the earthquake L_g spectrum is roughly a factor of ten or so larger than the corresponding L_g spectrum from the explosion. The biggest difference between the L_g spectra for these two latter events appears to occur at a frequency of about 4 Hz. In general, then, the L_g spectra for the regional earthquakes appear to be richer in high frequencies than those from the SR explosions with comparable regional P spectra recorded at WMQ.

This result is also apparent in the L_g/P spectral ratios computed for these events and plotted in the lower right portion of the figures. The explosion spectral ratios are observed to drop off precipitously from very high values at frequencies near 1 Hz to values about a factor of 40 lower above about 3 Hz. The earthquake L_g/P spectral ratios, on the other hand, start out at values near ten or so which are only slightly larger than the explosion ratios. However, the earthquake ratios decrease by only about a factor of ten within the frequency range shown. Thus, these results indicate that L_g/P spectral ratios for the earthquakes are relatively enriched at high frequencies compared to the explosions recorded at WMQ.

The L_g/P spectral ratios from the 11 SR explosions were averaged and the standard deviation computed assuming a log-normal distribution. Similar averaging was performed on the 8 DM explosions and the 27 regional earthquakes. Figure 19 presents the L_g/P spectral ratio averages for the SR explosions and the earthquakes. Differences between the SR and DM explosion ratios will be described in the following section of this report. As was observed for the individual ratios presented above, the average L_g/P ratios for earthquakes and explosions appear to be indistinguishable at frequencies near 1 Hz. However, the average explosion spectral ratio is seen to drop off by nearly two orders of magnitude toward higher frequencies ($\approx$ 6-7 Hz). Over the same interval the average L_g/P ratio for the earthquakes decreases by only about one-half order of magnitude. As a result, the L_g/P ratios are well separated at high frequencies. From the plots of the mean plus and minus one standard deviation in Figure 19, we see complete separation of the earthquake and explosion L_g/P spectral ratios above about 2 Hz. At higher frequencies the ratios are separated even further.

41
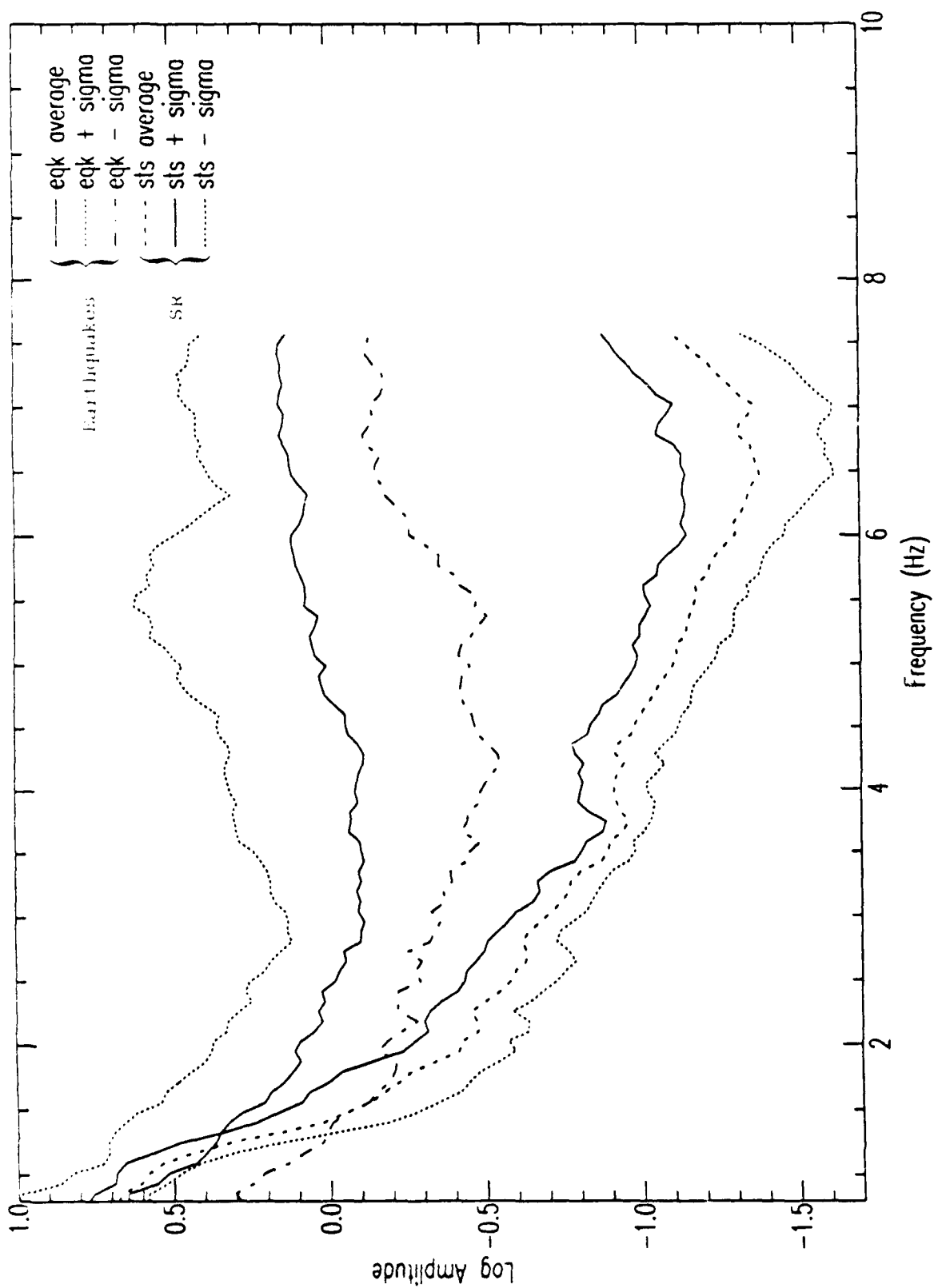
Figure 19.   Average Lg/P spectra ratios and their ± 1σ bounds for 11 SR explosions and 27 regional earthquakes measured at WMO.

42

These observations support our findings, from the band-pass measurements, that L_g/P spectral ratios for earthquakes are larger at high frequencies than for similar explosions recorded at WMQ. These lates. analyses confirm the same results for larger samples of both explosions and earthquakes. It should also be noted that these observations appear to be consistent with our previous findings (cf. Murphy and Bennett, 1982; Bennett and Murphy, 1986) for nearby explosions and earthquakes in the western U.S. In particular, it was found there that the earthquake L_g signals were relatively enriched at high frequencies while the regional P spectra from the earthquakes and explosions appeared to have quite similar shapes. In the following section of this report, we show results that indicate that differences in the L_g/P ratios between SR and DM explosions are inadequate to diminish the apparent discrimination capability of this measurement. The one outstanding problem appears to be the effects of regional path differences on the explosion and earthquake signals propagating to WMQ. Since we cannot identify co-located earthquakes and explosions in the areas of interest, the best approach to handling these factors appears to be by compensating for attenuation differences. To achieve this objective a better understanding of attenuation effects on regional P and L_g signals for regions of interest in and around the Soviet Union will be required. Results of some initial investigations toward this objective are presented in Section V of this report. In future work we will be performing similar analyses on regional signals recorded at other high quality digital stations, including the Soviet IRIS stations, and trying to develop a better theoretical understanding of the L_g/P spectral ratio behavior.

IV. Comparison of Shagan River and Degelen Mountain Explosions Recorded at WMQ

4.1 SR and DM Bias Differences

Application of regional phase signal measurements to discrimination and yield estimation has been hampered over the years by the lack of theoretical understanding of the excitation of these signals by explosion and earthquake sources. Of particular interest in this regard is whether different test sites produce different regional phase signals from otherwise comparable events. In proposing that L_g magnitudes could be used to estimate the yields of underground nuclear explosions, Nuttli (1986a,b) argued that explosions with equivalent energy release (i.e. yield) should produce L_g signals with equal amplitudes near the source. Thus, the L_g magnitude should provide a measure of explosion yield independent of the test site where the event occurred. Nuttli based this conclusion on a small number of explosions with announced yields in hard rock at a few different test sites.

Nuttli further suggested that observations of the differences between L_g magnitude and teleseismic m_b from different test sites could be related to attenuation of the teleseismic P waves in the upper mantle under the test sites. Thus, the difference between L_g magnitude and m_b should measure the teleseismic m_b bias of the test site. Nuttli (1986a,b) determined the test site biases for NTS and SR to be -0.31 and 0.036, respectively. Furthermore, Nuttli (1987) estimated the bias for DM to be 0.27. The large difference in biases between SR and DM was surprising considering that the two test sites are separated by only about 50 km. Based on this result Nuttli (1987) concluded that either P-wave amplitudes from DM explosions are 1.9 times larger than SR explosions or L_g amplitudes are 1.9 times smaller for DM explosions. To obtain additional insight into this problem, we have analyzed the behavior of the regional P and L_g signals recorded at WMQ from SR and DM events.

44

4.2 Regional Waveform Comparisons

As noted above in Section II, our database of explosions recorded at WMQ includes 18 SR explosions and 9 DM explosions. We presented the vertical component records at WMQ for all of these events above in Figure 2. Figure 20 shows three examples from each test site on a somewhat expanded scale for comparison. The selected events from each test site have roughly comparable magnitudes between 4.8 and 5.9 m_b. The records in Figure 20 appear to show nearly the opposite behavior to that observed by Nuttli. In particular, the regional P phases from the DM explosions are in all cases smaller than the L_g, whereas the regional P phases from the SR explosions are larger than the L_g. One of the main differences appears to be the large, relatively high-frequency, initial P phase for the SR explosions which is not apparent for the DM explosions. One explanation, consistent with Nuttli's observations, might be that for SR explosions some of the high-frequency energy normally contributing to teleseismic P is being trapped in the regional P waveguide; but several other possible explanations also need to be evaluated.

Figure 21 shows comparisons of the regional P and L_g signal levels at the two East Kazakh test sites for all 18 SR explosions and the 9 DM explosions as measured at WMQ. The plot presents the logarithms of the maximum P amplitudes measured from the broadband records versus the logarithms of the maximum L_g amplitudes also measured from the broadband records. The data show considerable scatter and some intermingling but are separated on average. Regression lines were fit to each data set. These are described by

$$\log P(max) = 0.744 \log L_g(max) + 0.909$$

for SR and

$$\log P(max) = 0.899 \log L_g(max) + 0.147$$

for DM. Within the range of overlap of the L_g amplitude measurements, the maximum regional P-wave amplitudes are separated by from 0.2 to 0.4

45

Snagan River Explosions

06/14/88 m_b 5.0

09/02/89 m_b 5.4

08/02/87 m_b 5.9

|———— 100 sec ————|

Degelen Mountain Explosions

04/22/88 m_b 4.8

11/23/88 m_b 5.3

07/17/87 m_b 5.8
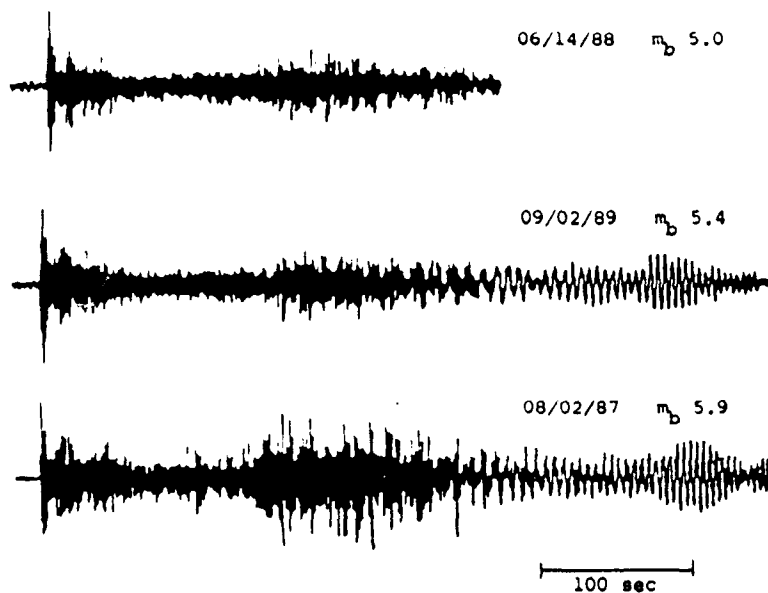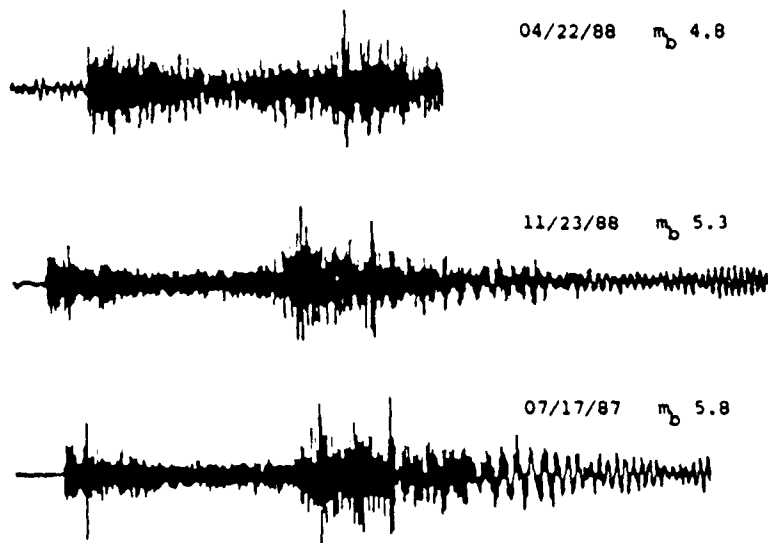
WMQ   R ≈ 960 km

Figure 20. Examples of WMQ records from similar magnitude
            nuclear tests at SR and DM.
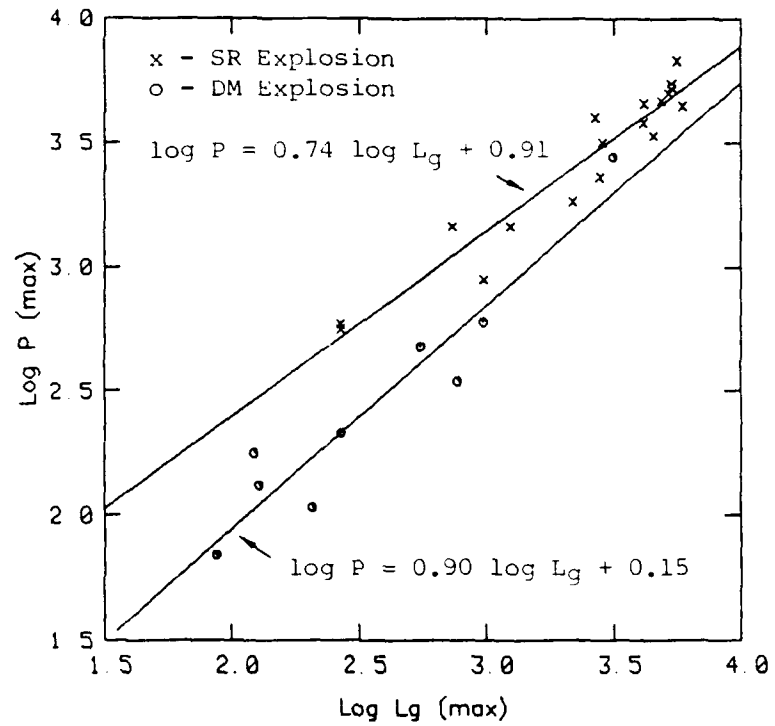
Figure 21. Regional P versus L_g maximum amplitude levels for SR and DM explosions recorded at WMQ.

47

magnitude units on average between the two test sites. As with the examples shown above, the regional P phases from the SR explosions for the total sample appear to be on average a factor of about two larger in amplitude than regional P phases from DM explosions which have comparable L_g amplitudes at WMQ. It should be noted that the standard deviations of the measurements relative to these regressions are large. It is also interesting that the regression lines tend to converge at larger amplitudes (i.e. larger magnitude), but this is to a large measure controlled by the single larger amplitude observation at DM which is intermingled with the SR data points.

4.3   Spectral Comparisons

We computed spectra for the initial P and L_g windows at WMQ from comparable magnitude SR and DM explosions, whose time histories were presented above in Figure 20. These are shown in Figure 22. In computing these spectra we used a short window (viz 12.8 seconds) including the initial P and a long window (viz 102.4 seconds) which encompassed nearly all the L_g energy. The time histories were tapered and the spectra smoothed using a running average. The instrument response for the WMQ broadband instrument was also removed prior to plotting the spectra in Figure 22. Aside from some minor fluctuations at certain frequencies, the L_g spectra appear to be quite consistent between the comparable SR and DM explosions. Although the L_g spectra for the DM explosions in both cases fall slightly below those for the SR explosions at a frequency near 1 Hz, this difference might be explained by the slightly lower magnitudes of the DM events. The differences in the regional P-wave spectra between the SR and DM events cover a broader range of frequencies and are generally larger. The latter differences probably cannot be explained by the small magnitude differences between the compared events. The observations suggest that the regional P waves from the SR explosions are enhanced over a broad range of frequencies relative to DM explosions with comparable L_g signals.

Spectral analyses were also performed on a larger sample of 11 SR and 8 DM explosions using the same procedures as those described in Section III for determining L_g/P spectral ratios. Figures 23 through 26 show the results of these analyses performed on two SR and two DM underground nuclear
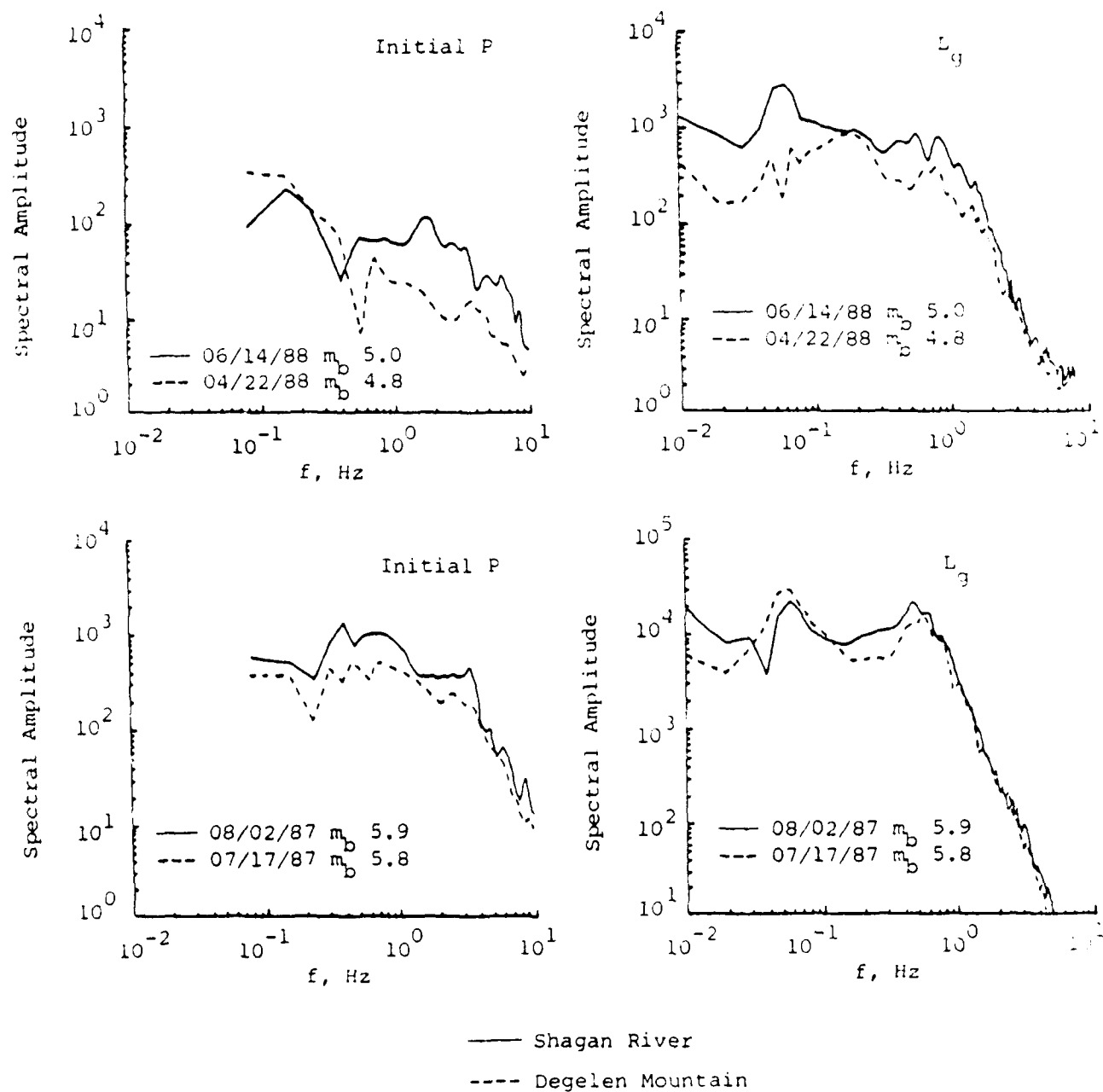
Figure 22. Spectral comparisons for initial P and Lg phases from
similar magnitude explosions at SR and DM recorded at
WMQ. Note that instrument response has been removed
from spectral shape.
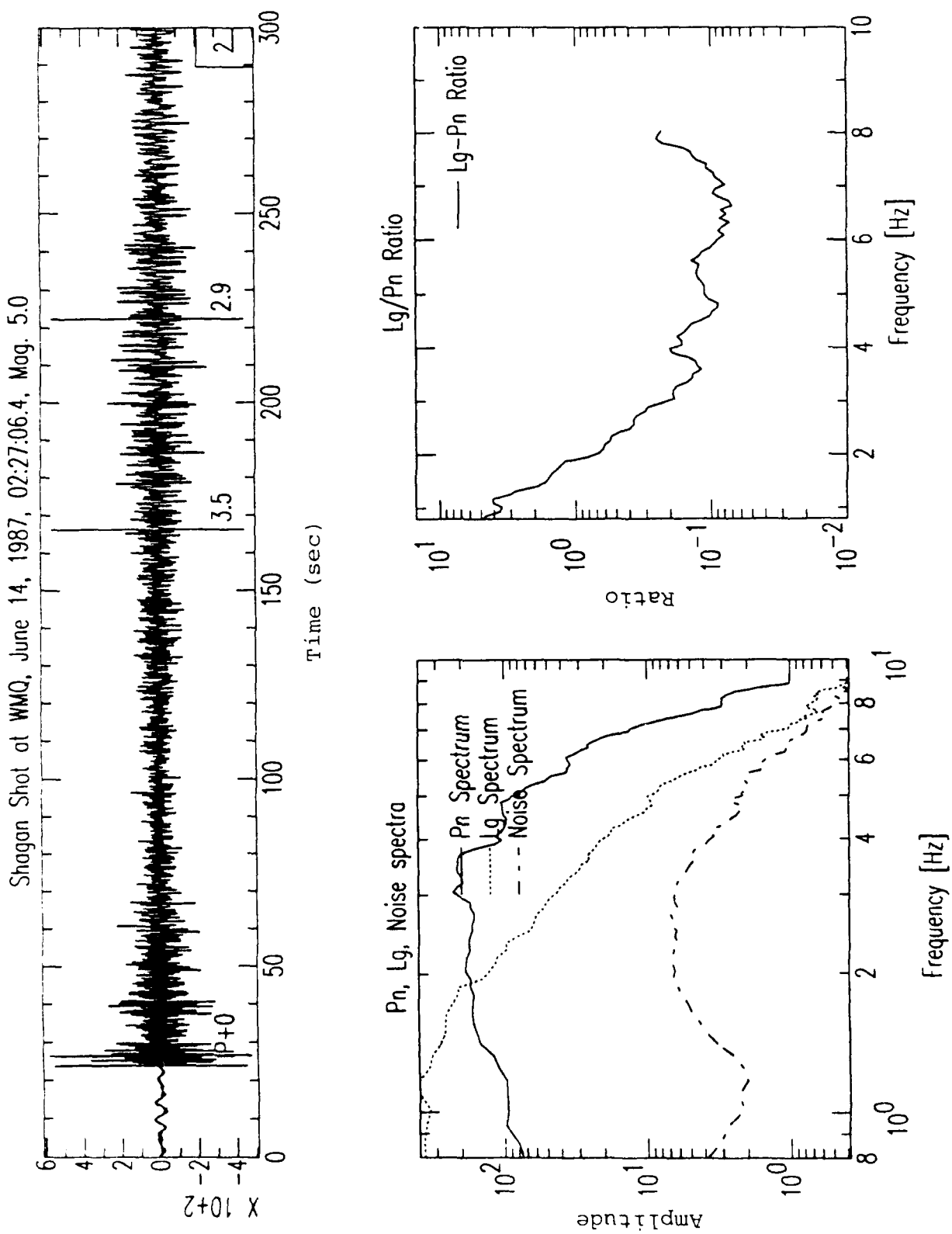
Figure 23. Spectral analysis of the WMQ record from the 06/14/88 SR explosion.
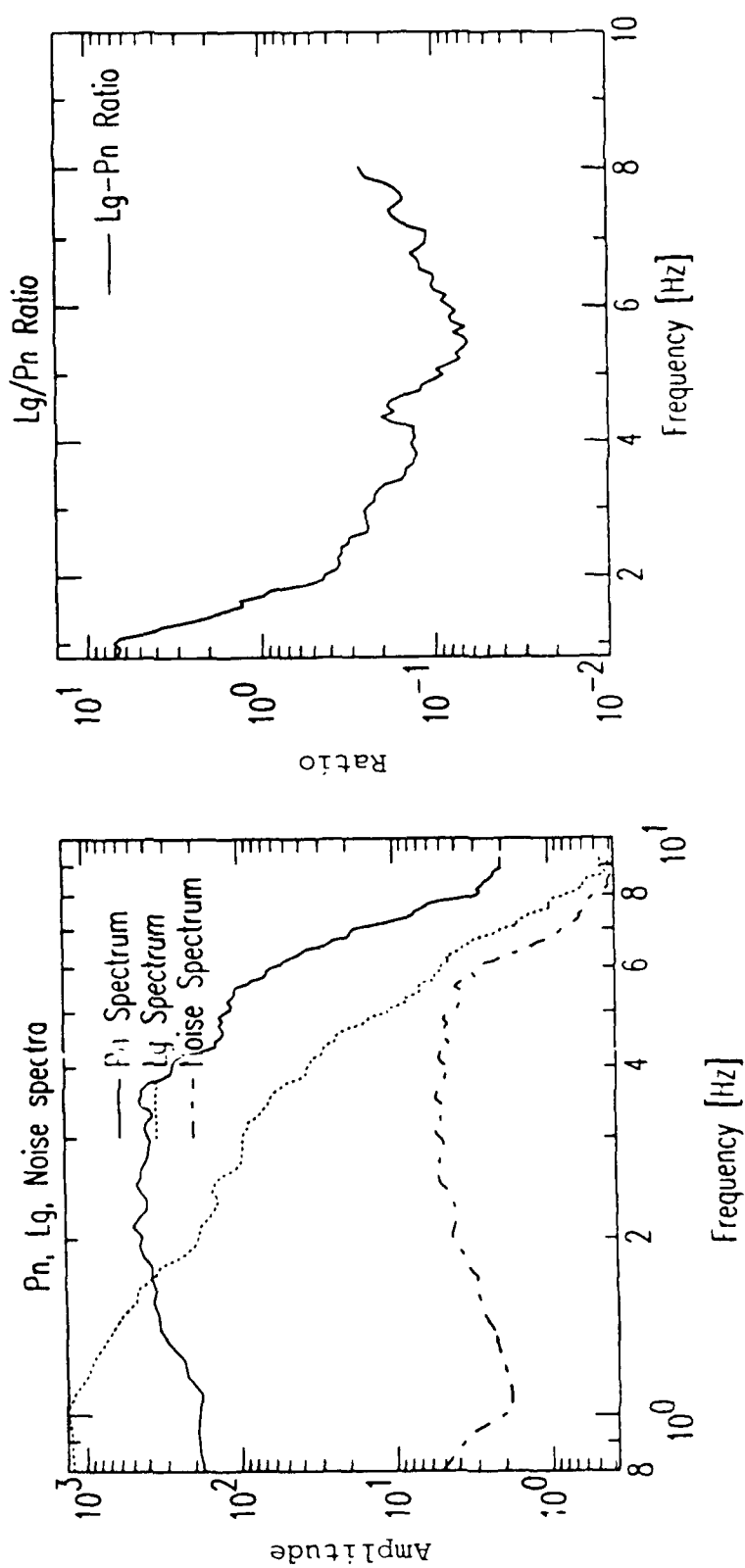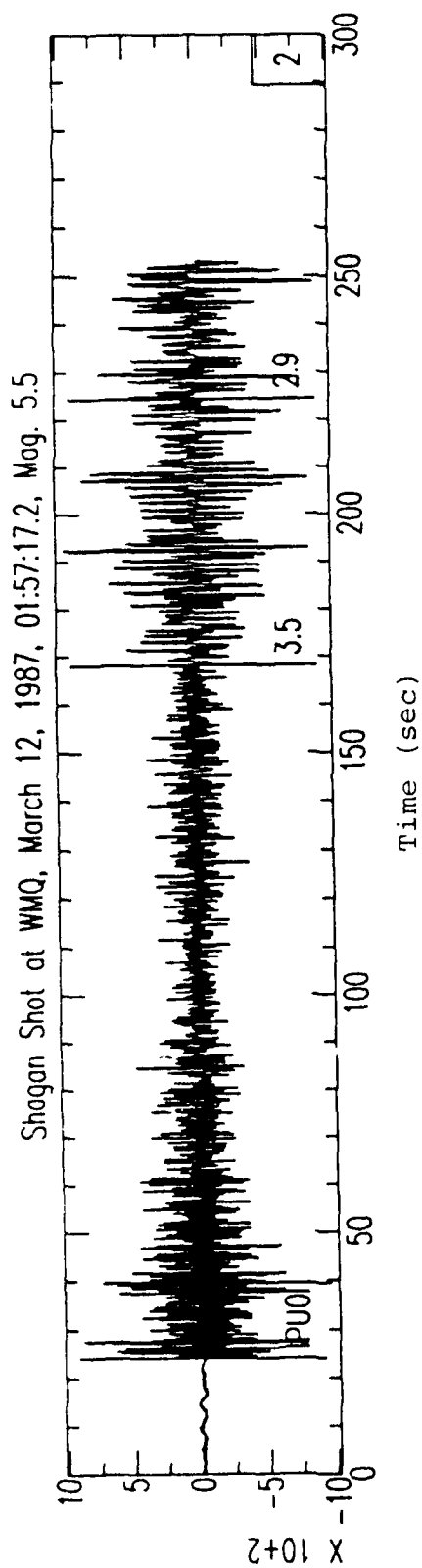
Figure 24. Spectral analysis of the WMQ record from the 03/12/87 SR explosion.
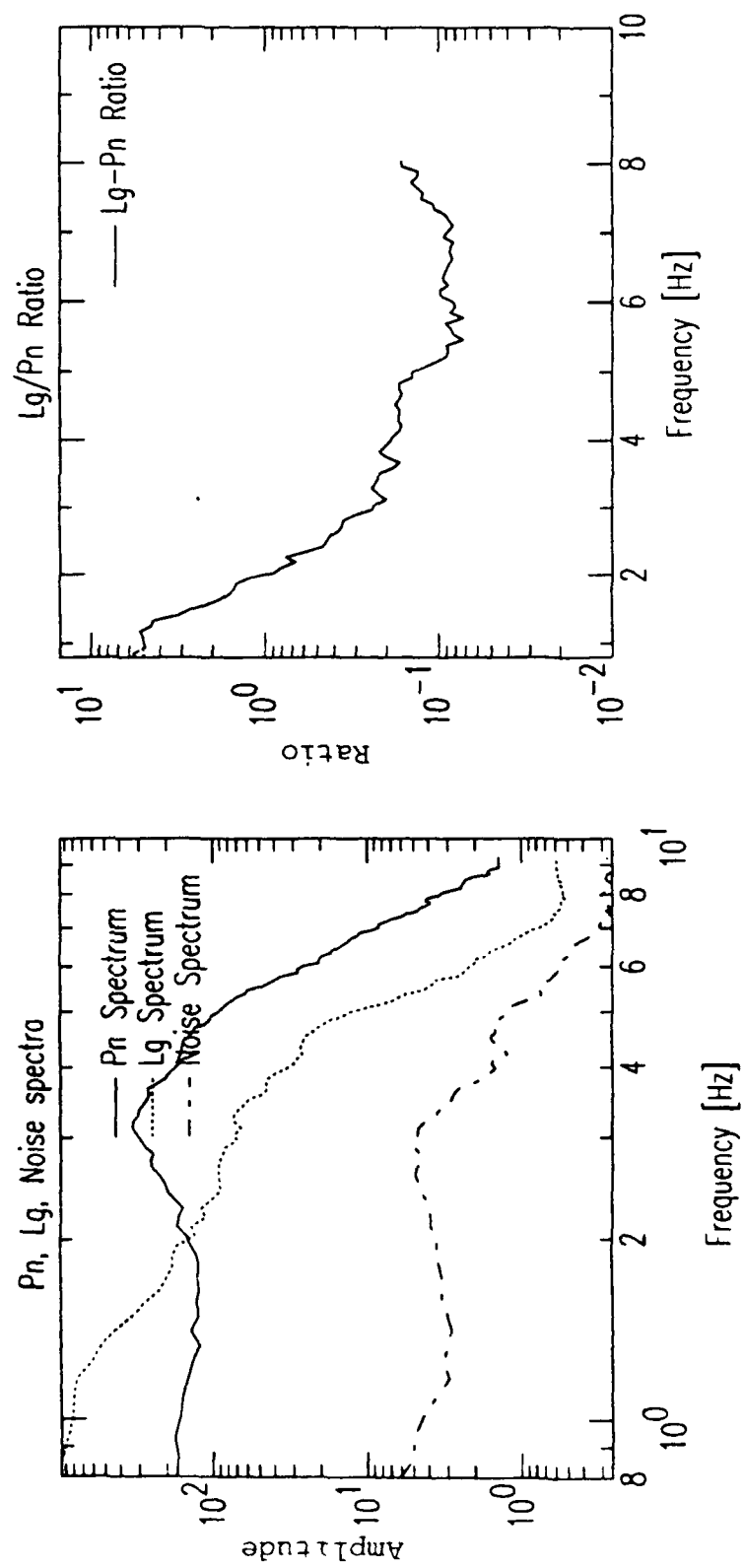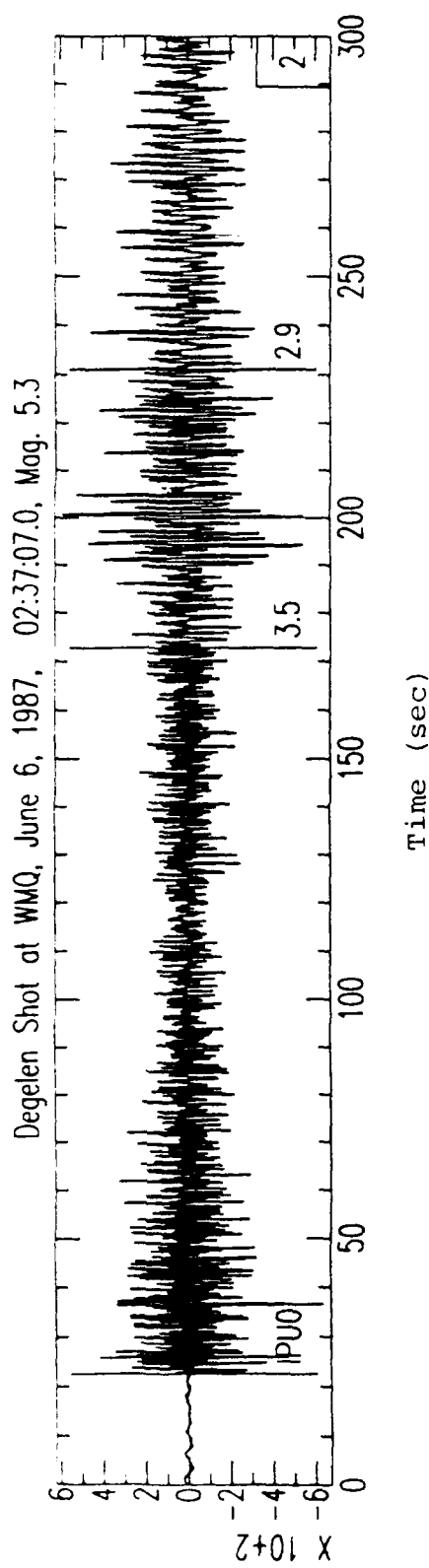
Figure 25. Spectral analysis of the WMQ record from the 06/06/87 DM explosion.
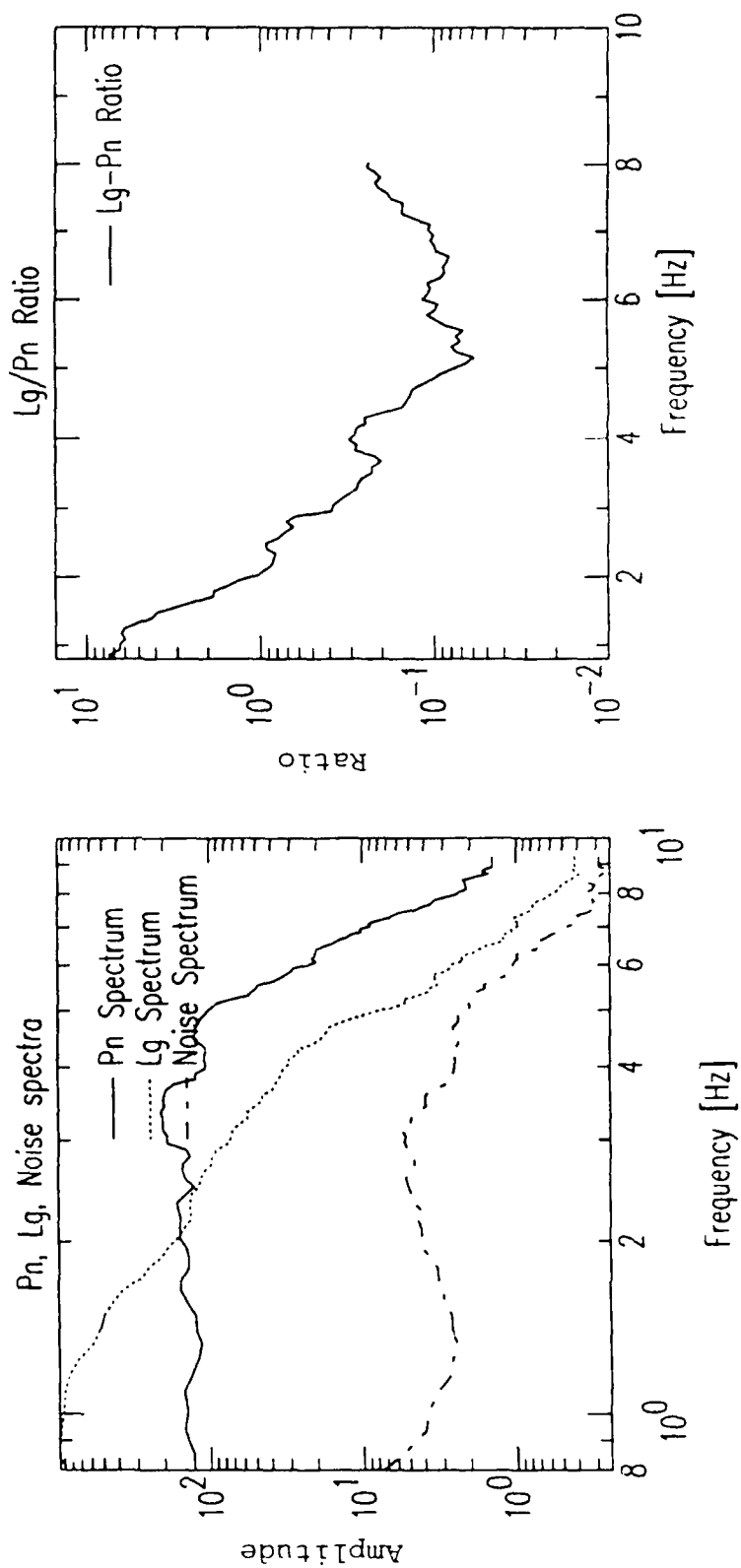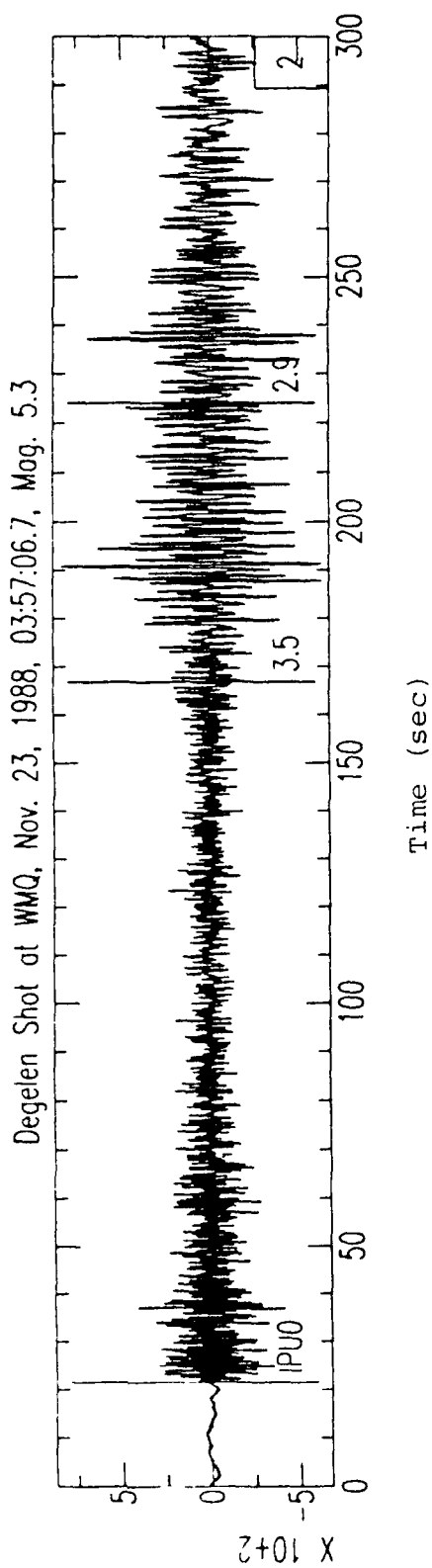
Figure 26. Spectral analysis of the WMQ record from the 11/23/88 DM explosion.

explosions with similar magnitudes in the range 5.0 to 5.5 m_b. The ground motion records, shown at the top of the figures, indicate the same tendency noted above with relatively larger regional P phases for the SR events versus DM events with comparable L_g signals. The results presented for the regional P spectra in Figures 23 through 26 correspond to a longer P-wave window (viz 25 seconds long and beginning 1 second prior to the initial P markers shown superimposed on the waveform traces). The L_g windows covered a group velocity range from 3.5 to 2.9 km/sec, indicated by the later markers, and clearly include most of the L_g energy. Although some additional L_g energy is seen to arrive after the end of the defined windows, we experimented with windows which included this energy also and found that the choice of the L_g window bounds made little difference in the spectral shape or level. The windows were tapered; discrete Fourier transforms were then computed and resampled and smoothed to provide equivalent frequency spacing for the regional P and L_g signal spectra. Finally, L_g/P spectral ratios were computed at each frequency.

The spectra in Figures 23 to 26 appear remarkably similar from event to event. In particular, over the frequency band shown in these figures, the L_g spectral shapes can be made to overlay almost exactly between all four events. Slight differences in the general level of the L_g spectra, however, are apparent from event to event. The regional P spectra are slightly more variable in both shape and level. Comparing first the two DM shots, which are equal in magnitude (viz 5.3 m_b), the only real difference is a very slight increase in the regional P-wave spectral level for the 06/06/87 event over the 11/23/88 event in the limited frequency band from about 2.0 to 5.0 Hz (cf. Figures 23 and 24). Comparing next the 06/06/87 DM event with the 03/12/87 SR event (5.5 m_b), we see that the L_g spectra match very closely in both shape and level (cf. Figures 23 and 25) even though the teleseismic m_b magnitudes are different by 0.2 magnitude units. In contrast, the regional P-wave spectrum for the 03/12/87 SR event lies generally above that of the 06/06/87 DM event with the greatest differences (up to a factor of three in amplitude) occurring in the frequency range from 1.0 to 3.0 Hz. Finally, comparison of the 06/06/87 DM event with the 06/14/87 SR event (5.0 m_b) indicates that the regional P-wave spectra match more closely in shape and level (cf. Figures 23 and 26); while the L_g spectrum for the smaller SR event lies somewhat below that of the

54

DM event over a limited frequency band from about 2.0 to 5.0 Hz. These results again appear to be consistent with relatively greater excitation of regional P signals at some frequencies from SR explosions which have the same level of L_g excitation as DM explosions.

The latter observation shows up as a relatively subtle effect in the L_g/P spectral ratios presented in Figures 23 to 26. Comparing first the L_g/P ratios for the shots at common test sites, it is seen that the ratios match quite closely over the entire frequency band presented. Comparisons of the L_g/P spectral ratios between SR and DM events indicates that the SR spectra generally lie slightly below the DM spectra at almost all frequencies. Figure 27 shows this same comparison for the suite of 11 SR events and 8 DM events. The figure presents the average L_g/P spectral ratios from these events along with $\pm$ 1(σ) bounds on these mean values as a function of frequency. The L_g/P ratios are observed to be nearly identical around 1 Hz and more separated at higher frequencies with the SR average lying below the DM average. Over most of the frequency band from 1 Hz to 8 Hz, the separation appears to hold at the $\pm$ 1(σ) level, although just barely.

From these analyses we would conclude that SR sources tend to be relatively more efficient in generating regional P than DM sources with equivalent L_g signals. Above we suggested an explanation consistent with Nuttli's observation of larger teleseismic P from DM events might be preferential trapping of P energy from the SR explosions in the crust and upper-mantle waveguide. Alternatively, these observations of relatively larger L_g/P ratios from DM events could also be interpreted as greater excitation of L_g by the DM sources. The latter might be caused by more efficient coupling between the L_g crustal waveguide at the DM source (in contrast to SR) and the transmission path waveguide to WMQ. If such effects exist they have not been demonstrated, and additional explanation of Nuttli's teleseismic P differences would be required. Other explanations for these observations also exist and require further study. We plan follow-on studies using the Soviet IRIS and other regional stations to further resolve these differences between SR and DM.
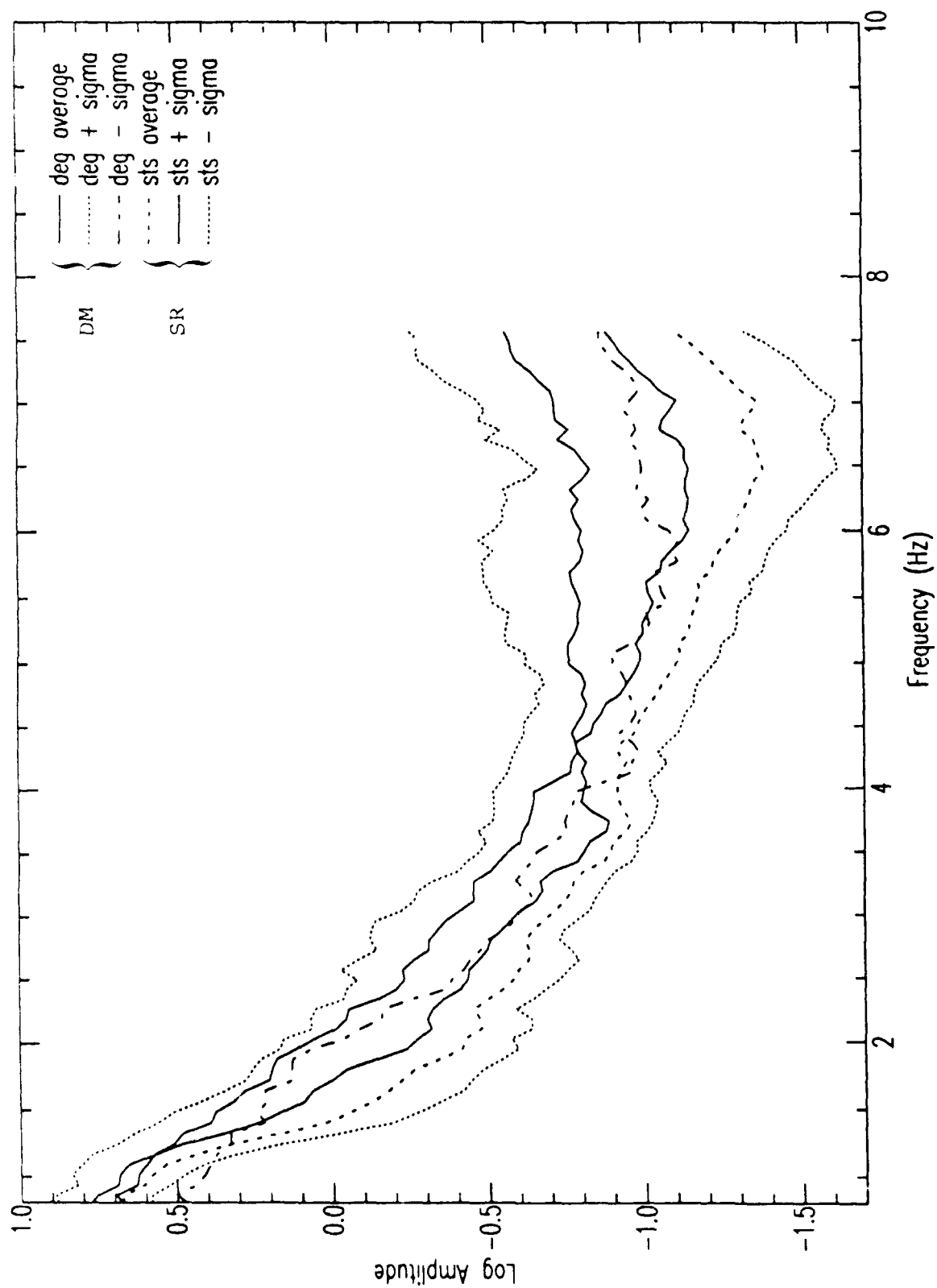
Figure 27. Average Lg/P spectral ratios and their ± 1σ bounds for 11 SR explosions and 8 DM explosions measured at WMQ.

It should also be noted that the differences between SR and DM tend to make the L_g/P spectral ratios for the DM events appear slightly more earthquake-like (cf. Section III above). However, it can be seen by comparing the observations in Figure 27 with the discrimination results, presented above in Figure 19, that there still appears to be good separation between the earthquake and explosion sample above about 3 Hz. We, therefore, conclude that test site differences like those between SR and DM are not sufficient to confound the discrimination differences seen in the L_g/P spectral ratios between underground nuclear explosions and earthquakes.

V. Investigation of Path Effects on Regional Signals

5.1   Attenuation Measurements

As noted above, one argument against the effectiveness of empirically derived discriminants, such as the L_g/P spectral ratios presented in Section III, is that they do not take into account the differences in propagation path effects when sources are not co-located. The results we showed above for East Kazakh explosions compared the observed ratios to those from earthquakes, which in some cases had similar ranges to WMQ, but whose epicenters were located in many cases along the southern Soviet border (cf. Figure 3 above). Therefore, the propagation paths to the station from underground nuclear tests are frequently quite different than those from the earthquakes used for comparisons. In our analysis we attempted to compensate for these effects to some degree by including earthquakes from a variety of locations so as not to bias the result toward a particular propagation path from a single earthquake source area. However, a clearly better approach would be to handle the propagation effects more directly by making appropriate adjustments to the signal or signal spectra from each source area for attenuation differences. Development of a better understanding of regional propagation effects for paths of interest in the Soviet Union is a major task. We have attempted to make some progress on this problem during the past year by analyzing L_g attenuation for paths to selected CDSN and Soviet IRIS stations from the East Kazakh source region. In the future it is anticipated that similar information can be developed into a regionalized attenuation model for the Soviet Union and surrounding areas of Eurasia which can in turn be used to correct regional phase spectra for propagation effects and identify source related differences.

It is clear that regional phase signals are affected by attenuation. In addition to the normal amplitude decrease associated with geometrical spreading, the regional phase signal loses energy due to inherent medium absorption and scattering by inhomogeneities in the waveguide. In developing the L_g magnitude scale, Nuttli (1973) used an analytic expression for geometrical spreading and an effective attenuation term, including both absorption and scattering

effects, to determine the near-source amplitude level. According to this model of the L_g signal, propagating energy is dissipated in relation to the time it spends in the medium, with the higher frequencies being preferentially absorbed. Since tha time a number of methods have evolved for deriving the effective Q, representative of attenuation, from observational data. Some of these methods involve measurement of the coda decay (e.g. Aki and Chouet, 1975; Herrmann, 1980; Nuttli, 1981, 1986a,b) while others are based on observation of the behavior of the signal spectrum at one or more stations (e.g. Chun et al., 1987; Baumgardt and Ziegler, 1988; Sereno et al., 1988). Information on coda behavior, spectral content, and calibration everus can be used to derive an effective Q_0 for the path from SR to WMQ. In the current study we have used the L_g amplitude differences between WMQ and HIA and the Soviet IRIS stations for common SR explosions to derive Q_0's for those paths as well.

5.2 L_g Attenuation for the Path to WMQ

In our initial analysis of L_g attenuation, we have focused on the path to station WMQ from SR events. As noted above, a relatively large database of strong L_g signals exists for this path. In a previous report Bennett et al. (1989) noted that the RSTN station RSSD recorded strong L_g signals from NTS explosions and that the general characteristics of the regional signals at WMQ and RSSD appeared quite similar, even though the stations were located at somewhat different distances from the respective source areas, 960 km from SR to WMQ and 1270 km from NTS to RSSD. To develop the effective attenuation for the paths to these stations, we have compared the amplitude and spectral characteristics of the L_g signals from explosions of equivalent yield at NTS and SR to determine to what extent those characteristics can be attributed to attenuation differences.

We first selected several, large magnitude events which were well-recorded at each station. Vertical component records for these events are shown in Figure 28. They include three SR explosions recorded at WMQ and four NTS explosions recorded at RSSD. Table 5 summarizes the source information on the seven events. To make the signal records more comparable between the two stations, we removed the different instrument responses from
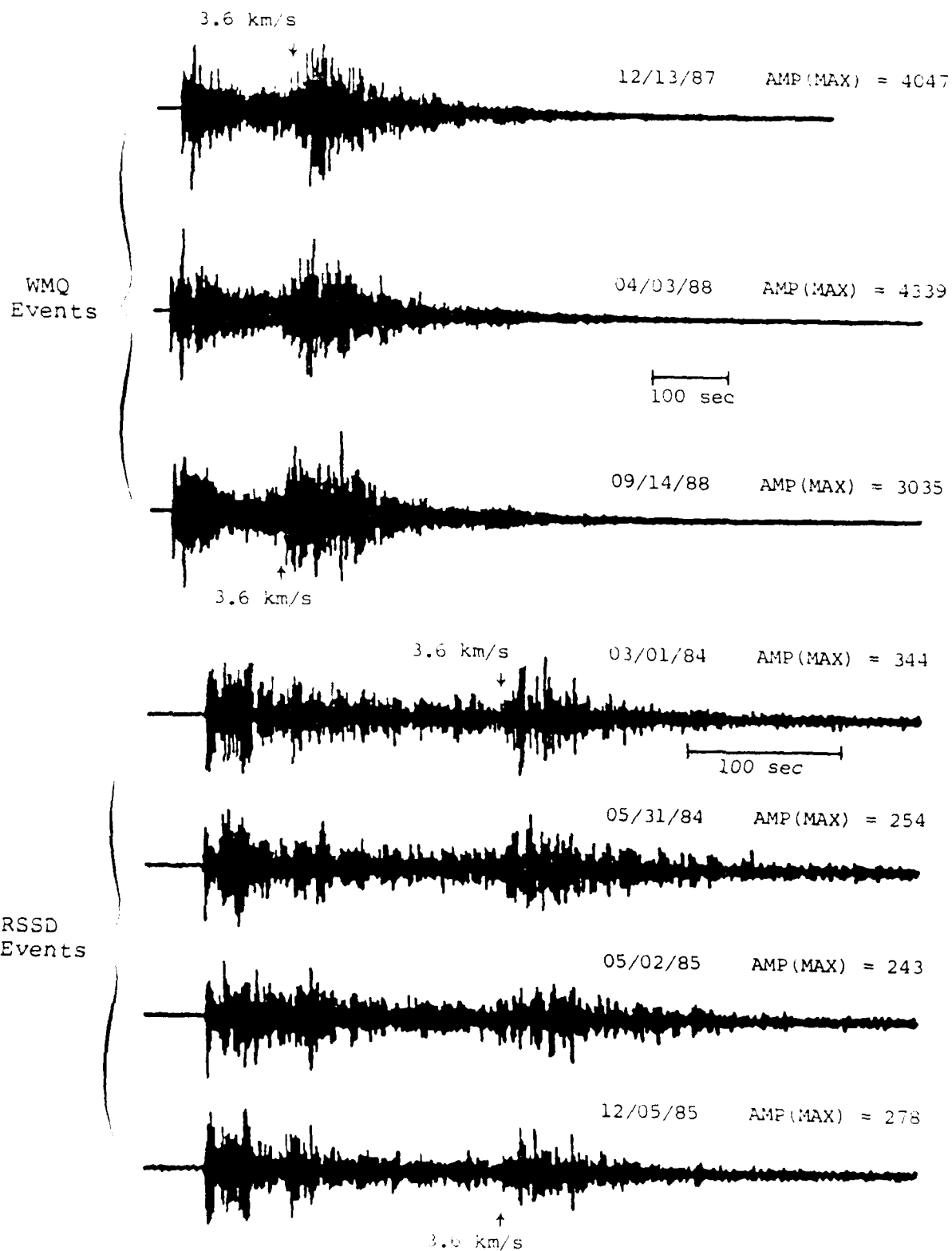
Figure 28. Vertical-component records at WMQ and RSSD for
three SR and four NTS explosions of approximately
equivalent yields.

Table 5. Source Information for Similar Yield Explosions at NTS and SR

	Event	Lat.	Lon.	m_b
NTS	03/01/84	37.07	-116.05	5.9
	05/31/84	37.10	-116.05	5.8
	05/02/85	37.25	-116.33	5.7
	12/05/85	37.05	-116.05	5.7
SR	12/13/87	49.99	78.84	6.1
	04/03/88	49.92	78.95	6.1
	09/14/88	49.83	78.81	6.1

the original records and reconvolved with the instrument response for the short-period WWSSN station to produce the records in Figure 28. The approximate beginning of the L_g windows is designated by the arrows at a group velocity of 3.6 km/sec.

As noted above in Section IV, Nuttli (1986a,b) estimated the teleseismic m_b bias for NTS to be -0.31 and for SR to be 0.036. Thus, equivalent-yield explosions at NTS and SR would be expected to have m_b values about 0.35 magnitude units larger for the SR explosions. In selecting the explosions in Table 5 we attempted to pick events with approximately this magnitude difference, so that the explosions at the two test sites are nearly equivalent in yield. In particular, pairs of explosions of nearly equivalent yield from each test site were identified and L_g spectra determined from the time histories recorded at the respective stations. Figure 29 shows the L_g spectra for two such explosion pairs (viz the 04/03/88 SR event paired with the 05/31/84 NTS event, on the left, and the 09/14/88 SR event paired with the 05/02/85 NTS event, on the right). The spectra plotted in the figure include the common WWSSN response referred to above. The L_g spectra are observed to be fairly sharply peaked at a frequency between 0.5 Hz and 1.0 Hz. The sharpness of the peak is to some extent related to the WWSSN response; the broadband spectra described above in Sections II and III had less exaggerated peaks. The spectral shapes appear to be consistent with the expected behavior of increased attenuation causing depletion of high-frequency energy at the more-distant station. The L_g spectra at WMQ show a steady decline above the peak before reaching an apparent noise floor at about 6 Hz. The L_g spectra at RSSD decline more rapidly above the peak and reach the apparent noise level at a much lower frequency (viz about 3 Hz). L_g spectral ratios determined for the two event pairs over a frequency band from 0 to 3 Hz are presented in Figure 30. The measured L_g spectral ratios are remarkably consistent between the two pairs. Ignoring the variations at very low frequencies, which may be related to inaccurate response information, the L_g spectral ratio (WMQ to RSSD) shows a steady increase over the range from 0.2 to 3.0 Hz. A slight tendency to roll-over and flatten-out toward the higher-frequency end is also apparent.
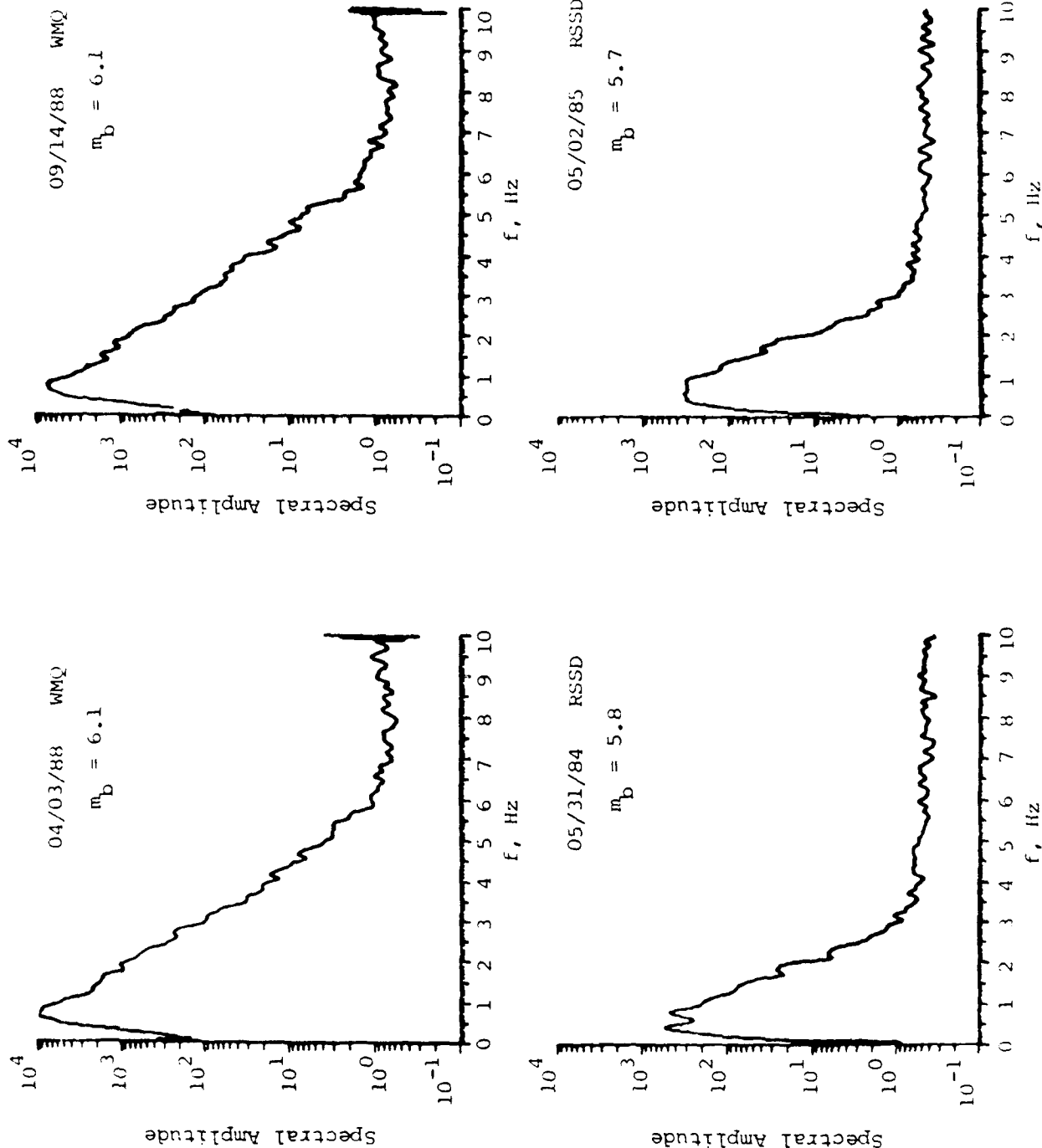
Figure 29. Lg spectral comparisons 04/03/88 SR event and 05/31/84 NTS event (left) and 09/14/88 SR event and 05/02/85 NTS event (right) after adjusting to equivalent instrument response.

63
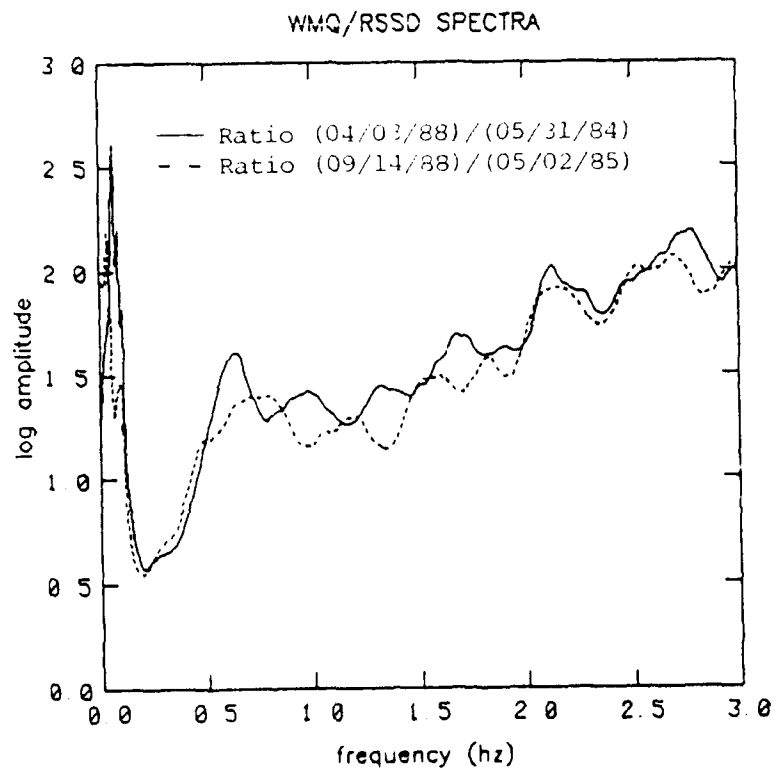
WMQ/RSSD SPECTRA

Figure 30.   Lg spectral ratios WMQ/RSSD for event pairs from Figure 29.

In analyzing this observation it is assumed that the observed L_g spectrum from an explosion source can be represented as

$$A(f) = A_o(f) \ I(f) \ G(R) \ S(f) \ H(f,R) \qquad (1)$$

where A_o is the source function effect, I is the instrument response, G is geometrical spreading, S is site response and H is path attenuation. Assuming equivalent source functions, instrument response, and station effects, then the spectral ratio of the L_g signals for the event pairs can be written as

$$P(f) = \frac{A_1(f)}{A_2(f)} = \frac{G(R_1)}{G(R_2)} \ \frac{H_1(f, R_1)}{H_2(f, R_2)} \qquad (2)$$

where

$$H(f,R) = \exp \ \frac{-\pi f \Delta t}{Q} = \exp \ \frac{-\pi f \ R}{Q \ U} \qquad (3)$$

and

$$G(R) = \left(\frac{R}{10}\right)^{\frac{1}{3}} \left[\frac{\sin(R/111.1)}{\sin(10/111.1)} \right]^{\frac{1}{2}} \qquad (4)$$

Thus,

$$P(f) = \frac{G(R_1)}{G(R_2)} \ \exp \left\{ -\pi f \left[\frac{R_1}{Q_1 \ U_1} - \frac{R_2}{Q_2 \ U_2} \right] \right\} \qquad (5)$$

So, the path Q functions can be used to predict the spectral ratios for the event pairs.

In these analyses we took the common representation of Q as

$$Q = Q_o \ f^c \qquad\qquad (6)$$

Studies of L_g attenuation in continental areas have typically found the frequency exponent, c, to have values between 0.4 and 0.6 (e.g. Mitchell, 1990; Sereno *et al.*, 1988) In the present study we have not attempted to determine the frequency dependence of Q but have instead assumed values in the appropriate range. Therefore, we initially assumed, based on preliminary analysis, that c was 0.4 for the path from SR to WMQ and 0.5 for the path from NTS to RSSD. Using this as a constraint, we determined values of Q_o which would give the appropriate spectral ratios when applied in Equation 5. Figure 31 shows the predicted spectral ratios for the explosion pairs under the assumption that $Q = 285 \ f^{0.4}$ for the path to WMQ and $Q = 200 \ f^{0.5}$ for the path to RSSD. The agreement between the predicted and observed behavior for the L_g spectral ratio appears to be reasonable, but the estimates of Q could be refined to provide even closer agreement. Furthermore, it should be noted that, even though the observed L_g spectral ratios are reasonably matched by predictions based on the path Q's, these Q values do not produce L_g magnitudes which would give the right teleseismic m_b bias with respect to $m_b(L_g)$. In particular, these Q values give L_g magnitudes which are too large for both paths.

The magnitude bias and the spectral ratio results can be made consistent by adjusting the attenuation for both paths. We, therefore, proceeded under the constraint that the L_g magnitudes measured from the records in Figure 28 should give the appropriate test site bias, as determined by Nuttli (1986a,b), when compared to the reported teleseismic m_b. The logarithms of the peak L_g amplitudes measured from the records in Figure 28 were used in an inversion scheme to determine the Q_o values for each event which would give L_g magnitudes that provided the correct test site bias (viz $m_b - m_o(L_g) = -0.31$ for NTS and $m_b - m_b(L_g) = 0.036$ for SR). For the three SR events recorded at WMQ in Table 5, we determined Q_o to be 452 with $\sigma = 34$. The four NTS events recorded at RSSD (cf. Table 5) gave a Q_o of 239 with $\sigma = 5$. The relatively small σ values suggest that the bias differences were quite consistent between events recorded at these stations.
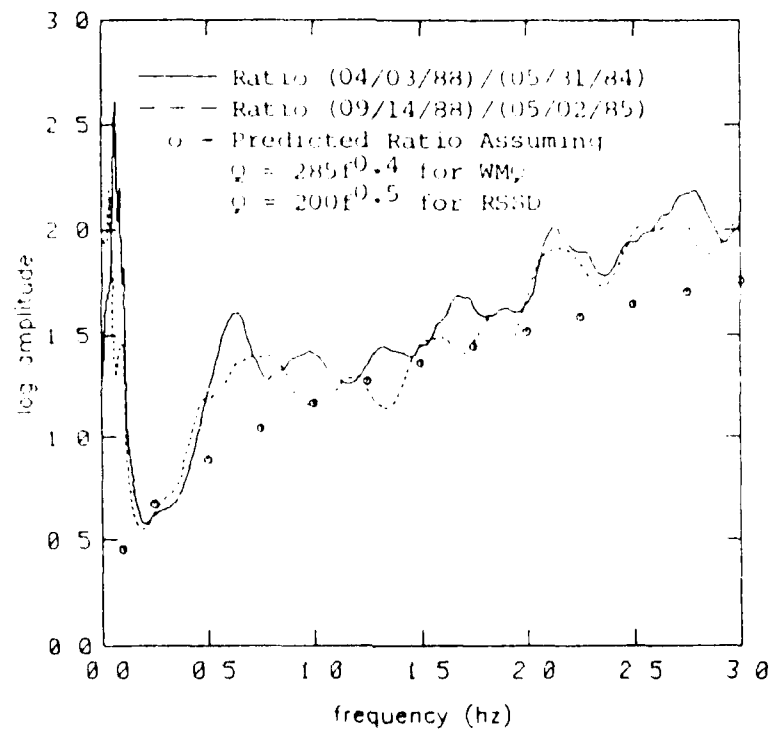
Figure 31. Comparison of observed and predicted L_q spectral ratios derived from attenuation models.

As a final check on these effective Q values for the paths SR/WMQ and NTS/RSSD, we reassessed the L_g spectral ratio for the comparable-yield explosions. For the SR/WMQ path we used $Q = 452\ f^{0.5}$, and for the NTS/RSSD path we used $Q = 239\ f^{0.5}$. Equation 5 above was again used to predict the spectral ratios. It can be seen in Figure 32, that these attenuation models do an excellent job of predicting the observed ratios. It's possible that attenuation models with different frequency dependence might also do a reasonable job of fitting these observations. However, we would expect that only minor variations for the Q_o's can be permitted to simultaneously satisfy the test site bias constraints. A more thorough analysis of the sensitivity of the attenuation estimates to these measurements would be useful.

5.3 Attenuation for Paths to Other Regional Stations

As pointed out above in Section II, strong L_g signals have been recorded at a regional network of stations from East Kazakh explosions. In this section we will determine the relative amplitudes of these L_g signals between stations and use these observations to estimate effective Q_o values for the paths from SR to the various stations. We start with Nuttli's definition of the L_g magnitude:

$$mb(L_g) = \log A(10km) + 2.96 \tag{7}$$

where

$$A(10km) = A(R)\ \left(\frac{R}{10}\right)^{\frac{1}{3}}\ \left[\frac{\sin(R/111.1)}{\sin(10/111.1)}\right]^{\frac{1}{2}}\ \exp\ \frac{\pi f(R-10)}{Q\ U} \tag{8}$$

where $A(R)$ is the L_g ground motion amplitude in μm measured on a WWSSN short-period, vertical-component instrument. The L_g magnitude difference between two stations recording the same event should, in the absence of measurements errors, be zero. So, we can write

$$\Delta m_b(L_g) = 0 \tag{9}$$

$$= \Delta m_b'(L_g)\ +\ \log\ \left\{\exp\left[\pi f\ \left(\frac{R_1 - 10}{U_1\ Q_1}\ -\ \frac{R_2 - 10}{U_2\ Q_2}\right)\right]\right\}$$

68
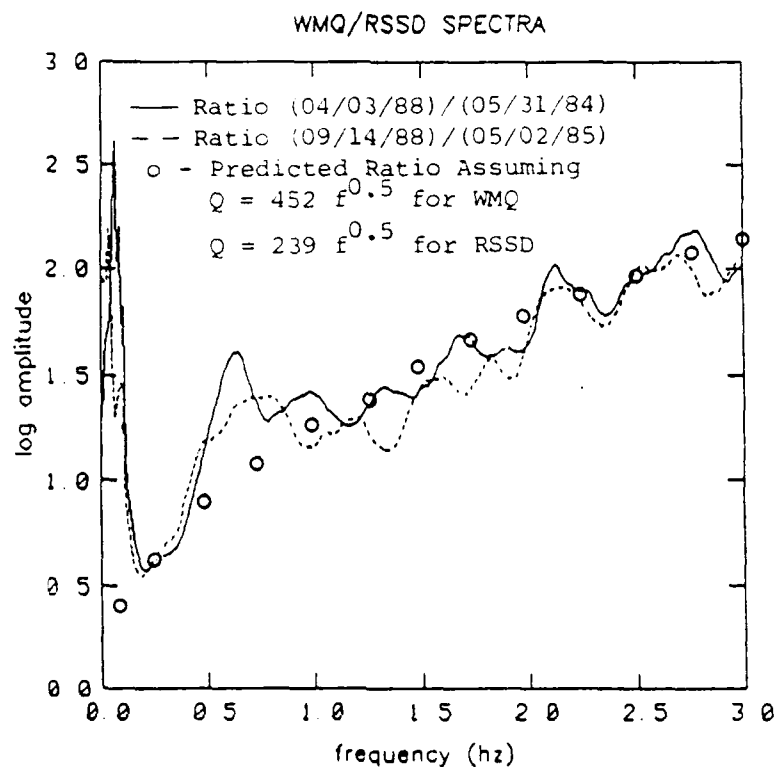
Figure 32. Comparison of observed and predicted Lg spectral ratio determined from revised Q models.

where

$$\Delta m_b{}'(L_g) = \log \frac{A(R_1)}{A(R_2)} + \frac{1}{3} \log \frac{R_1}{R_2} + \frac{1}{2} \log \frac{\sin(R_1/111.1)}{\sin(R_2/111.1)} \quad (10)$$

Then

$$\pi f \left(\frac{R_2 - 10}{U_2 Q_2} - \frac{R_1 - 10}{U_1 Q_1} \right) \log e = \Delta m_b{}'(L_g) \quad (11)$$

and

$$Q_2 = \frac{T_2 Q_1 \pi f \log e}{T_1 \pi f \log e + Q_1 \Delta m_b{}'(L_g)} \quad (12)$$

where $T = R/U$ and $R \gg 10$. In these analyses the L_g amplitude measurements were made from a seismogram which had been converted to WWSSN response, so we assumed that $f \approx 1$ Hz and that the Q_1 and Q_2 values then correspond to Q_o's for the station involved. Since we had some prior knowledge of the attenuation to station WMQ (based on the analyses presented in the preceding section) and a large amount of data recorded there, it was used as the reference station. L_g magnitude residuals relative to WMQ were then analyzed for the Soviet IRIS stations (viz GAR, ARU, OBN, and KIV) and for the other useful CDSN station (viz HIA) to determine the respective Q_o values for these paths from SR events.

The first step in this process was to convert all instrument responses to an equivalent WWSSN short-period instrument. To accomplish this the individual station responses were deconvolved from the observed records and the output reconvolved with a standard WWSSN response. Figures 33 and 34 illustrate the application of this process to the WMQ and ARU records for two SR explosions. For both stations the conversion process is seen to basically remove some of the lower-frequency energy in the records. In particular, this greatly reduces the low-frequency microseismic noise (enhancing the apparent signal-

70

WMQ

09/14/88 m_b 6.1

100 sec

11/12/88 m_b 5.3
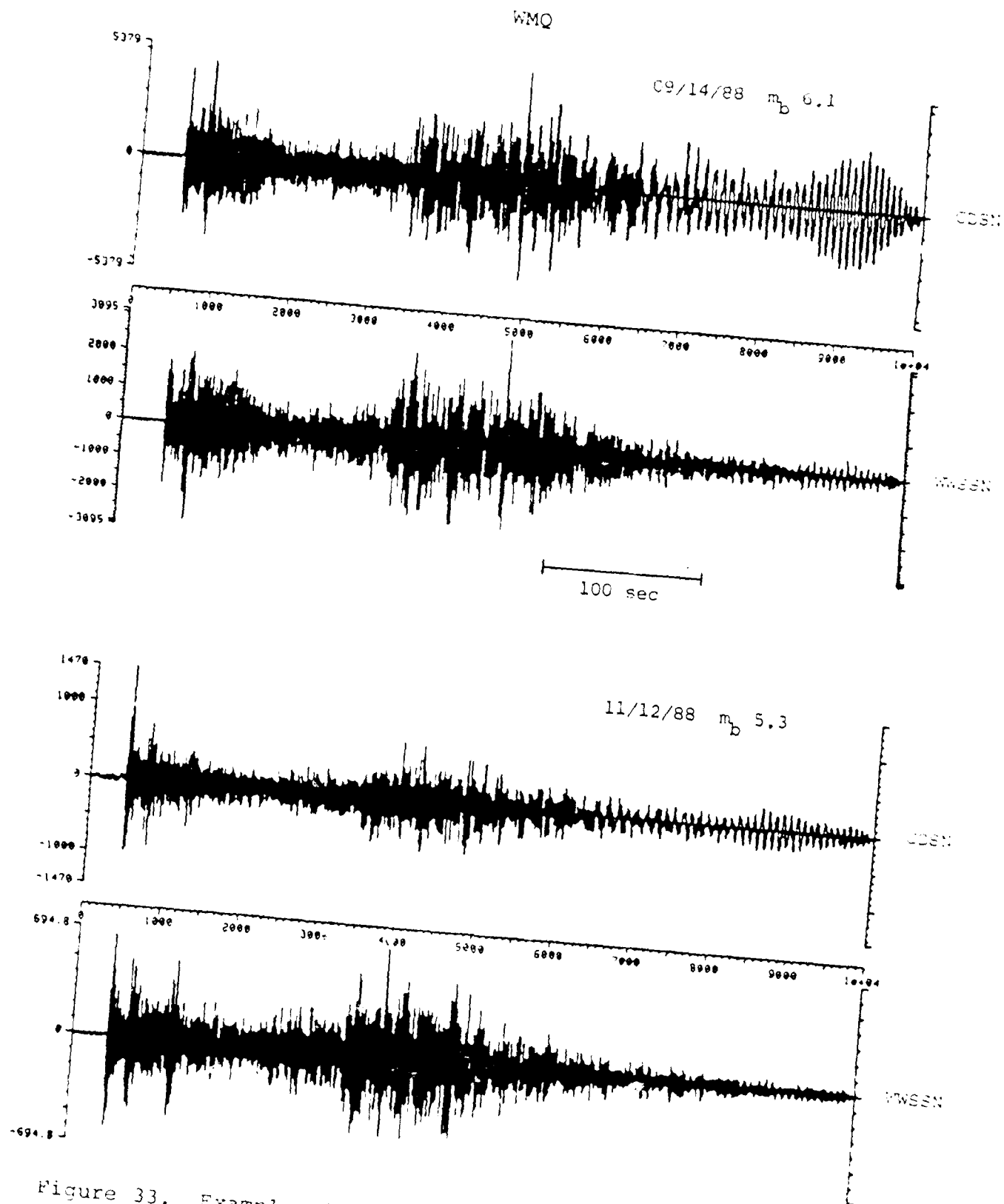
Figure 33.   Examples illustrating conversion of WMQ explosion records to WWSSN response.

71

ARU
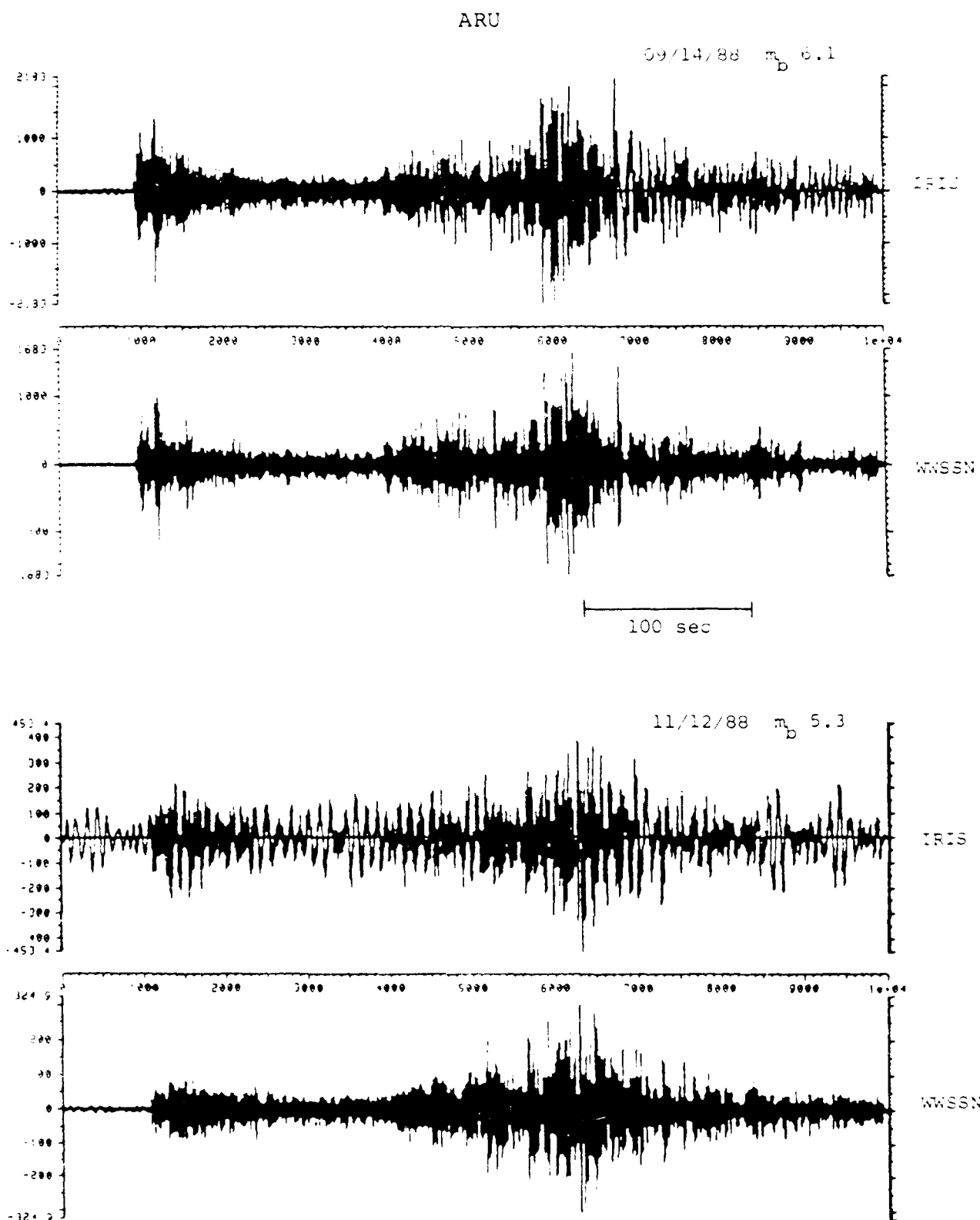
Figure 14. Examples illustrating conversion of ARU explosion records to WWSSN response.

72

to-noise) and also reduces the low-frequency surface waves.

We next measured the sustained L_g amplitudes using the procedures described by Nuttli (1973; 1986a,b) and computed the residuals (i.e. $\Delta m_b'(L_g)$ for the common events. Table 6 summarizes the data that were analyzed in this way. The residuals for each event/station path were converted to estimates of Q_o for these paths using the relationship in equation 12. The average Q_o values for the paths are shown in Figure 35. The values range from a low-Q path value of 428 to station GAR up to a high-Q path of 761 to OBN. The Q_o value of 580 determined for the path to KIV is surprisingly large considering the low L_g signal level normally observed there and probably represents a maximum estimate. For comparison we show in Figure 36 Q_o values derived by Nuttli for paths to Eurasian WWSSN stations from East Kazakh test site events. The Q_o values determined in the present study are quite consistent with Nuttli's values for similar paths. They also agree generally with Q values recently reported by Xie and Mitchell (1990) based on spectral studies of L_g for central Asian paths from explosions and earthquakes. In particular, we find relatively low Q's to the south of the test site consistent with high attenuation of L_g in the complex tectonic region of the southern Soviet border. On the other hand, Q's for the northwestern paths are high corresponding to low attenuation of L_g in the stable continental platform area of the Soviet interior. The largest uncertainties on the Q_o values estimated from the L_g magnitude residuals are associated with station ARU and OBN. We would expect some refinement of these estimates as additional data become available. We also plan to more fully investigate the frequency dependence of Q over the rather limited band of frequencies which these data will permit.

Table 6. Q_0 Estimates Derived From Measured L_g Magnitude Residuals

Date	WMQ	HIA	ARU	GAR	OBN	KIV
09/14/88	452	559	707	433	818	571
10/18/88	452	-	641	410	-	-
11/12/88	452	-	675	451	-	-
12/17/88	452	577	645	-	734	-
02/12/89	452	560	577	-	-	-
02/17/89	452	-	507	417	-	-
07/08/89	452	575	604	428	731	589
	452*	568±10	622±66	428±16	761±49	580±13

* The Q_0 value at the reference station WMQ was fixed at 452 based on previous analyses.
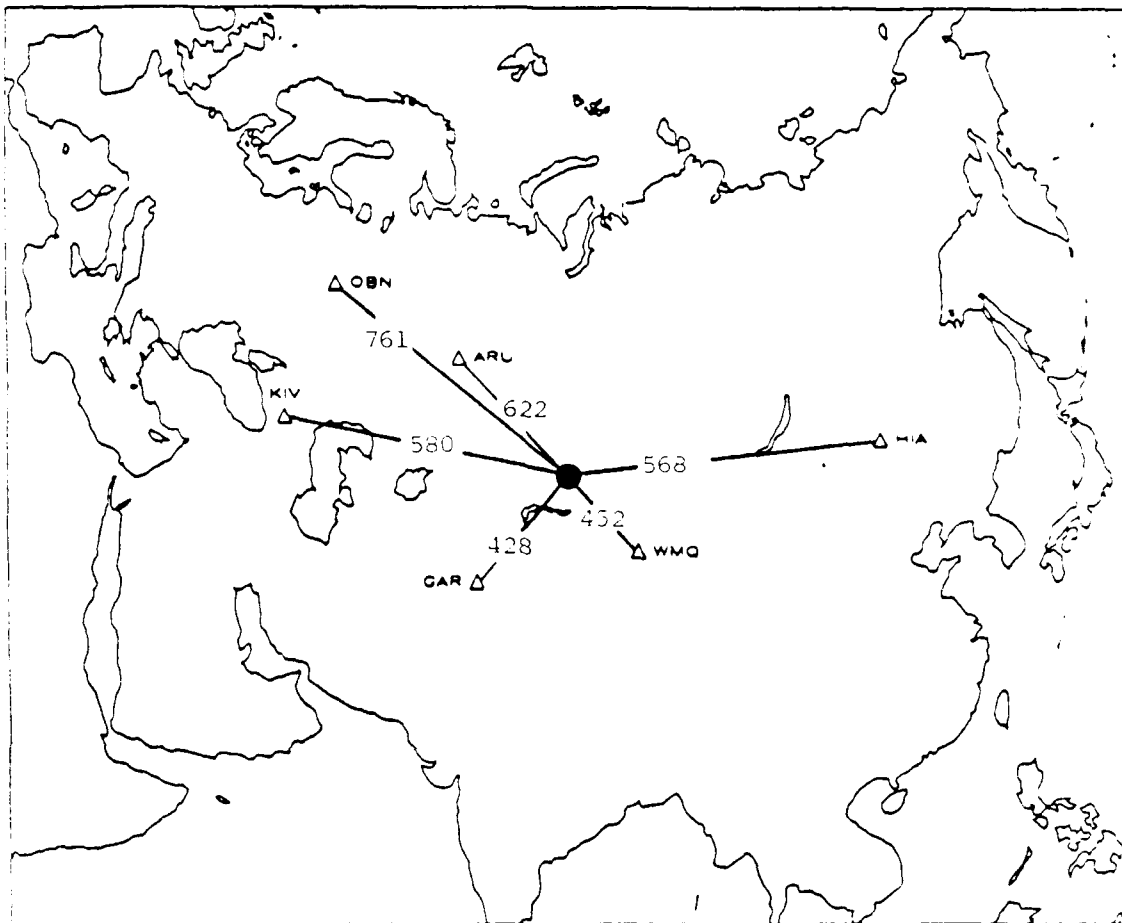
Figure 35. Path Q_O values to IRIS and CDSN stations derived from L_g magnitude residuals.
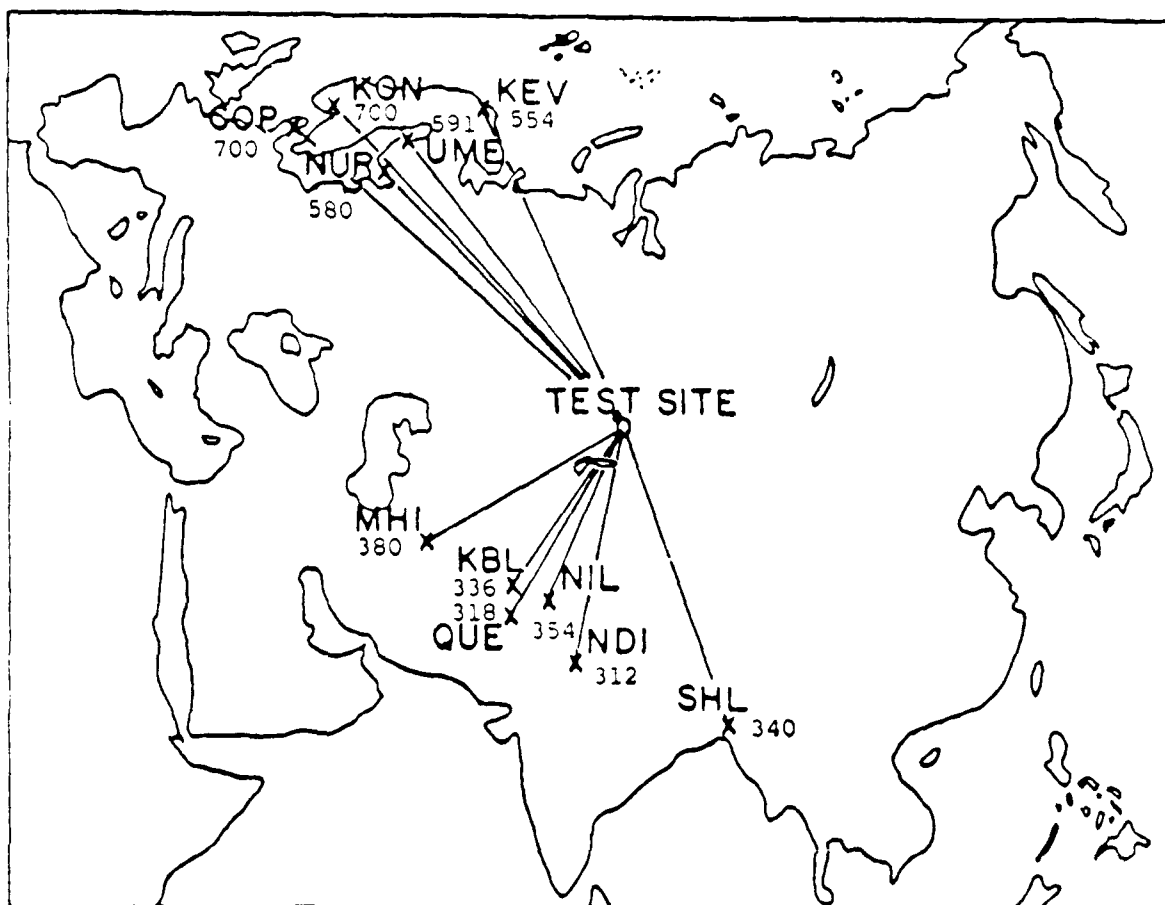
Figure 36. Q_O values determined by Nuttli (1986b) for paths from SR to WWSSN stations.

VI. Summary and Conclusions

6.1 Summary of Research Program

The research described here represents the first year's effort of a three year program designed to evaluate the capability of regional seismic stations to discriminate underground nuclear explosions from earthquakes and non-nuclear explosions. This effort to date has focused on investigation of the regional signals recorded at CDSN and Soviet IRIS stations. These two sources of data have become available only within the last few years and an experience base needs to be developed in order to understand their capability for monitoring seismic events within the Soviet Union.

The overall objective of this research program is to systematically evaluate a wide variety of regional discriminant measures, to identify the reliability of those discriminants for application to events in the Soviet Union, and ultimately to formulate a winnowing procedure utilizing those regional discriminants which can be used to identify Soviet events. In prior investigations we have applied a range of regional signal measurements, which included new as well as previously proposed discriminant measures, to the available regional phase signals from seismic events in tectonic environments including the Soviet Union, the western U. S. and eastern North America. These measurements included time domain phase amplitude comparisons and spectral differences for events in each of the tectonic environments. The results of these studies have suggested that a number of such regional measurements may be useful in distinguishing undergound nuclear explosions from other seismic events including earthquakes and non-nuclear blasts. However, it is only recently that suitable regional data from a large sample of Soviet explosions and nearby regional earthquakes have become available to permit testing of those procedures on a relevant database.

Therefore, during this first year, we have directed efforts at expanding the database of events from the Soviet Union and comparable events from nearby border regions. This database currently includes 28 East Kazakh underground

nuclear explosions and 32 regional earthquakes recorded at CDSN stations (primarily at station WMQ). In addition, the database of Soviet events includes nine East Kazakh explosions recorded at the Soviet IRIS stations, and we are in the process of recovering a comparable sample of regional earthquakes recorded at these same stations. Additional regional recordings of Soviet underground nuclear explosions obtained from these stations are also being incorporated into the database as they become available.

We have performed several analyses on these regional recordings concentrating primarily on determining the detection capability of the stations and the amplitude and spectral characteristics of the L_g and regional P signals. Comparisons of L_g versus regional P signal levels have been analyzed for differences related to source type. The latter included investigation of frequency dependence in the relative excitation of L_g and regional P from the explosion and earthquake sources. We also studied differences in the relative excitation of L_g and regional P signals between the two principal explosion test areas at East Kazakh: Shagan River and Degelen Mountain.

Finally, we made some preliminary investigations of the effects of propagation path differences on regional signals which could eventually be useful for making appropriate adjustments to regional phase measurements in discrimination analyses. In particular, since co-located earthquake and explosion sources do not always exist, propagation paths to regional monitoring stations from explosions and comparable earthquake sources may be different. To get at source-dependent excitation differences more directly, signal measurements should be compensated for attenuation differences. In the current study we performed analyses to determine the extent to which L_g signal differences at the available CDSN and Soviet IRIS stations could be explained by attenuation differences for the propagation paths to the stations from common events. The L_g signal differences from such common events were used to derive effective Q values representative of the various propagation paths.

6.2 Conclusions

The studies described in this report have revealed many interesting characteristics of the behavior of regional signals from Soviet explosions and

comparable earthquakes. In particular, the larger database of events recorded at station WMQ, which was analyzed in this study, again showed that L_g/P ratios for regional earthquakes were relatively enriched at high frequencies compared to similar explosions. These L_g/P ratios were found to be intermingled at frequencies near 1 Hz but completely separated above 2 Hz for SR explosions and regional earthquakes. This observation continues to have the potential for becoming a valuable discriminant, but effects of propagation path differences between events with different source types need further study.

Another interesting conclusion, based on analyses of WMQ recordings of SR and DM explosions, was that the regional P signals from SR explosions are relatively stronger than from DM explosions with similar L_g signals. This appears to be opposite of Nuttli's finding based on comparison of teleseismic P from the two source areas. Spectral analyses of the WMQ signals from SR and DM explosions indicated a tendency for the DM explosions to have somewhat larger L_g/P ratios at higher frequencies, which would make them appear more earthquake-like. However, this effect was relatively small compared to the differences between explosion and earthquake spectral ratios determined in the discrimination studies. Therefore, it does not severely limit the discrimination potential of such measurements.

An issue which will require considerable study before discrimination results can be extrapolated into uncalibrated areas is the effect of propagation path differences and attenuation on the regional discriminant measurements. It has been argued that this might be a contributing factor to the L_g/P ratio differences between explosions and earthquakes observed at WMQ, which were described above. To better understand these effects, we derived Q values representative of L_g attenuation for the path from East Kazakh to WMQ and the other regional stations. For the path to WMQ we found a Q_o value of 452 representing effective L_g attenuation. Q_o values to the other stations derived from L_g magnitude residuals for common events ranged from a low value of 428 for IRIS station GAR to a high value of 761 for IRIS station OBN. It is envisioned that observations like these may eventually be useful in adjusting discriminant measurements for propagation differences.

In addition, some other observations made during the course of this study seem noteworthy. We found, in general, that East Kazakh explosions and regional earthquakes frequently produced strong L_g signals which were recorded at CDSN and Soviet IRIS stations out to ranges in excess of 2000 km. For the triggered CDSN stations, the most complete sample of data was available from the station WMQ nearest the East Kazakh test site which has recorded explosion signals to magnitudes as low as 4.8 m_b. P-wave signals at WMQ from East Kazakh explosions were seen to be quite complex. Spectral analyses of these regional P signals revealed that selection of the window length appeared to produce some small effects on computed spectra, primarily at lower frequencies. Long windows encompassing all P energy produced spectra which were somewhat larger than the corresponding spectral levels obtained for short windows including only the initial P. As a result, L_g/P spectral ratios obtained using the short windows tended to be lower and somewhat more earthquake-like than ratios based on the longer P-wave windows. Possible causes for this observation need additional study. CDSN station HIA at a range of more than 2900 km from the test site also recorded strong L_g signals from many of the larger East Kazakh explosions. However, the useful frequency band of these signals was found to be limited to rather low frequencies. Unfortunately, other CDSN stations have not recorded useful L_g signals from Soviet explosions apparently because their normal trigger level is set higher than the amplitudes generated by the signals at these ranges.

Much of our analysis of the Soviet IRIS station data is preliminary at this time since we are still developing the earthquake database. However, we have found that stations ARU and GAR frequently record strong L_g and regional P signals from East Kazakh explosions down to fairly low magnitudes. Spectral analysis of these signals indicates that the maximum signal-to-noise level for these events is in a passband near 1 Hz. In fact, we found that, by band-pass filtering the ARU records in a frequency band from 0.8 to 1.6 Hz, L_g signal levels could be enhanced to three times the noise level for a SR explosion with a magnitude of only about 3.8 m_b. Similar enhancement also is attainable for L_g signals recorded at IRIS station GAR. However, at the more distant Soviet IRIS stations, the L_g signals from East Kazakh explosions have spectral peaks at frequencies less than 1 Hz and drop off rapidly to the noise level at higher frequencies. As a result, it appears that stations considerably closer than OBN

and KIV will probably be required to obtain L_g signals at frequencies above 1 Hz. This may impede some types of regional discriminant measures which require broadband spectral estimates of signal strength.

References

Aki, K. and B. Chouet (1975). "Origin of Coda Waves: Source, Attenuation, and Scattering Effects," *J. Geophys. Res., 80,* pp. 3322-3342.

Allen, R. (1982). "Automatic Phase Pickers: Their Present Use and Future Prospects," *Bull. Seism. Soc. Am., 72,* pp. S225-S242.

Baumgardt, D. R. and K. A. Ziegler (1988). "Spectral Evidence of Source Multiplicity in Explosions: Application to Regional Discrimination of Earthquakes and Explosions," *Bull. Seism. Soc. Am., 78,* pp. 1773-1795.

Bennett, T. J., D. G. Lambert, J. R. Murphy, J. M. Savino, and C. B. Archambeau (1981). "Regional Discrimination Research," S-CUBED Report SSS-R-81-5032, Technical Report on Contract No. F08606-80-C-0016.

Bennett, T. J., and J. R. Murphy (1986). "Analysis of Seismic Discrimination Capabilities Using Regional Data from Western United States Events," *Bull. Seism. Soc. Am., 76,* pp. 1069-1086.

Bennett, T. J., B. W. Barker, K. L. McLaughlin, and J. R. Murphy (1989). "Regional Discrimination of Quarry Blasts, Earthquakes and Underground Nuclear Explosions," S-CUBED Report, SSS-TR-89-10385, GL-TR-89-0114, ADA223148.

Blandford, R. R. (1981). "Seismic Discrimination Problems at Regional Distances," in *Identification of Seismic Source - Earthquake or Underground Explosion,* D. Reidel Publishing Co.

Chun, K.-Y., G. F. West, R. J. Kokoski and C. Samson (1987). "A Novel Technique for Measuring L_g Attenuation - Results from Eastern Canada Between 1 to 10 Hz," *Bull. Seism. Soc. Am., 77,* pp. 398-419.

Hansen, R. A., F. Ringdal, and P. G. Richards (1990). "The Stability of RMS L_g Measurements, and Their Potential for Accurate Estimation of the Yields of Soviet Underground Nuclear Explosions," Paper Presented at NORSAR Symposium on Studies with Seismic Arrays, February, 1990.

Herrmann, R. B. (1980). "Q Estimates Using the Coda of Local Earthquakes," *Bull. Seism. Soc. Am.*, *70*, pp. 447-468.

Mitchell, B. J. (1990). "Regional Variations of Q_β and Q_{L_g} in Continental Regions - Implications for Crustal Evolution," *EOS, 71*, p. 566.

Murphy, J. R. and T. J. Bennett (1982). "A Discrimination Analysis of Short-Period Regional Seismic Data Recorded at Tonto Forest Observatory," *Bull. Seism. Soc. Am.*, *72*, pp. 1351-1366.

Nuttli, O. w. (1973). "Seismic Wave Attenuation and Magnitude Relations for Eastern North America," *J. Geophys. Res.*, *78*, pp. 876-885.

Nuttli, O. W. (1981). "On the Attenuation of L_g Waves in Western and Central Asia and Their Use as a Discriminant Between Earthquakes and Explosions," *Bull. Seism. Soc. Am.*, *71*, pp. 249-261.

Nuttli, O. W. (1986a). "Yield Estimates of Nevada Test Site Explosions Obtained from Seismic L_g Waves," *J. Geophys. Res.*, *91*, pp. 2137-2151.

Nuttli, O. W. (1986b). "L_g Magnitudes of Selected East Kazakhstan Underground Explosions," *Bull. Seism. Soc. Am.*, *76*, pp. 1241-1251.

Nuttli, O. W. (1987). "L_g Magnitudes of Degelen, East Kazakhstan, Underground Explosions," *Bull. Seism. Soc. Am.*, *77*, pp. 679-681.

Piwinskii, A. J., and D. L. Springer (1978). "Propagation of L_g Waves Across Eastern Europe and Asia," Lawrence Livermore National Laboratory Report, Number UCRL-52494.

Pomeroy, P. W., W. J. Best, and T. V. McEvilly (1982). "Test Ban Treaty Verification with Regional Data - A Review," *Bull. Seism. Soc. Am., 72.* pp. S89-S129.

Sereno, T., S. Bratt, and T. Bache (1988). "Simultaneous Inversion of Regional Wave Spectra for Attenuation and Seismic Moment in Scandinavia," *J. Geophys. Res., 93,* pp. 2019-2035.

Wiggins, R. A. (1976). "A Fast, New Computational Algorithm for Free Oscillations and Surface Waves," *Geophys. J., 47,* pp. 135-150.

Xie, J., and B. J. Mitchell (1990). "L_g Coda Q in Eurasia - Preliminary Results," *EOS, 71,* p. 566.

Prof. Thomas Ahrens
Seismological Lab, 252-21
Division of Geological & Planetary Sciences
California Institute of Technology
Pasadena, CA 91125

Prof. Charles B. Archambeau
CIRES
University of Colorado
Boulder, CO 80309

Dr. Thomas C. Bache, Jr.
Science Applications Int'l Corp.
10260 Campus Point Drive
San Diego, CA 92121   (2 copies)

Prof. Muawia Barazangi
Institute for the Study of the Continent
Cornell University
Ithaca, NY 14853

Dr. Douglas R. Baumgardt
ENSCO, Inc
5400 Port Royal Road
Springfield, VA 22151-2388

Prof. Jonathan Berger
IGPP, A-025
Scripps Institution of Oceanography
University of California, San Diego
La Jolla, CA 92093

Dr. Lawrence J. Burdick
Woodward-Clyde Consultants
566 El Dorado Street
Pasadena, CA 91109-3245

Dr. Jerry Carter
Center for Seismic Studies
1300 North 17th St., Suite 1450
Arlington, VA 22209-2308

Dr. Karl Coyner
New England Research, Inc.
76 Olcott Drive
White River Junction, VT 05001

Prof. Vernon F. Cormier
Department of Geology & Geophysics
U-45, Room 207
The University of Connecticut
Storrs, CT 06268

Professor Anton W. Dainty
Earth Resources Laboratory
Massachusetts Institute of Technology
42 Carleton Street
Cambridge, MA 02142

Prof. Steven Day
Department of Geological Sciences
San Diego State University
San Diego, CA 92182

Dr. Zoltan A. Der
ENSCO, Inc.
5400 Port Royal Road
Springfield, VA 22151-2388

Prof. John Ferguson
Center for Lithospheric Studies
The University of Texas at Dallas
P.O. Box 830688
Richardson, TX 75083-0688

Prof. Stanley Flatte
Applied Sciences Building
University of California
Santa Cruz, CA 95064

Dr. Alexander Florence
SRI International
333 Ravenswood Avenue
Menlo Park, CA 94025-3493

Prof. Stephen Grand
University of Texas at Austin
Department of Geological Sciences
Austin, TX 78713-7909

Prof. Henry L. Gray
Vice Provost and Dean
Department of Statistical Sciences
Southern Methodist University
Dallas, TX 75275

Dr. Indra Gupta
Teledyne Geotech
314 Montgomery Street
Alexandria, VA 22314

Prof. David G. Harkrider
Seismological Laboratory
Division of Geological & Planetary Sciences
California Institute of Technology
Pasadena, CA 91125

Prof. Donald V. Helmberger
Seismological Laboratory
Division of Geological & Planetary Sciences
California Institute of Technology
Pasadena, CA 91125

Prof. Eugene Herrin
Institute for the Study of Earth and Man
GeophysicalLaboratory
Southern Methodist University
Dallas, TX 75275

Prof. Robert B. Herrmann
Department of Earth & Atmospheric Sciences
St. Louis University
St. Louis, MO 63156

Prof. Bryan Isacks
Cornell University
Department of Geological Sciences
SNEE Hall
ithaca, NY 14850

Dr. Rong-Song Jih
Teledyne Geotech
314 Montgomery Street
Alexandria, VA 22314

Prof. Lane R. Johnson
Seismographic Station
University of California
Berkeley, CA 94720

Prof. Alan Kafka
Department of Geology & Geophysics
Boston College
Chestnut Hill, MA 02167

Dr. Richard LaCoss
MIT-Lincoln Laboratory
M-200B
P. O. Box 73
Lexington, MA 02173-0073 (3 copies)

Prof Fred K. Lamb
University of Illinois at Urbana-Champaign
Department of Physics
1110 West Green Street
Urbana, IL 61801

Prof. Charles A. Langston
Geosciences Department
403 Deike Building
The Pennsylvania State University
University Park, PA 16802

Prof. Thorne Lay
Institute of Tectonics
Earth Science Board
University of California, Santa Cruz
Santa Cruz, CA 95064

Prof. Arthur Lerner-Lam
Lamont-Doherty Geological Observatory
of Columbia University
Palisades, NY 10964

Dr. Christopher Lynnes
Teledyne Geotech
314 Montgomery Street
Alexandria, VA 22314

Prof. Peter Malin
University of California at Santa Barbara
Institute for Crustal Studies
Santa Barbara, CA 93106

Dr. Randolph Martin, III
New England Research, Inc.
76 Olcott Drive
White River Junction, VT 05001

Dr. Gary McCartor
Mission Research Corporation
735 State Street
P.O. Drawer 719
Santa Barbara, CA 93102 (2 copies)

Prof. Thomas V. McEvilly
Seismographic Station
University of California
Berkeley, CA 94720

Dr. Keith L. McLaughlin
S-CUBED
A Division of Maxwell Laboratory
P.O. Box 1620
La Jolla, CA 92038-1620

Prof. William Menke
Lamont-Doherty Geological Observatory
of Columbia University
Palisades, NY 10964

Stephen Miller
SRI International
333 Ravenswood Avenue
Box AF 116
Menlo Park, CA 94025-3493

2

Prof. Bernard Minster
IGPP, A-025
Scripps Institute of Oceanography
University of California, San Diego
La Jolla, CA 92093

Prof. Brian J. Mitchell
Department of Earth & Atmospheric Sciences
St. Louis University
St. Louis, MO 63156

Mr. Jack Murphy
S-CUBED, A Division of Maxwell Laboratory
11800 Sunrise Valley Drive
Suite 1212
Reston, VA 22091 (2 copies)

Dr. Bao Nguyen
GL/LWH
Hanscom AFB, MA 01731-5000

Prof. John A. Orcutt
IGPP, A-025
Scripps Institute of Oceanography
University of California, San Diego
La Jolla, CA 92093

Prof. Keith Priestley
University of Cambridge
Bullard Labs, Dept. of Earth Sciences
Madingley Rise, Madingley Rd.
Cambridge CB3 OEZ, ENGLAND

Prof. Paul G. Richards
Lamont Doherty Geological Observatory
 of Columbia University
Palisades, NY 10964

Dr. Wilmer Rivers
Teledyne Geotech
314 Montgomery Street
Alexandria, VA 22314

Prof. Charles G. Sammis
Center for Earth Sciences
University of Southern California
University Park
Los Angeles, CA 90089-0741

Prof. Christopher H. Scholz
Lamont-Doherty Geological Observatory
of Columbia University
Palisades, NY 10964

Thomas J. Sereno, Jr.
Science Application Int'l Corp.
10260 Campus Point Drive
San Diego, CA 92121

Prof. David G. Simpson
Lamont-Doherty Geological Observatory
of Columbia University
Palisades, NY 10964

Dr. Jeffrey Stevens
S-CUBED
A Division of Maxwell Laboratory
P.O. Box 1620
La Jolla, CA 92038-1620

Prof. Brian Stump
Institute for the Study of Earth & Man
Geophysical Laboratory
Southern Methodist University
Dallas, TX 75275

Prof. Jeremiah Sullivan
University of Illinois at Urbana-Champaign
Department of Physics
1110 West Green Street
Urbana, IL 61801

Prof. Clifford Thurber
University of Wisconsin-Madison
Department of Geology & Geophysics
1215 West Dayton Street
Madison, WS 53706

Prof. M. Nafi Toksoz
Earth Resources Lab
Massachusetts Institute of Technology
42 Carleton Street
Cambridge, MA 02142

Prof. John E. Vidale
University of California at Santa Cruz
Seismological Laboratory
Santa Cruz, CA 95064

Prof. Terry C. Wallace
Department of Geosciences
Building #77
University of Arizona
Tucson, AZ 85721

Dr. Raymond Willeman
GL/LWH
Hanscom AFB, MA 01731-5000

Dr. Lorraine Wolf
GL/LWH
Hanscom AFB, MA 01731-5000

3

Dr. Monem Abdel-Gawad
Rockwell International Science Center
1049 Camino Dos Rios
Thousand Oaks, CA 91360

Prof. Keiiti Aki
Center for Earth Sciences
University of Southern California
University Park
Los Angeles, CA 90089-0741

Prof. Shelton S. Alexander
Geosciences Department
403 Deike Building
The Pennsylvania State University
University Park, PA 16802

Dr. Kenneth Anderson
BBNSTC
Mail Stop 14/1B
Cambridge, MA 02238

Dr. Ralph Archuleta
Department of Geological Sciences
University of California at Santa Barbara
Santa Barbara, CA 93102

Dr. Jeff Barker
Department of Geological Sciences
State University of New York
at Binghamton
Vestal, NY 13901

Dr. Susan Beck
Department of Geosciences, Bldg # 77
University of Arizona
Tucson, AZ 85721

Dr. T.J. Bennett
S-CUBED
A Division of Maxwell Laboratory
11800 Sunrise Valley Drive, Suite 1212
Reston, VA 22091

Mr. William J. Best
907 Westwood Drive
Vienna, VA 22180

Dr. N. Biswas
Geophysical Institute
University of Alaska
Fairbanks, AK 99701

Dr. G.A. Bollinger
Department of Geological Sciences
Virginia Polytechnical Institute
21044 Derring Hall
Blacksburg, VA 24061

Dr. Stephen Bratt
Center for Seismic Studies
1300 North 17th Street
Suite 1450
Arlington, VA 22209

Michael Browne
Teledyne Geotech
3401 Shiloh Road
Garland, TX 75041

Mr. Roy Burger
1221 Serry Road
Schenectady, NY 12309

Dr. Robert Burridge
Schlumberger-Doll Research Center
Old Quarry Road
Ridgefield, CT 06877

Dr. W. Winston Chan
Teledyne Geotech
314 Montgomery Street
Alexandria, VA 22314-1581

Dr. Theodore Cherry
Science Horizons, Inc.
710 Encinitas Blvd., Suite 200
Encinitas, CA 92024 (2 copies)

Prof. Jon F. Claerbout
Department of Geophysics
Stanford University
Stanford, CA 94305

Prof. Robert W. Clayton
Seismological Laboratory
Division of Geological & Planetary Sciences
California Institute of Technology
Pasadena, CA 91125

Prof. F. A. Dahlen
Geological and Geophysical Sciences
Princeton University
Princeton, NJ 08544-0636

4

Prof. Adam Dziewonski
Hoffman Laboratory
Harvard University
20 Oxford St
Cambridge, MA 02138

Prof. John Ebel
Department of Geology & Geophysics
Boston College
Chestnut Hill, MA 02167

Eric Fielding
SNEE Hall
INSTOC
Cornell University
Ithaca, NY 14853

Prof. Donald Forsyth
Department of Geological Sciences
Brown University
Providence, RI 02912

Dr. Cliff Frolich
Institute of Geophysics
8701 North Mopac
Austin, TX 78759

Dr. Anthony Gangi
Texas A&M University
Department of Geophysics
College Station, TX 77843

Dr. Freeman Gilbert
IGPP, A-025
Scripps Institute of Oceanography
University of California
La Jolla, CA 92093

Mr. Edward Giller
Pacific Sierra Research Corp.
1401 Wilson Boulevard
Arlington, VA 22209

Dr. Jeffrey W. Given
SAIC
10260 Campus Point Drive
San Diego, CA 92121

Prof. Roy Greenfield
Geosciences Department
403 Deike Building
The Pennsylvania State University
University Park, PA 16802

Dan N. Hagedorn
Battelle
Pacific Northwest Laboratories
Battelle Boulevard
Richland, WA 99352

Kevin Hutchenson
Department of Earth Sciences
St. Louis University
3507 Laclede
St. Louis, MO 63103

Dr. Hans Israelsson
Center for Seismic Studies
1300 N. 17th Street, Suite 1450
Arlington, VA 22209-2308

Prof. Thomas H. Jordan
Department of Earth, Atmospheric
   and Planetary Sciences
Massachusetts Institute of Technology
Cambridge, MA 02139

Robert C. Kemerait
ENSCO, Inc.
445 Pineda Court
Melbourne, FL 32940

William Kikendall
Teledyne Geotech
3401 Shiloh Road
Garland, TX 75041

Prof. Leon Knopoff
University of California
Institute of Geophysics & Planetary Physics
Los Angeles, CA 90024

Prof. L. Timothy Long
School of Geophysical Sciences
Georgia Institute of Technology
Atlanta, GA 30332

Prof. Art McGarr
Mail Stop 977
Geological Survey
345 Middlefield Rd.
Menlo Park, CA 94025

Dr. George Mellman
Sierra Geophysics
11255 Kirkland Way
Kirkland, WA 98033

5

Prof. John Nabelek
College of Oceanography
Oregon State University
Corvallis, OR 97331

Dr. Susan Schwartz
Institute of Tectonics
1156 High St.
Santa Cruz, CA 95064

Prof. Geza Nagy
University of California, San Diego
Department of Ames, M.S. B-010
La Jolla, CA 92093

John Sherwin
Teledyne Geotech
3401 Shiloh Road
Garland, TX 75041

Prof. Amos Nur
Department of Geophysics
Stanford University
Stanford, CA 94305

Dr. Matthew Sibol
Virginia Tech
Seismological Observatory
4044 Derring Hall
Blacksburg, VA 24061-0420

Prof. Jack Oliver
Department of Geology
Cornell University
Ithaca, NY 14850

Prof. Robert Smith
Department of Geophysics
University of Utah
1400 East 2nd South
Salt Lake City, UT 84112

Prof. Robert Phinney
Geological & Geophysical Sciences
Princeton University
Princeton, NJ 08544-0636

Dr. Stewart W. Smith
Geophysics AK-50
University of Washington
Seattle, WA 98195

Dr. Paul Pomeroy
Rondout Associates
P.O. Box 224
Stone Ridge, NY 12484

Dr. George Sutton
Rondout Associates
P.O. Box 224
Stone Ridge, NY 12484

Dr. Jay Pulli
RADIX System, Inc.
2 Taft Court, Suite 203
Rockville, MD 20850

Prof. L. Sykes
Lamont-Doherty Geological Observatory
of Columbia University
Palisades, NY 10964

Dr. Norton Rimer
S-CUBED
A Division of Maxwell Laboratory
P.O. Box 1620
La Jolla, CA 92038-1620

Prof. Pradeep Talwani
Department of Geological Sciences
University of South Carolina
Columbia, SC 29208

Prof. Larry J. Ruff
Department of Geological Sciences
1006 C.C. Little Building
University of Michigan
Ann Arbor, MI 48109-1063

Prof. Ta-liang Teng
Center for Earth Sciences
University of Southern California
University Park
Los Angeles, CA 90089-0741

Dr. Richard Sailor
TASC Inc.
55 Walkers Brook Drive
Reading, MA 01867

Dr. R.B. Tittmann
Rockwell International Science Center
1049 Camino Dos Rios
P.O. Box 1085
Thousand Oaks, CA 91360

Dr. Gregory van der Vink
IRIS, Inc.
1616 North Fort Myer Drive
Suite 1440
Arlington, VA 22209

Professor Daniel Walker
University of Hawaii
Institute of Geophysics
Honolulu, HI 96822

William R. Walter
Seismological Laboratory
University of Nevada
Reno, NV 89557

Dr. Gregory Wojcik
Weidlinger Associates
4410 El Camino Real
Suite 110
Los Altos, CA 94022

Prof. John H. Woodhouse
Hoffman Laboratory
Harvard University
20 Oxford St.
Cambridge, MA 02138

Prof. Francis T. Wu
Department of Geological Sciences
State University of New York
at Binghamton
Vestal, NY 13901

Dr. Gregory B. Young
ENSCO, Inc.
5400 Port Royal Road
Springfield, VA 22151-2388

Dr. Ralph Alewine III
DARPA/NMRO
1400 Wilson Boulevard
Arlington, VA 22209-2308

Mr. James C. Battis
GL/LWH
Hanscom AFB, MA 01731-5000

Dr. Robert Blandford
DARPA/NMRO
1400 Wilson Boulevard
Arlington, VA 22209-2308

Eric Chael
Division 9241
Sandia Laboratory
Albuquerque, NM 87185

Dr. John J. Cipar
GL/LWH
Hanscom AFB, MA 01731-5000

Cecil Davis
Group P 15, Mail Stop D406
P.O. Box 1663
Los Alamos National Laboratory
Los Alamos, NM 87544

Mr. Jeff Duncan
Office of Congressman Markey
2133 Rayburn House Bldg.
Washington, DC 20515

Dr. Jack Evernden
USGS - Earthquake Studies
345 Middlefield Road
Menlo Park, CA 94025

Art Frankel
USGS
922 National Center
Reston, VA 22092

Dr. Dale Glover
DIA/DT-1B
Washington, DC 20301

Dr. T. Hanks
USGS
Nat'l Earthquake Research Center
345 Middlefield Road
Menlo Park, CA 94025

Dr. James Hannon
Lawrence Livermore Nat'l Laboratory
P.O. Box 808
Livermore, CA 94550

Paul Johnson
ESS-4, Mail Stop J979
Los Alamos National Laboratory
Los Alamos, NM 87545

Janet Johnston
GL/LWH
Hanscom AFB, MA 01731-5000

Dr. Katharine Kadinsky-Cade
GL/LWH
Hanscom AFB, MA 01731-5000

Ms. Ann Kerr
IGPP, A-025
Scripps Institute of Oceanography
University of California, San Diego
La Jolla, CA 92093

Dr. Max Koontz
US Dept of Energy/DP 5
Forrestal Building
1000 Independence Avenue
Washington, DC 20585

Dr. W.H.K. Lee
Office of Earthquakes, Volcanoes,
& Engineering
345 Middlefield Road
Menlo Park, CA 94025

Dr. William Leith
U.S. Geological Survey
Mail Stop 928
Reston, VA 22092

Dr. Richard Lewis
Director, Earthquake Engineering & Geophysics
U.S. Army Corps of Engineers
Box 631
Vicksburg, MS 39180

James F. Lewkowicz
GL/LWH
Hanscom AFB, MA 01731-5000

Mr. Chris Paine
Office of Senator Kennedy
SR 315
United States Senate
Washington, DC 20510

Mr. Alfred Lieberman
ACDA/VI-OA'State Department Bldg
Room 5726
320 - 21st Street, NW
Washington, DC 20451

Colonel Jerry J. Perrizo
AFOSR/NP, Building 410
Bolling AFB
Washington, DC 20332-6448

Stephen Mangino
GL/LWH
Hanscom AFB, MA 01731-5000

Dr. Frank F. Pilotte
HQ AFTAC/TT
Patrick AFB, FL 32925-6001

Dr. Robert Masse
Box 25046, Mail Stop 967
Denver Federal Center
Denver, CO 80225

Katie Poley
CIA-OSWR/NED
Washington, DC 20505

Art McGarr
U.S. Geological Survey, MS-977
345 Middlefield Road
Menlo Park, CA 94025

Mr. Jack Rachlin
U.S. Geological Survey
Geology, Rm 3 C136
Mail Stop 928 National Center
Reston, VA 22092

Richard Morrow
ACDA/VI, Room 5741
320 21st Street N.W
Washington, DC 20451

Dr. Robert Reinke
WL/NTESG
Kirtland AFB, NM 87117-6008

Dr. Keith K. Nakanishi
Lawrence Livermore National Laboratory
P.O. Box 808, L-205
Livermore, CA 94550

Dr. Byron Ristvet
HQ DNA, Nevada Operations Office
Attn: NVCG
P.O. Box 98539
Las Vegas, NV 89193

Dr. Carl Newton
Los Alamos National Laboratory
P.O. Box 1663
Mail Stop C335, Group ESS-3
Los Alamos, NM 87545

Dr. George Rothe
HQ AFTAC/TTR
Patrick AFB, FL 32925-6001

Dr. Kenneth H. Olsen
Los Alamos Scientific Laboratory
P.O. Box 1663
Mail Stop D-406
Los Alamos, NM 87545

Dr. Alan S. Ryall, Jr.
DARPA/NMRO
1400 Wilson Boulevard
Arlington, VA 22209-2308

Howard J. Patton
Lawrence Livermore National Laboratory
P.O. Box 808, L-205
Livermore, CA 94550

Dr. Michael Shore
Defense Nuclear Agency/SPSS
6801 Telegraph Road
Alexandria, VA 22310

Dr. Albert Smith
Los Alamos National Laboratory
L-205
P. O. Box 808
Livermore. CA 94550

Office of the Secretary Defense
DDR & E
Washington, DC 20330

Donald L. Springer
Lawrence Livermore National Laboratory
L-205
P. O. Box 808
Livermore , CA 94550

HQ DNA
Attn: Technical Library
Washington, DC 20305

Mr. Charles L. Taylor
GL/LWG
Hanscom AFB, MA 01731-5000

DARPA/RMO/RETRIEVAL
1400 Wilson Boulevard
Arlington, VA 22209

Dr. Steven R. Taylor
Lawrence Livermore National Laboratory
L-205
P. O. Box 808
Livermore, CA 94550

DARPA/RMO/Security Office
1400 Wilson Boulevard
Arlington, VA 22209

Dr. Larry Turnbull
CIA-OSWR/NED
Washington, DC 20505

Geophysics Laboratory
Attn: XO
Hanscom AFB, MA 01731-5000

Dr. Eileen Vergino
Lawrence Livermore National Laboratory
L-205
P. O. Box 808
Livermore, CA 94550

Geophysics Laboratory
Attn: LW
Hanscom AFB, MA 01731-5000

Dr. Thomas Weaver
Los Alamos National Laboratory
P.O. Box 1663, Mail Stop C335
Los Alamos, NM 87545

DARPA/PM
1400 Wilson Boulevard
Arlington, VA 22209

J.J. Zucca
Lawrence Livermore National Laboratory
P. O. Box 808
Livermore, CA 94550

Defense Technical Information Center
Cameron Station
Alexandria, VA 22314 (5 copies)

GL/SULL
Research Library
Hanscom AFB , MA 01731-5000 (2 copies)

Defense Intelligence Agency
Directorate for Scientific
& Technical IntelligenceAttn: DTIB
Washington, DC 20340-6158

Secretary of the Air Force
(SAFRD)
Washington, DC 20330

AFTAC/CA
(STINFO)
Patrick AFB, FL 32925-600!

TACTEC - Battelle Memorial Institute
505 King Ave.
Columbus, OH 43201   (FINAL REPORT ONLY)

10

Dr. Ramon Cabre, S.J.
Observatorio San Calixto
Casilla 5939
La Paz, Bolivia

Prof. Hans-Peter Harjes
Institute for Geophysik
Ruhr University/Bochum
P.O. Box 102148
4630 Bochum 1, FRG

Prof. Eystein Husebye
NTNF/NORSAR
P.O. Box 51
N-2007 Kjeller, NORWAY

Prof. Brian L.N. Kennett
Research School of Earth Sciences
Institute of Advanced Studies
G.P.O. Box 4
Canberra 2601, AUSTRALIA

Dr. Bernard Massinon
Societe Radiomana
27 rue Claude Bernard
75005 Paris, FRANCE (2 Copies)

Dr. Pierre Mecheler
Societe Radiomana
27 rue Claude Bernard
75005 Paris, FRANCE

Dr. Svein Mykkeltveit
NTNF/NORSAR
P.O. Box 51
N-2007 Kjeller, NORWAY

Dr. Peter Basham
Earth Physics Branch
Geological Survey of Canada
1 Observatory Crescent
Ottawa, Ontario, CANADA K1A 0Y3

Dr. Eduard Berg
Institute of Geophysics
University of Hawaii
Honolulu, HI 96822

Dr. Michel Bouchon
I.R.I.G.M.-B.P. 68
38402 St. Martin D'Heres
Cedex, FRANCE

Dr. Hilmar Bungum
NTNF/NORSAR
P.O. Box 51
N-2007 Kjeller, NORWAY

Dr. Michel Campillo
Observatoire de Grenoble
I.R.I.G.M.-B.P. 53
38041 Grenoble, FRANCE

Dr. Kin Yip Chun
Geophysics Division
Physics Department
University of Toronto
Ontario, CANADA M5S 1A7

Dr. Alan Douglas
Ministry of Defense
Blacknest, Brimpton
Reading RG7-4RS, UNITED KINGDOM

Dr. Roger Hansen
NTNF/NORSAR
P.O. Box 51
N-2007 Kjeller, NORWAY

Dr. Manfred Henger
Federal Institute for Geosciences & Nat'l Res.
Postfach 510153
D-3000 Hanover 51, FRG

Ms. Eva Johannisson
Senior Research Officer
National Defense Research Inst.
P.O. Box 27322
S-102 54 Stockholm, SWEDEN

Dr. Fekadu Kebede
Seismological Section
Box 12019
S-750 Uppsala, SWEDEN

Dr. Tormod Kvaerna
NTNF/NORSAR
P.O. Box 51
N-2007 Kjeller, NORWAY

Dr. Peter Marshal
Procurement Executive
Minisuy of Defense
Blacknest, Brimpton
Reading FG7-4RS, UNITED KINGDOM

Prof. Ari Ben-Menahem
Department of Applied Mathematics
Weizman Institute of Science
Rehovot, ISRAEL 951729

Dr. Robert North
Geophysics Division
Geological Survey of Canada
1 Observatory Crescent
Ottawa, Ontario, CANADA K1A 0Y3

Dr. Frode Ringdal
NTNF/NORSAR
P.O. Box 51
N-2007 Kjeller, NORWAY

Dr. Jorg Schlittenhardt
Federal Institute for Geosciences & Nat'l Res.
Postfach 510153
D-3000 Hannover 51, FEDERAL REPUBLIC OF
GERMANY